# a-scope biomass coreh2o flex premier traq

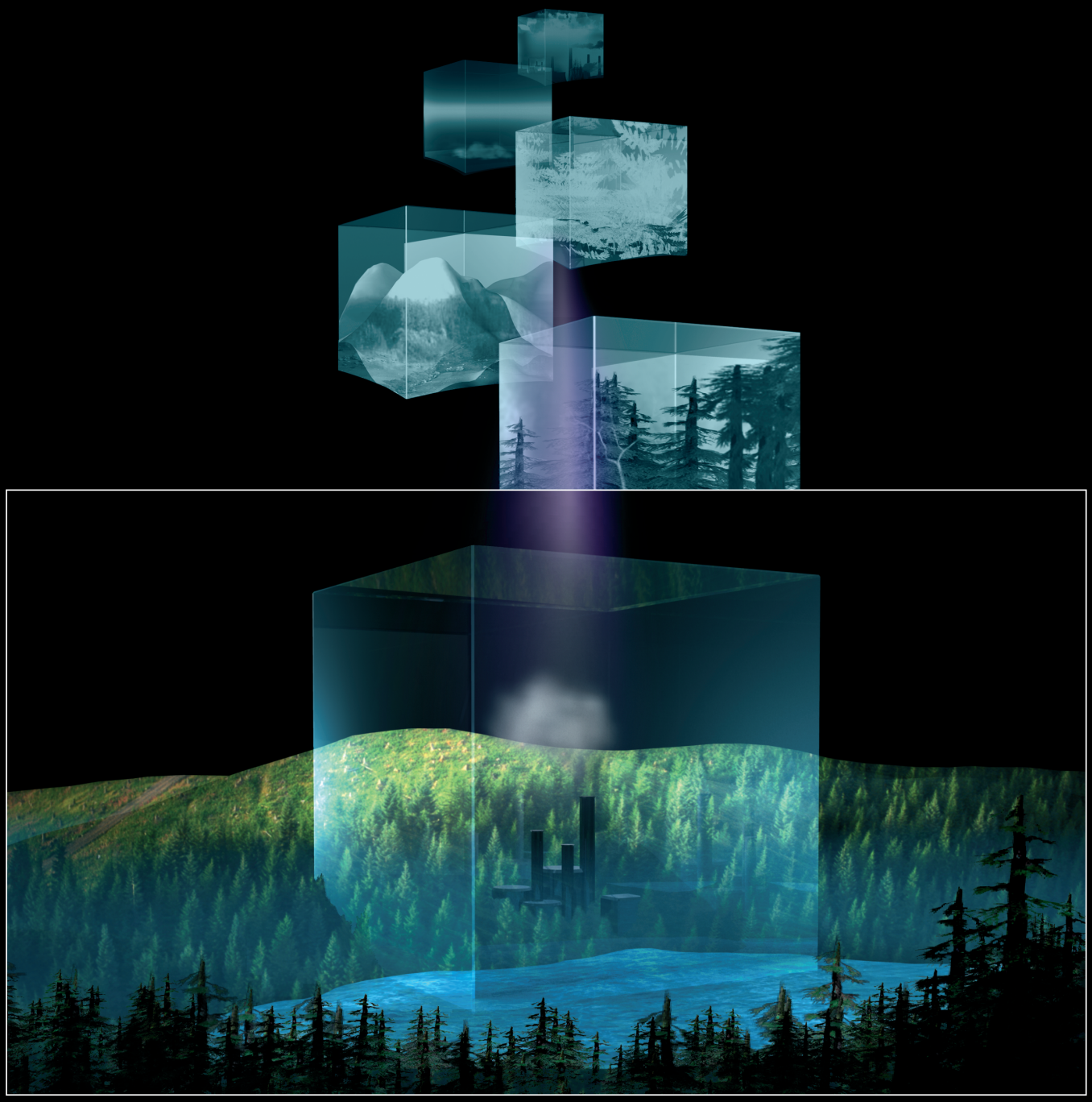

## → TO OBSERVE ATMOSPHERIC CARBON DIOXIDE FOR A BETTER UNDERSTANDING OF THE CARBON CYCLE

Six Candidate Earth Explorer Core Missions – Report for Assessment 1

www.esa.int

European Space Agency

CANDIDATE EARTH EXPLORER CORE MISSION

# a-scope – advanced space carbon and climate observation of planet earth

Report for Assessment
November 2008
SP-1313/1

**ESA SP-1313/1 Candidate Earth Explorer Core Missions – Reports for Assessment:**
**A-SCOPE – Advanced Space Carbon and climate Observation of Planet Earth**

| | |
|---|---|
| Scientific coordinator: | Mission Science Division<br>P. Ingmann |
| Technical coordinators: | Future Missions Division<br>P. Bensi |
| | Instrument Pre-Development Division<br>Y. Durand |
| Production & layout: | A. Griva |
| Editor: | P. Clissold |
| Cover: | AOES Medialab |
| Published by: | ESA Communication Production Office<br>ESTEC, PO Box 299<br>2200 AG Noordwijk<br>The Netherlands |
| Copyright: | © 2008 European Space Agency<br>ISBN 978-92-9221-406-7<br>ISSN 0379-6566 |

## Table of Contents

Chapter 1. Introduction. . . . . 1
1.1 Mission Summary . . . . . 3
Chapter 2. Background and Scientific Justification . . . . . 5
2.1 Introduction. . . . . 5
2.2 The role of $CO_2$ in the Earth system. . . . . 8
2.2.1 Radiative forcing (present, expected for 2050?). . . . . 8
2.2.2 Sources and sinks in the global carbon cycle. . . . . 9
2.2.3 Trends and future developments . . . . . 13
2.3 The use of atmospheric $CO_2$ to define sources and sinks . . . . . 15
2.3.1 A short historical overview . . . . . 15
2.3.2 Status . . . . . 17
2.3.3 Fundamental limitations at present . . . . . 21
2.4 Current and planned observational systems . . . . . 22
2.4.1 Current surface networks . . . . . 22
2.4.2 Airborne measurements . . . . . 23
2.4.3 Plans for surface network expansion . . . . . 24
2.4.4 Satellite missions for $CO_2$ monitoring . . . . . 25
2.5 A-SCOPE's observational system. . . . . 26
2.5.1 Nature of the sampling . . . . . 26
2.5.2 Nature of the data . . . . . 28
2.5.3 Expected improvement of source and sink estimation . . . . . 29
2.5.4 Expected impact on process understanding. . . . . 32
2.5.5 Expected impact on science and policy . . . . . 32
2.5.6 Ancillary benefits . . . . . 33
2.6 Uniqueness of A-SCOPE . . . . . 34
Chapter 3. Research Objectives . . . . . 37
3.1 Introduction. . . . . 37
3.2 The global carbon cycle and climate change . . . . . 37
3.3 Surface fluxes and modelling . . . . . 38
3.4 Emission inventories and protocols . . . . . 38
3.5 Conclusions . . . . . 39
Chapter 4. Observation Requirements . . . . . 41
4.1 Introduction. . . . . 41
4.2 Target and threshold. . . . . 42
4.3 Translation of flux uncertainty to $XCO_2$ precision. . . . . 42
4.4 Requirement Definition . . . . . 43
4.4.1 Accuracy and precision. . . . . 44
4.4.2 Vertical sensitivity . . . . . 44

4.4.3 Coverage . . . . . 44
4.4.4 Resolution . . . . . 45
4.4.5 Ranging capabilities . . . . . 45
4.4.6 Timeliness . . . . . 45
4.5 Observational requirements for $XCO_2$ . . . . . 45
4.6 Auxiliary data . . . . . 47
4.7 Spin-off products . . . . . 49
4.8 Performance simulations . . . . . 49
4.9 Conclusions . . . . . 51

Chapter 5. The Mission Elements . . . . . 53
5.1. Introduction . . . . . 53
5.2 Space segment . . . . . 53
5.2.1 Observational principle . . . . . 54
5.2.2 Ancillary data requirement . . . . . 57
5.3 Ground segment . . . . . 58
5.4. Processing requirements for $XCO_2$ . . . . . 58
5.5 Validation . . . . . 59
5.6 Additional geophysical products . . . . . 60
5.6.1 Canopy height and vertical structure . . . . . 60
5.6.2 Cloud boundaries and elevated aerosol layer . . . . . 61
5.6.3 Surface retro-reflectance . . . . . 61
5.7 Summary of A-SCOPE geophysical products . . . . . 62
5.8 Relation with other missions . . . . . 62
5.9 Proof of concept . . . . . 63
5.10 Summary . . . . . 66

Chapter 6. System Concept . . . . . 69
6.1 Introduction . . . . . 69
6.2 Mission architecture overview . . . . . 69
6.3 Orbit . . . . . 71
6.4 Space segment . . . . . 71
6.4.1 Payload . . . . . 72
6.4.2 Platform . . . . . 80
6.4.3 Satellite . . . . . 84
6.4.4 Launcher . . . . . 85
6.5 Ground segment and data processing . . . . . 87
6.5.1 General . . . . . 87
6.5.2 Ground segment elements . . . . . 87
6.5.3 Data processing . . . . . 88
6.6 Operation and utilisation concept . . . . . 89
6.7 Performance Aspects . . . . . 90

6.7.1 Random errors and instrument sizing . . . . . 90
6.7.2 Systematic errors and measurement accuracy . . . . . 91
6.7.3 Scattering surface elevation . . . . . 92
6.7.4 Comparison B1/B2 . . . . . 93

Chapter 7. Programmatics . . . . . 95
7.1 Introduction . . . . . 95
7.2 Technical maturity, critical areas and risk . . . . . 95
7.2.1 Transmitter . . . . . 95
7.2.2 Detector . . . . . 96
7.2.3 Frequency stabilisation . . . . . 96
7.2.4 Power monitoring measurements . . . . . 97
7.3 Development approach and schedule . . . . . 97

References . . . . . 99

Acronyms . . . . . 107

## Chapter 1. Introduction

Earth Explorer missions focus on the science and research elements of ESA's Living Planet Programme. Encompassing a new approach to observing the Earth from space, Earth Explorers are developed in direct response to scientific challenges identified by the scientific community. The fundamental principle of defining, developing and operating missions in close cooperation with the scientific community provides an efficient tool to address pressing Earth-science questions as effectively as possible.

Since the science and research elements of ESA's Living Planet Programme were established in the mid-1990s, this on-going user-driven strategy has, so far, resulted in six Explorer missions selected for implementation. Together, they cover a broad range of issues to further our understanding of the Earth system and the impact of human activity. In addition, the scientific questions addressed also form the basis for the development of new applications for Earth observation data.

Earth Explorers missions are split into two categories – 'Core' and 'Opportunity'. Core Earth Explorers are large missions addressing complex issues of scientific interest whilst Opportunity missions are smaller and supported scientifically by the proposing team. Through a process of selection, Core and Opportunity missions are implemented in separate cycles to ensure a steady flow of missions to address key Earth-science questions.

The first cycle for Core missions resulted in the Gravity field and steady-state Ocean Circulation Explorer (GOCE) launched in October 2008, and the Atmospheric Dynamics Mission ADM-Aeolus (due for launch in 2010). The second cycle, initiated in 2000, resulted in the Earth Clouds Aerosols and Radiation Explorer (EarthCARE), due for launch in 2013. The first cycle for Opportunity missions resulted in the ice mission CryoSat, which is currently being rebuilt following a launch failure in 2005 and scheduled for launch in 2009, and the Soil Moisture and Ocean Salinity (SMOS) mission, also scheduled for launch in 2009. The second cycle resulted in the magnetic field mission Swarm, which is due for launch in 2010.

A third cycle of Earth Explorer Core missions was initiated by a Call for Ideas released in March 2005. In May 2006, six of the candidate missions were selected for Assessment Study (Phase 0) following a peer review of 24 proposed mission ideas. Prior to the next stage – the selection of missions for Feasibility Study (Phase A) – a Report for Assessment has been prepared for each of the six Candidate Earth Explorer Core Missions.

The following Reports for Assessment for each of the Candidate Earth Explorer Core Missions being provided to the Earth Observation research community prior to the User Consultation Meeting to be held in January 2009 in Lisbon, Portugal:

- A-SCOPE – to observe atmospheric carbon dioxide for a better understanding of the carbon cycle,

- BIOMASS – to observe global forest biomass for a better understanding of the carbon cycle,
- CoRe$H_2O$ – to observe snow and ice for a better understanding of the water cycle,
- FLEX – to observe photosynthesis for a better understanding of the carbon cycle,
- PREMIER – to observe trace gases for a better understanding of atmospheric chemistry and climate interactions,
- TRAQ – to observe the composition of the troposphere for a better understanding of air quality.

The six Reports for Assessment all follow a common structure comprising this introductory first chapter and six subsequent chapters as follows:

- Chapter 2 – identifies the issues of concern to be addressed by the mission, considers related past and present activities, justifies the mission set within the post-2015 time frame and includes a review of the current scientific understanding of the issue in question while identifying the potential 'delta' that the mission could provide,
- Chapter 3 – drawing on arguments presented in Chapter 2, this chapter details the specific research objectives of the mission,
- Chapter 4 – specifies the observational requirements within the context of the scientific objectives, including geophysical parameters and associated data products, space/time sampling requirements, timing of the mission etc.,
- Chapter 5 – provides an overview of the mission elements, including the space segment, ground segments, and products that are required to fulfil the observational requirements,
- Chapter 6 – details the complete system concept and reviews the technological challenges and levels of technical maturity,
- Chapter 7 – outlines a programme of implementation. Drawing on previous chapters, this chapter also addresses technical maturity, the development status of key technologies, risks, logistics and schedules.

This Report for Assessment covers the Advanced Space Carbon and Climate Observation of Planet Earth (A-SCOPE) mission and is based on contributions from the following members of the Mission Assessment Group (MAG):

Pierre Flamant – MAG Chairman (Laboratoire de Météorologie Dynamique, Palaiseau, France),

François-Marie Bréon (Laboratoire des Sciences du Climat et de L'Environnement, Gif-sur-Yvette, France),

Han Dolman (Faculty of Earth and Life Sciences, Vrije Universiteit Amsterdam, The Netherlands),

Gerhard Ehret (DLR Institute for Atmospheric Physics, Oberpfaffenhofen, Germany),

Nicolas Gruber (Eidgenössische Technische Hochschule, Zürich, Switzerland),

Sander Houweling (Stichting Ruimte Onderzoek Nederland, Utrecht, The Netherlands),

Marko Scholze (Department of Earth Sciences, University of Bristol, United Kingdom).

They are supported by an observer:

Robert T. Menzies (California Institute of Technology, Jet Propulsion Laboratory, Pasadena, USA).

The scientific content of the report has been compiled by Paul Ingmann. The technical content of the report has been compiled by Paolo Bensi, Jean-Loup Bézy, Marc Bouvet, Jerome Caron, Yannig Durand, David Evans, Arnaud Lecuyot, based on inputs derived from the industrial Phase 0 studies.

## 1.1 Mission Summary

### *Objectives*

The overarching objective of A-SCOPE is the observation of the spatial and temporal gradients of atmospheric $CO_2$ with a precision and accuracy sufficient to constrain $CO_2$ fluxes significantly better than with the current and future *in situ* and space-borne observation system, i.e. to constrain the fluxes to within 0.02 Pg C $yr^{-1}$ on a scale of 1000 km × 1000 km.

### *Science*

The A-SCOPE measurements, together with appropriate modelling and interpretative activities, will allow the constraining and further development of models of the terrestrial biosphere and of the oceans. This will improve the projections of future trends in carbon sources and sinks. In addition, the mission will monitor the impact of large-scale climatic disturbances (such as El Niño) and other factors (such as forest fire, insect plagues or afforestation/deforestation) on

regional carbon budgets. Such information is urgently needed, for example, for the development of optimal carbon mitigation strategies.

### *Mission*

A-SCOPE will demonstrate the value of active remote sensing of carbon dioxide from space. As such, it will establish the basis for future missions of long duration, as, for instance, required for the verification of future emissions reduction commitments or for the detection of trends. Indeed, large vegetation changes and associated carbon fluxes are expected during the 21st century as a response to climate change. A global and reliable monitoring of carbon fluxes will be essential in this context and A-SCOPE may be seen as a demonstration mission for this objective. The key feature of the A-SCOPE mission is high accuracy $CO_2$ measurements (1 ppm) with no bias.

[Credits: Nicolas Gruber, ETH]

# Chapter 2. Background and Scientific Justification

*Carbon dioxide is the most important anthropogenic greenhouse gas .... The atmospheric concentration of carbon dioxide in 2005 exceeds by far the natural range over the last 650 000 years (180 to 300 ppm) as determined from ice cores. The annual carbon dioxide concentration growth rate was larger during the last 10 years ..., than it has been since the beginning of continuous direct atmospheric measurements.*

*Intergovernmental Panel on Climate Change (IPCC) Summary for Policymakers of Working Group I, 2007 (IPCC, 2007a)*

## 2.1 Introduction

Carbon dioxide ($CO_2$) is the most important anthropogenic greenhouse gas (Figure 2.1). At present, it contributes to more than half of the total anthropogenic change in the Earth's radiation budget, and its relative contribution is bound to increase in the future. The observed rise in atmospheric $CO_2$ of more than 30% since pre-industrial times has been identified in the last assessment report by the Intergovernmental Panel on Climate Change (IPCC) as the main driver for the increase in global mean temperature over the same period, and particularly for the warming over the last 30 years. There is no doubt that the main cause of this atmospheric $CO_2$ increase is the emissions from the burning of fossil fuels and from land-use change, but the atmospheric $CO_2$ observations reveal also that less than half of the total anthropogenic emissions have remained in the atmosphere, with the remainder having been taken up by either the ocean or the land biosphere. This atmospheric fraction reflects the balance between anthropogenic carbon emissions and the dynamics of terrestrial and oceanic processes that remove $CO_2$ from the atmosphere (Sarmiento and Gruber, 2002). The long-term evolution of this balance is key to understanding and predicting the speed and magnitude of human induced climate change. There are indications that the land and ocean sink cannot keep up pace with increasing emissions and eventually may turn from a sink into a source (e.g. Cox et al., 2000).

The current knowledge about the sinks, particularly those over the land, comes to a substantial part from observations of small, but measurable spatial variations in atmospheric $CO_2$. This is because more direct means to measure these fluxes, such as eddy-covariance measurements or biomass inventories are either not reliable enough due to severe undersampling or are limited in scope due to measuring only above ground properties. By contrast, the atmosphere acts as a large-scale integrator, whose atmospheric $CO_2$ variations reflect where $CO_2$ has been added to or removed from the atmosphere. The interpretation of these variations is not entirely straightforward, but by using information about transport and mixing from atmospheric transport models, one can, in principle, determine where the sources and sinks for carbon dioxide are, how large they are, and how they have varied through time (Figure 2.2).

The present ability to use such *inverse* methods with sufficient reliability and at high spatial resolution is seriously hampered by the presently available observations of

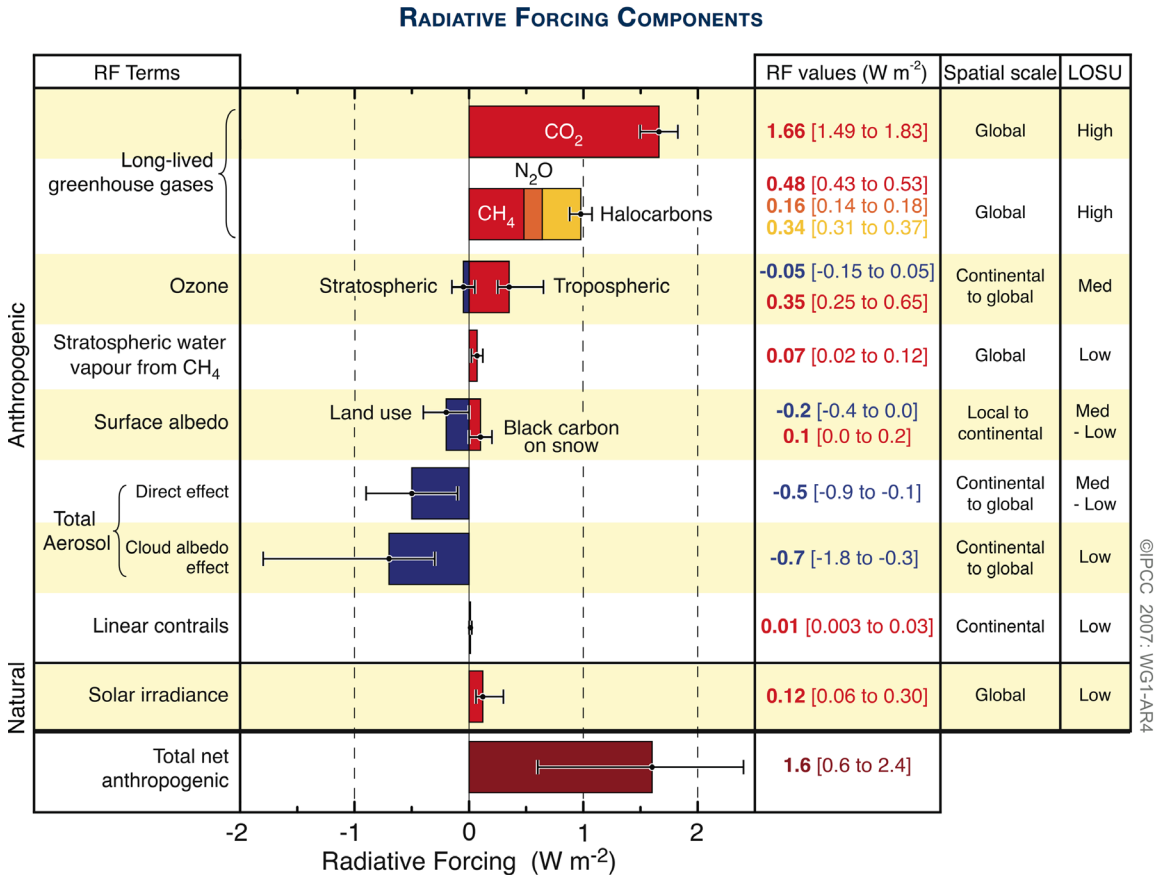


Figure 2.1: Global average Radiative Forcing (RF) estimates and ranges in 2005 for anthropogenic carbon dioxide ($CO_2$), methane ($CH_4$), nitrous oxide ($N_2O$) and other important agents and mechanisms, together with the typical geographical extent (spatial scale) of the forcing and the assessed Level Of Scientific understanding (LOSU). The net anthropogenic radiative forcing and its range are also shown. At present, anthropogenic $CO_2$ is the main forcing factor, being at least twice as influential as any other forcing factor. [Credits: IPCC (2007a) © IPCC]

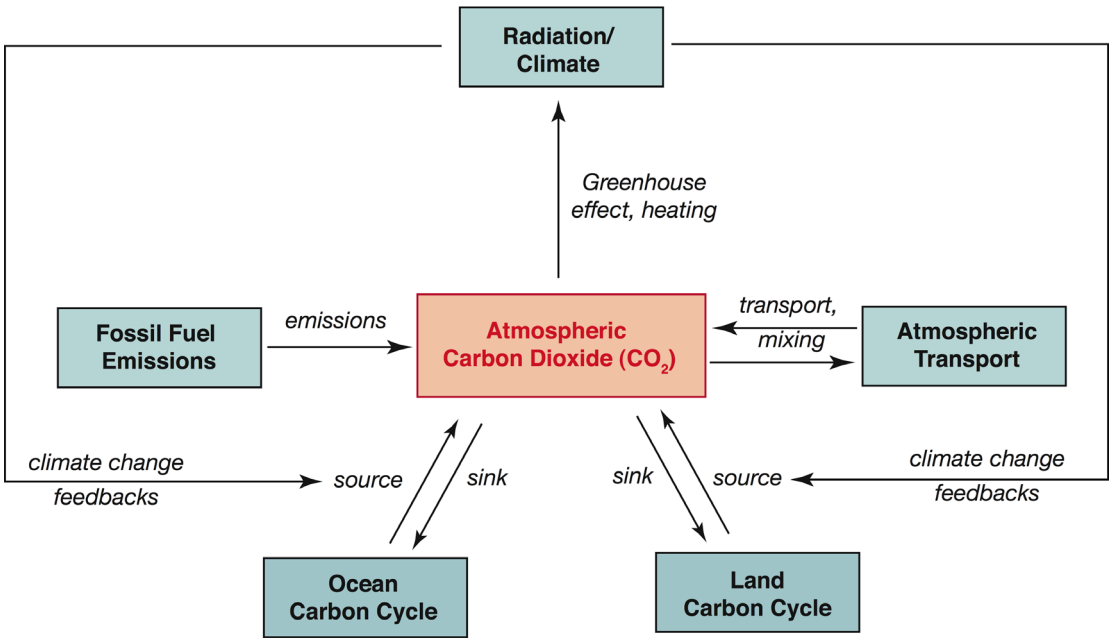


Figure 2.2: The importance of atmospheric $CO_2$ in the Earth system. [Credits: Nicolas Gruber, ETH]

atmospheric $CO_2$. Atmospheric $CO_2$ is measured regularly only at a limited set of monitoring stations (about 70), most of which are located in the Northern Hemisphere and at maritime locations, with almost no coverage, for example, over tropical land. In addition, at nearly all of these stations the observations are limited to near-ground, with only a handful of stations undertaking vertical profile measurements by aircraft. As a result of this limited observational network, current estimates of the regional distribution of $CO_2$ sources and sinks from atmospheric inversions are rather uncertain, unless they are constrained by *a priori* estimates or additional information. But even then, one currently cannot estimate the mean fluxes of $CO_2$ on the scale of entire continents to much better than about 1 Pg C $yr^{-1}$ (1 Pg = $10^{15}$ g = $10^{12}$ kg), which is very large considering, for example, that the fossil fuel emissions of the European Union were about 1.1 Pg C $yr^{-1}$ in the past decade.

The goal of the proposed A-SCOPE mission is to improve this situation dramatically, by enhancing the atmospheric $CO_2$ observations to the point where continental-scale $CO_2$ fluxes can be estimated to generally within less than 0.02 Pg C $yr^{-1}$ at the scale of one million square kilometres, i.e. 1000 km × 1000 km. This requires high-precision and high accuracy observations that only an active measurement can provide, while the presently planned $CO_2$ missions by the Japanese Space Agency (Greenhouse gases Observing SATellite, GOSAT) and U.S. NASA (Orbiting Carbon Observatory, OCO) use a passive technique, which imposes strong limits on precision and accuracy, as well as spatial and temporal coverage due to cloud cover, aerosol interference, and lack of sunlight. Of particular concern are the inability of passive systems to make measurements in the high-latitudes during the winter months, leaving large areas of the globe unobserved for a considerable amount of time, and their high sensitivity to aerosols, making the passive measurements vulnerable to biases. An additional major benefit of the proposed active mission is that it provides constraints about the distribution of the height and structure of the terrestrial vegetation.

Knowledge about the spatial distribution of sources and sinks of $CO_2$ with unprecedented accuracy will provide urgently needed process information about the global carbon cycle (Figure 2.2). For example, the distribution and causes of the current net uptake of $CO_2$ by the terrestrial biosphere is not well understood. Neither are the causes that drive the changes through time on an interannual to decadal scale, or those that may eventually decrease the capacity of the land to absorb $CO_2$. Among the various hypotheses to explain the current sink are:

- regrowth of previously cultivated areas,
- fertilisation of land plants by the elevated $CO_2$,
- growth of high latitude forests as a response to warming, and
- fertilisation by nitrogen deposits.

These processes have a distinct spatial and temporal structure with regard to both $CO_2$ fluxes and changes in the height of the terrestrial vegetation, so that the proposed mission is expected to be able to differentiate between these hypotheses. Whether one or the other dominates the current sink has strong implications for

the future behaviour of the terrestrial carbon sink. Similarly, it is unclear what the net effect of climate change on the land sink is. The lengthening of the growing season has often been assumed to be a negative feedback on the atmospheric growth rate (i.e., longer growing seasons should increase carbon uptake), but recent work shows that the opposite may in fact be the case. In many environments a longer growing season results in lengthening seasonal drought conditions and can ultimately reduce carbon uptake. Similarly, large scale droughts associated with heatwaves have potential to significantly reduce the carbon uptake by the land.

In a world that is moving forward with the implementation of the United Nations' Framework Convention on Climate Change (UNFCCC), which requires "the stabilisation of atmospheric greenhouse gases at a level that prevents dangerous interference with the climate system", these differences mean that humankind has to reduce its $CO_2$ emissions in order not to exceed a particular atmospheric $CO_2$ trajectory. Knowing by how much this reduction has to proceed is fundamental to climate change mitigation and adaptation policies. At current $CO_2$ mitigation costs of between € 10 and € 100 /tonne $CO_2$, an additional reduction of the emissions by 100 Pg C amounts to a cost of € 3–30 billion. In addition, verification of agreed emission targets by nations or groups of nations is vital for any international carbon management scheme. The proposed high-accuracy estimation of the net carbon balance (0.02 Pg C $yr^{-1}$) of regions at the million square kilometre scale is essential for the international verification of emission targets.

The A-SCOPE mission is thus uniquely positioned to provide data that is not only of scientific value, but also is of fundamental importance from a societal and political perspective (for example, UNFCCC).

Moreover, A-SCOPE will address several of the key challenges identified in ESA's updated strategy for Earth Observation (ESA, 2006). As outlined in more detail in chapter 3, A-SCOPE will provide fundamental observations to better describe and understand the terrestrial and oceanic processes as well as the composition of the Earth's atmosphere (Challenges of the atmosphere, ocean and land). Hence, this mission will contribute fundamentally to our understanding of the functioning of three out of the five spheres of the Earth system, highlighting the importance of the global carbon cycle in this system.

## 2.2 The role of $CO_2$ in the Earth system

### *2.2.1 Radiative forcing (present, expected for 2050?)*

Carbon dioxide ($CO_2$) in the atmosphere is a 'greenhouse gas', i.e. it interacts with the Earth's energy flow in such a manner that it does not affect the amount of incoming shortwave radiation from the Sun, but it tends to absorb the longwave radiation that is being emitted by Earth's surface. As a result, $CO_2$ tends to trap heat in the lower levels of the atmosphere, so that the more $CO_2$ the atmosphere contains, the warmer it will get. On the other hand, i.e. without the presence of greenhouse gases in the atmosphere, the Earth's mean temperature would be

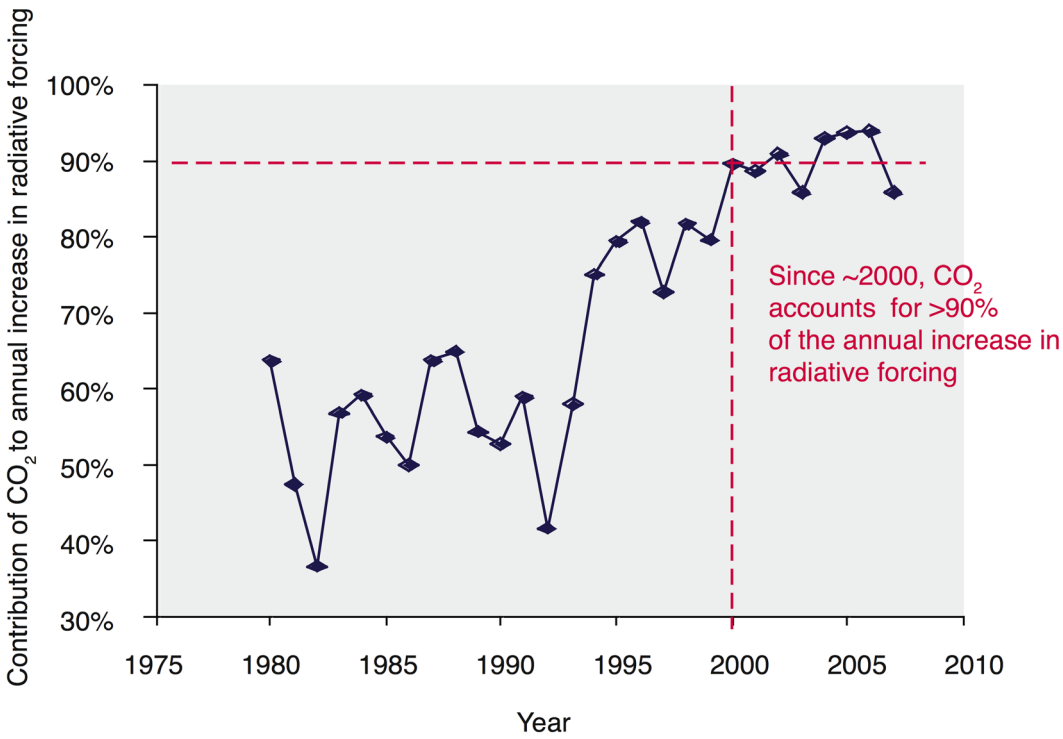


Figure 2.3: Time series plot of the relative contribution of atmospheric $CO_2$ to the annual increase in total radiative forcing. In the 1980s, the contribution of $CO_2$ was about 50% to the cumulative contribution, (see also Figure 2.1), but in the 1990s, the $CO_2$ contribution has increased to about 90% of the overall annual increase. This trend is expected to persist in the future, as the rate of growth of the other greenhouse gases is expected to remain small, while that of $CO_2$ very likely will remain high for quite some time. [Based on the annual greenhouse gas index provided by NOAA GMD (*www.esrl.noaa.gov/gmd/aggi*)]. [Credits: Nicolas Gruber, ETH, Han Dolman, VU]

about 30°C colder than today, rendering Earth largely uninhabitable. While the direct effect of the addition of greenhouse gases on the radiative forcing balance of the Earth is well understood (Figure 2.1), the exact amount of warming for a given increase in atmospheric $CO_2$ (the so-called climate sensitivity) is not well quantified, as it depends on a number of feedbacks between the various subelements of the Earth's climate system (e.g. hydrological cycle, oceanic circulation, carbon cycle) (IPCC, 2007b). The globally-averaged forcing since pre-industrial times has been dominated by $CO_2$ (Figure 2.1). In addition, since about 2000, the contribution of atmospheric $CO_2$ has become overwhelming, being responsible for about 90% of the annual increase in total radiative forcing (Figure 2.3). As the rate of increase in atmospheric $CO_2$ is expected to increase in the future and concentrations of other greenhouse gases may level off, this recent trend will very likely persist, so that the cumulative contribution of $CO_2$ to the radiative forcing budgets is likely to increase as well (IPCC, 2007b).

### *2.2.2 Sources and sinks in the global carbon cycle*

The amount of carbon dioxide in the atmosphere is miniscule relative to the amount of carbon stored in the ocean and in the land biosphere (living vegetation and soils) (Figure 2.4). The ocean alone contains 60 times more carbon than the atmosphere (about 38 000 Pg C relative to the 590 Pg C stored in the pre-industrial

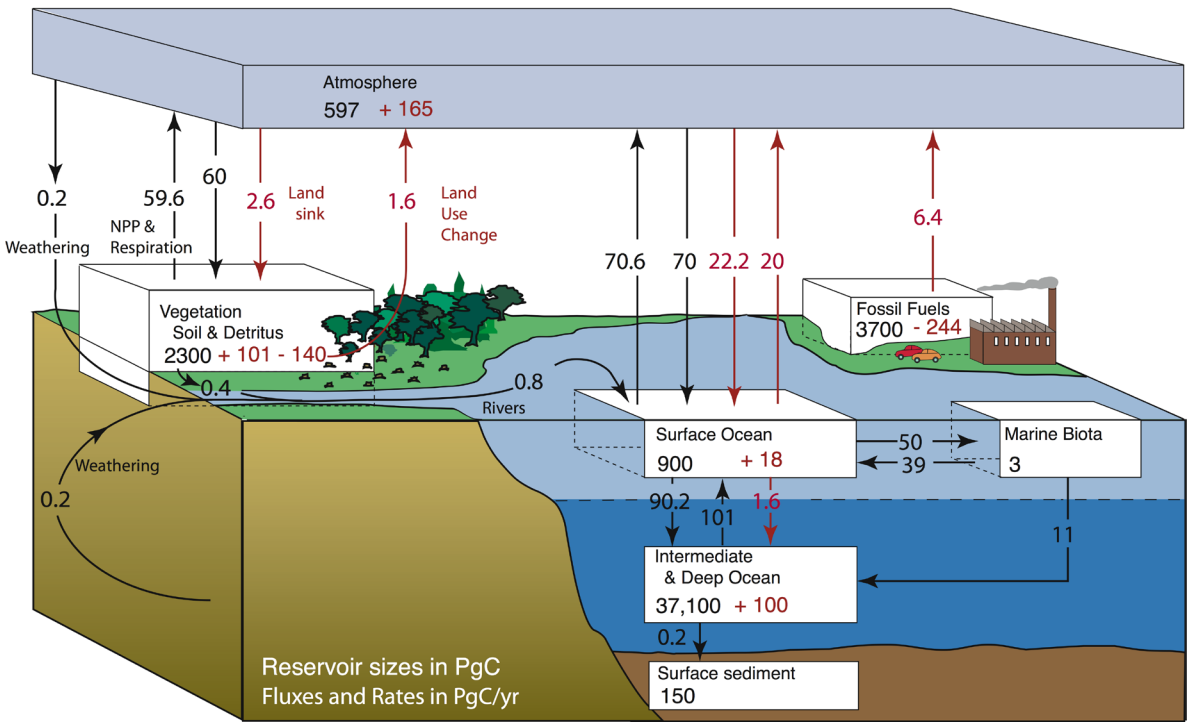


Figure 2.4: The global carbon cycle for the 1990s, showing main annual fluxes in PgC $yr^{-1}$: preindustrial 'natural' fluxes in black and 'anthropogenic' fluxes in red. Modified from Sarmiento and Gruber (2002) to reflect the fluxes for decade of the 1990s using data from Sabine *et al.* (2004). The net terrestrial loss of –39 Pg C is inferred from cumulative (fossil fuel emissions – atmospheric increase – ocean storage). The loss of –140 Pg C from the 'Vegetation, Soil & detritus' compartment represents the cumulative emissions from land use change (Houghton, 2003), and requires a terrestrial biosphere sink of 101 Pg C. [Credits: Nicolas Gruber, ETH]

atmosphere, the carbon stored in the land biosphere is also at least 4 times that in the atmosphere (about 2300 Pg C). Before the onset of the industrial revolution, some 200 years ago, the atmospheric $CO_2$ concentration was determined almost solely by the exchange processes of (natural) carbon between the atmosphere and ocean, and between the atmosphere and land biosphere, respectively. These exchanges are very vigorous (order of 100 Pg C $yr^{-1}$), turning the entire atmospheric $CO_2$ content over in less than 5 years. Despite this short residence time, atmospheric $CO_2$ concentrations have remained remarkably stable over the last 10 000 years, until the start of the industrial revolution, varying only between about 260 and 280 ppm.

The onset of the industrial revolution led to a dramatic perturbation of this natural carbon cycle. The emissions of $CO_2$ from the burning of fossil fuel and from changes in land-use, mostly the conversion of forests into agriculturally used land, have led to a nearly 40% increase in atmospheric $CO_2$ over the last 250 years (mean atmospheric $CO_2$ concentration in 2007 was about 380 ppm) (Figure 2.5). A comparison of this increase with the estimated emissions reveals that only about 40% of the cumulative anthropogenic emissions, which by now total nearly the pre-industrial $CO_2$ content of the atmosphere, have actually remained in the atmosphere. The rest was removed by sink processes in the ocean and in the land biosphere. The currently best estimates suggest that between 1800 and 1994, the ocean has taken up about 120 Pg C, while the terrestrial biosphere was a net source

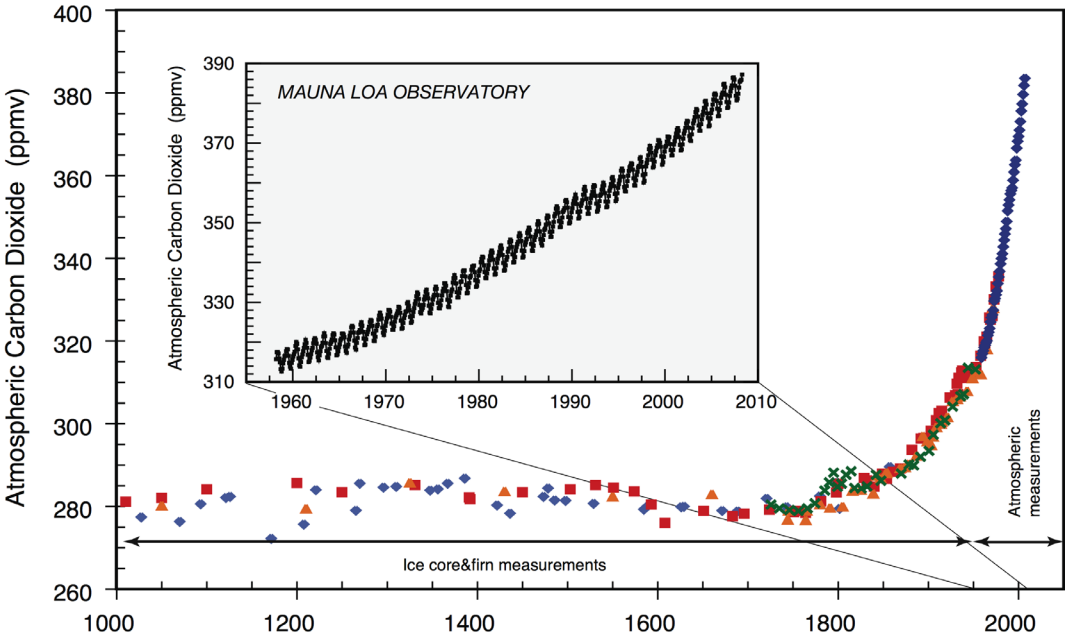


Figure 2.5: Atmospheric $CO_2$ evolution over the last 1000 years. The atmospheric carbon dioxide levels have increased by more than 30% since the industrial revolution started in the mid 18th century. Before then, atmospheric $CO_2$ had been at 280 ppm for several millennia. Data before 1958 stem from measurements of air bubbles trapped in ice cores recovered from several sites in Antarctica. The $CO_2$ data displayed in the inset were measured on air samples taken by Charles D. Keeling and collaborators at Mauna Loa, Hawaii. The seasonal variations evident there reflect the seasonal breathing of the terrestrial biosphere in the Northern Hemisphere: $CO_2$ is removed by strong growth in spring and summer and returned by respiration and remineralisation in the fall and winter (updated from Sarmiento and Gruber, 2002). [Credits: Nicolas Gruber, ETH]

of about 40 Pg C (Figure 2.4) (Sabine et al., 2004). The latter flux consists of the sum of a land-use change source, which resulted in the loss of about 140 Pg C over this period (primarily a consequence of the conversion of forests into agricultural land), and a land sink (mostly by forests), which removed about 100 Pg C. Thus, the carbon cycle on land and in the ocean has slowed down the atmospheric $CO_2$ increase substantially. Without these sink processes, the atmospheric $CO_2$ concentration today would be nearly twice that in pre-industrial times, i.e. well above 500 ppm rather than the current 380 ppm.

The primary mechanism driving the present oceanic sink is the equilibration of the anthropogenic $CO_2$ across the air-sea interface and the subsequent transport of this anthropogenic $CO_2$ bearing water into the ocean interior. Eventually, this mechanism will remove about 80% of the anthropogenic $CO_2$ emissions, but due to the slowness of interior ocean circulation, it will take several thousand years to reach this equilibration. This explains why the oceanic uptake fraction of anthropogenic $CO_2$ is much smaller than might be expected on the basis of the atmosphere-ocean carbon distribution in pre-industrial times. The primary mechanism driving the land biosphere sink is an excess of photosynthesis over the mechanisms responsible for carbon losses, i.e. respiration, decomposition, fire and harvest. However, the relative roles of these various terms in driving changes in the long-term carbon storage on land are not well established. Several particular processes have been proposed, such as $CO_2$ fertilisation, increased growth due to more favourable

growth conditions (e.g. in boreal forests), recovery from past land-use change, and nitrogen fertilisation, but no consensus the attribution has yet emerged.

The sources and sinks for $CO_2$ have varied substantially from year to year, and even from decade to decade (Figure 2.6). These variations are not driven by changes in fossil fuel emissions, which have increased relatively steadily over the last 50 years, but primarily by changes in the terrestrial carbon sink. In the year following an El Niño event in the Pacific, the terrestrial biosphere often becomes a net source of $CO_2$, while in the years following a La Niña event, the terrestrial biosphere is an anomalously strong sink, with the amplitude of these changes amounting to more

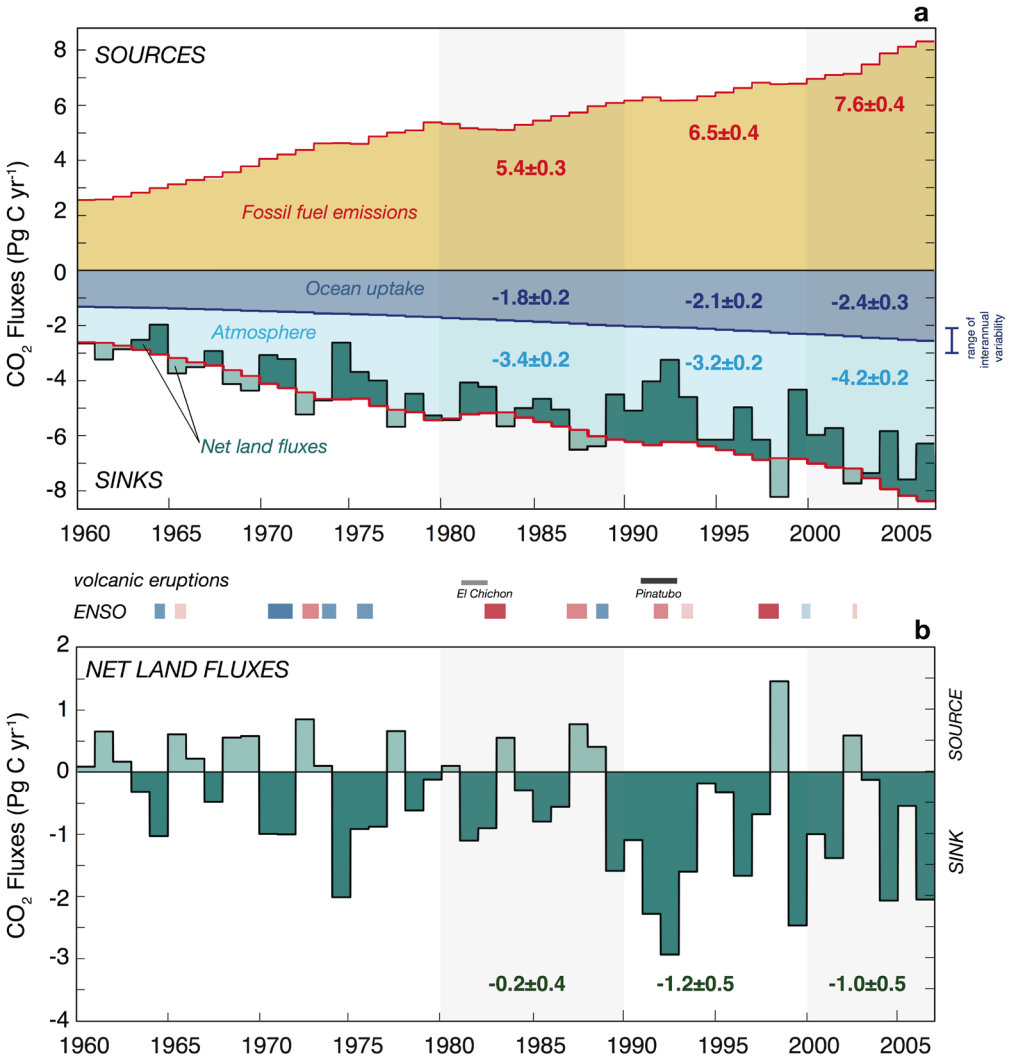


Figure 2.6: Time history of the global fate of the anthropogenic carbon emitted by fossil-fuel burning and cement production. (a) Time series of fossil-fuel emissions from 1958 until 2006 (upper half) and how they were redistributed in the global carbon system, i.e. uptake by the ocean, accumulation in the atmosphere, and exchange with the terrestrial biosphere (lower half). The time history of the oceanic uptake flux does not contain any interannual variability, but this is believed to be relatively small (about ± 0.5 Pg C $yr^{-1}$ as indicated by the vertical bar) (b) Time series of net exchange flux of $CO_2$ between the atmosphere and the terrestrial biosphere. This flux is the sum of a land sink flux and emissions from land-use change. The net land fluxes vary strongly from year to year, often in association with climatic perturbations such as El Niño's (red), La Niña's (blue) and volcanic eruptions, as shown by the horizontal bars. [Credits: Nicolas Gruber, ETH]

than 4 Pg C $yr^{-1}$. These large changes in the magnitude of the terrestrial fluxes lead to substantial year-to-year changes in the atmospheric $CO_2$ growth rate. By contrast, the oceanic uptake varies much less from year to year, with an amplitude likely less than 1 Pg C $yr^{-1}$ (Peylin et al., 2005).

There exists a strong consensus that the rapid increase in atmospheric $CO_2$ over the last 250 years (Figure 2.5) is the most important driver for the observed warming of about 0.8°C over this period, especially for that during the last 30 years (IPCC, 2007b). The future evolution of Earth's climate will likely depend to an even greater degree on the evolution of atmospheric $CO_2$ than has been the case in the past (Figure 2.1), as the relative contribution of other greenhouse gases, such as methane, chlorofluorocarbons, and nitrous oxide will likely decrease in the future, cf. Figure 2.3.

### *2.2.3 Trends and future developments*

Future atmospheric $CO_2$ will depend on the magnitude of future anthropogenic $CO_2$ emissions, as well as on the future evolution of the sink strengths of the land and ocean. The emissions will be determined by trends in global population and economic growth, as well as by energy consumption patterns and the types of energy sources being used, which may well change in response to both experienced and expected additional climate change. This adds a new feedback into the global carbon cycle, which will have a profound influence on the future of the Earth system, as humankind begins to grapple with the challenge of managing its planetary environment.

The other important factor determining future $CO_2$ levels and hence climate change is the evolution of the carbon sinks. Although these carbon sinks in the ocean and in the land biosphere have removed a substantial fraction of the emitted $CO_2$ in the past, it is unclear whether and how these sinks will continue into the future. If the sink strengths become weaker with a warmer climate, as many studies currently suggest (for example, Figure 2.7), future atmospheric $CO_2$ will rise faster, causing additional warming, which makes the sinks even weaker. Thus the carbon cycle could form a positive feedback cycle that will significantly impact the future trajectory of the Earth's climate. However, this interaction between the physical climate system and the global carbon cycle is poorly understood and is a very substantial source of uncertainty in climate projections (IPCC, 2007b, Chapter 7).

To illustrate the level of uncertainty, Figure 2.7 shows the results from an intercomparison of 11 coupled carbon-climate models that simulate the anthropogenic perturbation during the 21st century based on emission scenarios of the IPCC (Friedlingstein et al., 2006). All models simulate an accelerated increase of atmospheric $CO_2$ as a result of impacts of climate change on the carbon cycle. The magnitude of this feedback varies, however, considerably between the various simulations. The resulting concentration of $CO_2$ in the atmosphere varies from 700 to 1000 ppm between the models, while the difference between the coupled and uncoupled runs varies from 25 to 300 ppm. At the moment, our scientific understanding is insufficient to clearly refute the scenario of any model, but almost

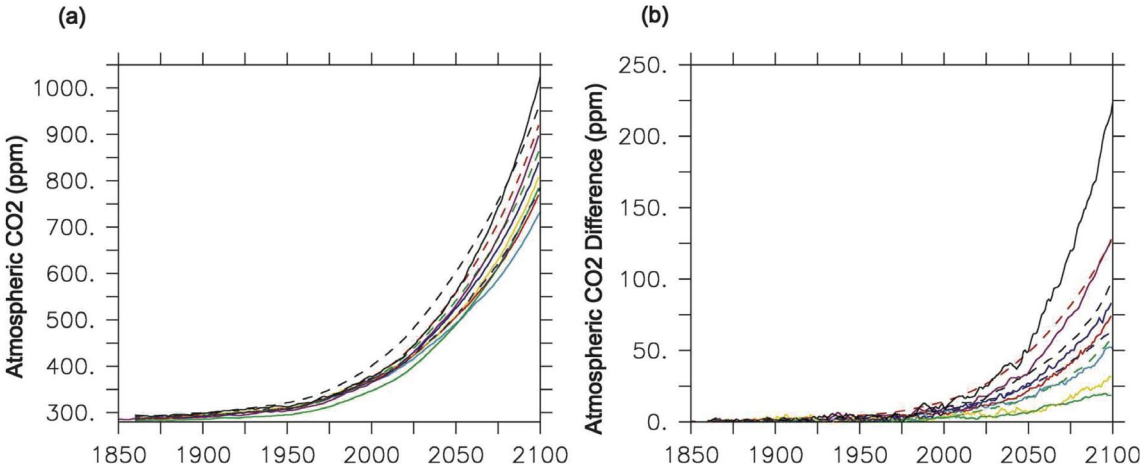


Figure 2.7: Model simulated $CO_2$ concentration in the atmosphere for a given $CO_2$ emission scenario (IPCC SRES A2) as simulated by 11 models that participated in the C4MIP model intercomparison. (a) Simulated $CO_2$ concentrations when climate-carbon feedbacks are permitted, i.e. when carbon cycle models are interactively coupled with climate models. (b) Difference between coupled and uncoupled simulation, i.e. the difference in atmospheric $CO_2$ arising from carbon-climate feedbacks. Note that this difference is positive for all models. There is thus a growing consensus that the sign of the carbon-climate feedback is positive, i.e. that the response of the global carbon cycle to global warming will be a reduced uptake, causing a larger fraction of the emitted $CO_2$ to stay in the atmosphere. [Credits: Friedlingstein et al., (2006) © AMS]

all models investigated to this date confirm that the overall feedback between the carbon-cycle and climate is positive, i.e. it tends to accelerate global warming (Friedlingstein et al., 2006). However, one out of twelve models shows a negative feedback (Thornton et al., 2007).

Current projections of future atmospheric $CO_2$ levels on the basis of a range of assumptions about the future evolution of the anthropogenic $CO_2$ carbon emissions and the future evolution of the carbon sinks include scenarios that suggest $CO_2$ concentrations at the end of this century may be approaching, in the worst case scenario, 1000 ppm (Figure 2.7). They correspond to an incease in the global mean temperature exceeding 6°C. With great confidence, such changes have no precedent in Earth's climate for the last one million years and quite likely not for the past 20 million years. Thus, humankind is moving into uncharted territory, where the past cannot be used as a good guide for the future. This makes the uncertainty with regard to the processes governing the sinks of $CO_2$ even more disturbing.

Quantifying and understanding the present sources and sinks of $CO_2$ represents, however, a key necessity for improving our ability to predict and guide the joint future of our planet and its human inhabitants. Accurate knowledge of the carbon cycle variability and feedback on climate is thus key to planning mitigation scenarios as Figure 2.8 shows (Friedlingstein, 2008). A mission like A-SCOPE could become instrumental in reducing the errors in climate prediction models. In turn, this could improve climate prediction. In particular, A-SCOPE observations could be used to (in)validate models and the parameterisations employed, by so doing, increase confidence in climate predictions.

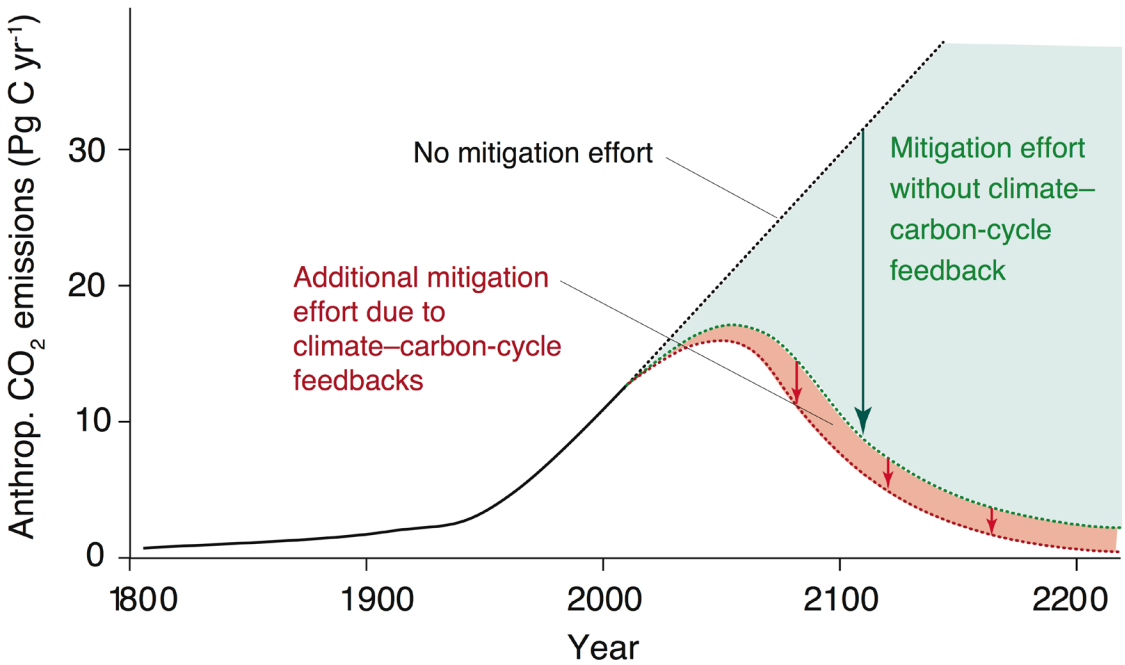


Figure 2.8: Past and projected trajectories of anthropogenic $CO_2$ emissions. The amount of $CO_2$ emitted from 1800 to the present is shown in black (solid line). Three projected trajectories of anthropogenic $CO_2$ emissions are also shown (dashed lines): no effort to reduce emissions (black), and $CO_2$ stabilisation scenarios that do (red) or do not (green) take into account the positive feedback between climate and the carbon cycle. A greater reduction in emissions will be required to stabilise climate when feedbacks involving the carbon cycle are considered (adapted from Friedlingstein, 2008). [Credits: Nicolas Gruber, ETH, Han Dolman, VU]

## 2.3 The use of atmospheric $CO_2$ to define sources and sinks

### *2.3.1 A short historical overview*

Measurements of atmospheric $CO_2$ have played an extraordinary role in elucidating the global carbon cycle and the sources and sinks that determine its evolution. In fact, the problem of the anthropogenic perturbation of the global carbon cycle was not recognised until the first detailed and accurate measurements of atmospheric $CO_2$ unambiguously showed that atmospheric $CO_2$ was increasing. To date, the atmospheric $CO_2$ curve from Mauna Loa and the South Pole (the Keeling curve), when extended backwards in time with atmospheric $CO_2$ measurements from air bubbles conserved in ice cores, is perhaps the single most important illustration of the extraordinary and global-scale impact of humans on the environment (c.f. Figure 2.5).

Over the past few decades, the addition of a substantial number of additional atmospheric $CO_2$ measurements sites to the Mauna Loa and the South Pole sites has provided sufficient information to portray natural seasonal and latitudinal variations superimposed on the secular global abundance trend. Atmospheric $CO_2$ exhibits a seasonal cycle, with peak to mean amplitude of about 1 ppm in the Southern Hemisphere, increasing to about 15 ppm in the higher latitudes of the Northern Hemisphere (55° to 65° N) (Figure 2.9a). This seasonal cycle is mostly governed by the seasonal exchange of $CO_2$ between the atmosphere and the terrestrial biosphere,

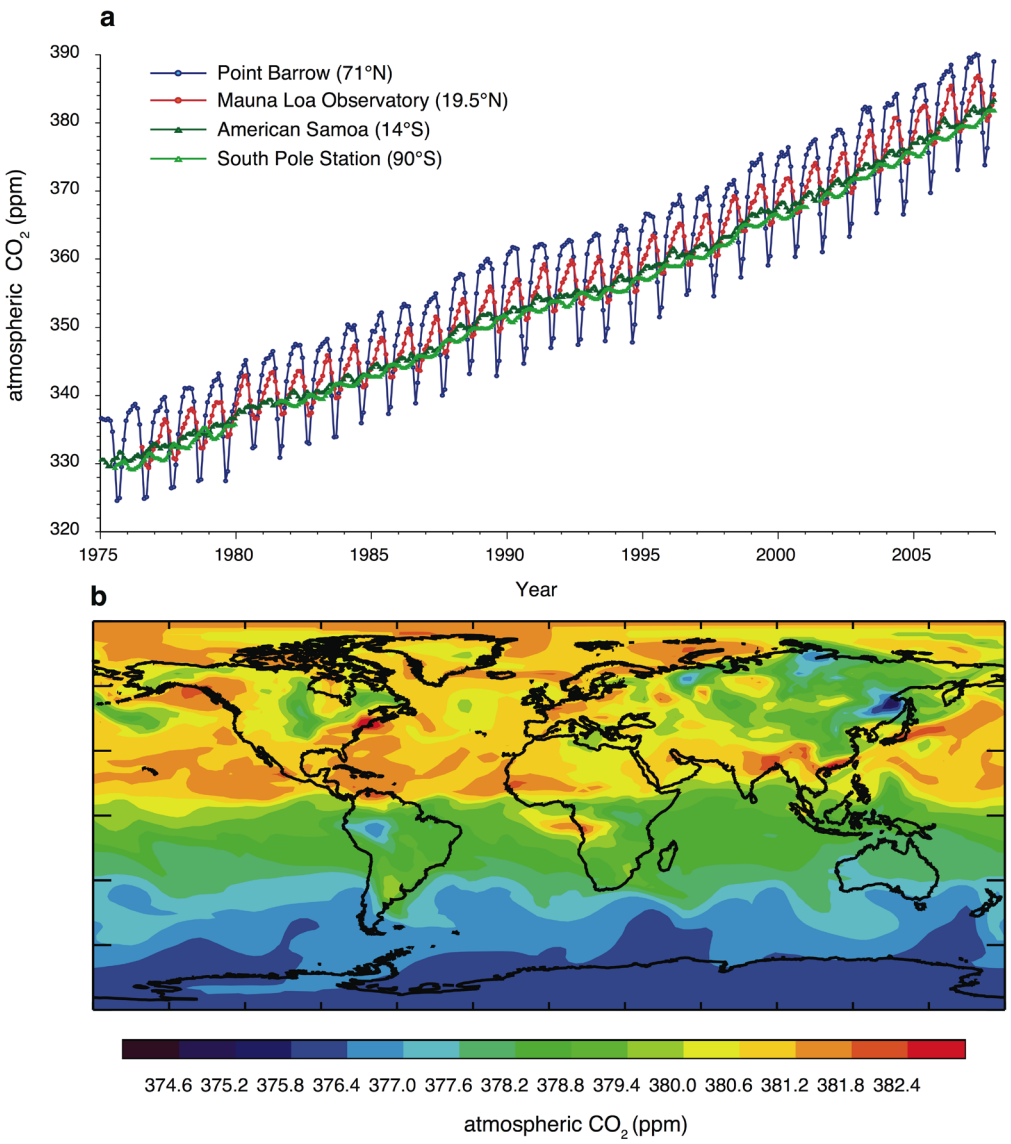


Figure 2.9: (a) Measured atmospheric $CO_2$ concentrations from 1975 until 2007 at selected surface stations (Barrow 71°N, 156°W; Mauna Loa 19.5°N, 155°W; Samoa 14°S, 172°W and at the South Pole) (data obtained by NOAA Global Monitoring Division). (b) Model simulated instantaneous snapshot of the column integrated atmospheric $CO_2$ concentration. [Credits: Nicolas Gruber, ETH, Sander Houweling, SRON]

which is disproportionally located in the Northern Hemisphere. This signal does not get mixed out by atmospheric transport and mixing, since in contrast to the relatively fast mixing of signals from the ground to the free troposphere, it takes about 3 months to mix signals from the pole to tropics, and about two years to mix signals between the two hemispheres. This long mixing time-scale also permits the presence of a distinct north-to-south gradient in yearly averaged atmospheric $CO_2$ concentrations, largely driven by the fossil fuel emissions, most of which occur in the Northern Hemisphere. Interestingly, the observed interhemispheric gradient is smaller than one would expect on the basis of the fossil fuel emissions. This indicates the presence of sink processes that are larger in the Northern than in the Southern Hemisphere.

Hidden within the smooth interhemispheric gradient in atmospheric $CO_2$ are strong spatial variations that exist even in the atmospheric $CO_2$ column mean (Figure 2.9b). These variations emerge from the interaction of sources and sinks at the Earth's surface with atmospheric dynamics.

Such differences in atmospheric $CO_2$ concentrations from site to site have been exploited very successfully to infer the spatial and temporal distribution of sources and sinks. In fact, atmospheric $CO_2$ measurements have so far been the most important source of information about the global-scale carbon balance. This is because direct measurements of $CO_2$ fluxes are difficult to obtain, and hence sparse in time and space, which prevents their extrapolation to larger scales. The inversion methods used to infer such sources and sinks from atmospheric $CO_2$ measurements have undergone rapid development and have become very sophisticated. Methods have been developed to not only invert the atmospheric $CO_2$ concentrations at the global scale, but also for individual regions with high spatial resolution. However, our present ability to use this constraint on the global carbon cycle is substantially limited by the present network of surface measurements which provide poor spatial coverage. To meet the future needs requires the availability of global observations only satellite-based instruments can provide.

### *2.3.2 Status*

So far, most applications of inverse modelling to the estimation of $CO_2$ sources and sinks have focused on large-scales, using measurements from global flask sampling networks (for example, NOAA-ESRL, CSIRO). The measurements can be used either to estimate net fluxes in space and time (referred to as flux inversions) or to optimise uncertain parameters of a coupled process-based model of the fluxes (referred to as parameter inversions). In both cases, measurements from remote sampling sites are selected, so that the air samples can be considered representative of large air masses, facilitating comparison with coarse resolution global models. Because of the background measurement selection, however, the flux resolving power of global inversions on smaller scales is generally rather low. This is explained by the fact that atmospheric mixing largely disperses the concentration signals of terrestrial carbon sources and sinks before they reach the remote sampling sites. In practise, global flux inversions only truly resolve the net fluxes of broad latitudinal bands. This is illustrated in Figure 2.10, showing the results of an atmospheric inverse modelling intercomparison in the framework of the TransCom Project (Gurney et al., 2002). The plot reveals that uncertainties of the annual (sub-)continental $CO_2$ fluxes are large and roughly similar in size to the fluxes themselves, i.e. the estimated fluxes do not differ in a statistically significant manner from zero. This is a major shortcoming in scientist's ability to shed light on the regional distribution of fluxes.

The relatively efficient atmospheric mixing in the longitudinal direction limits the resolution of longitudinally separated fluxes. As a result, global flux inversions show a limited skill in separating, for example, annual $CO_2$ fluxes from the ocean and the land without additional constraints on the land-ocean partitioning, which

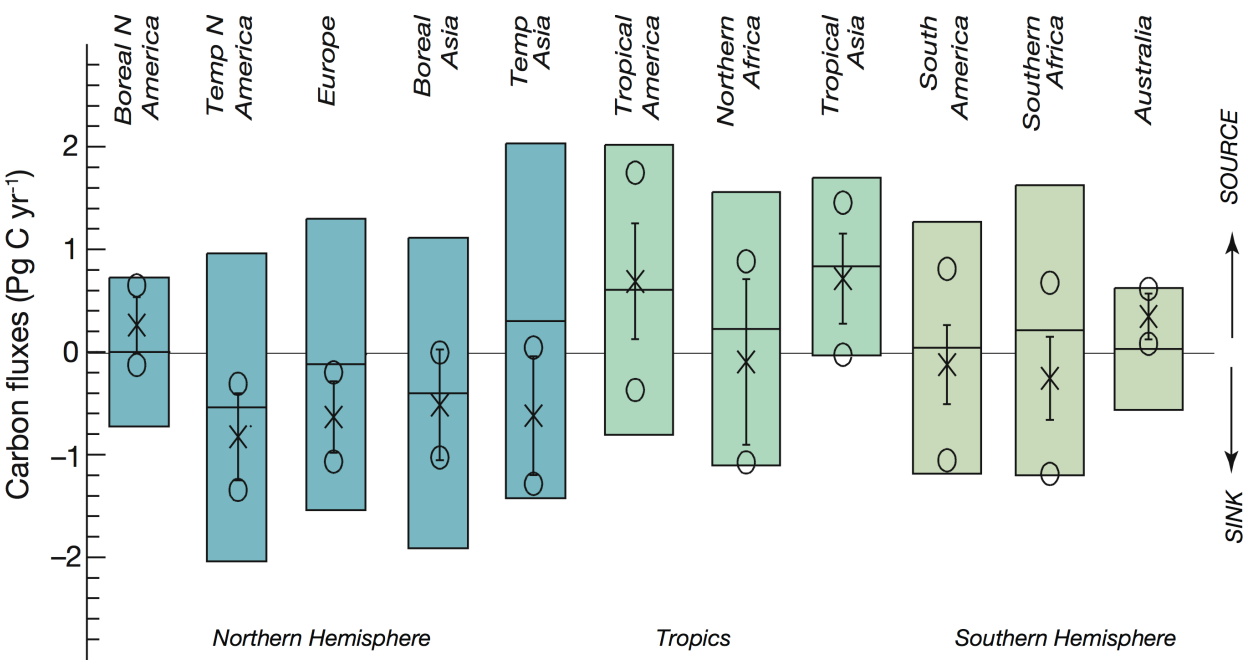


Figure 2.10: Net land fluxes estimated by a global inversion of annual mean atmospheric $CO_2$ concentrations. Mean estimated fluxes are shown by crosses. The prior flux estimates and their uncertainties are indicated by the boxes; the central horizontal bar indicates the prior flux estimate, and the top and bottom of the box give the prior flux uncertainty range. The mean estimated uncertainty across all models (the 'within-model' uncertainty) is indicated by the circles. The standard deviation of the models estimated fluxes (the 'between-model' uncertainty) is indicated by the 'error bars'. Colours refer to the broad latitudinal bands indicated at the bottom. Based on data provided by the TransCom experiment (Gurney et al., 2002). [Credits: Gruber, ETH]

can be derived from measurements of $O_2/N_2$ or $^{13}CO_2$. A recent development is to perform coupled ocean-atmosphere inversions using ocean interior measurements, which has proven a highly effective approach to reduce the uncertainty of the oceanic uptake of $CO_2$ and to provide new constraints on the land fluxes (Jacobson et al., 2007a,b) (Figure 2.11). The flux resolving power of global $CO_2$ inversions is more favourable in time than in space, as demonstrated by robust estimates of interannual flux variations. The results of multi-annual inversions highlight, for example, the sensitivity of the terrestrial biosphere to climatic variations, such as El Niño Southern Oscillation (ENSO) (Bousquet et al., 2000; Baker et al., 2006). The flux variations derived from these inversions are generally considered more reliable than the estimated long-term means. This is probably caused by the spatially inhomogeneous geometry of the sampling network in combination with systematic transport model errors.

Improved spatial resolution over land can be obtained using high-frequency measurements from networks of tall towers, which are presently under development in Europe and the US (CarboEurope, North American Carbon Project). Regional inverse modelling of these measurements requires an atmospheric transport model that is operated at a high spatial resolution. So far, exploratory studies have mainly focused on assessing the model performance on these scales. Substantial differences between models are found, which emphasise the importance of model resolution and boundary-layer dynamics. Although transport

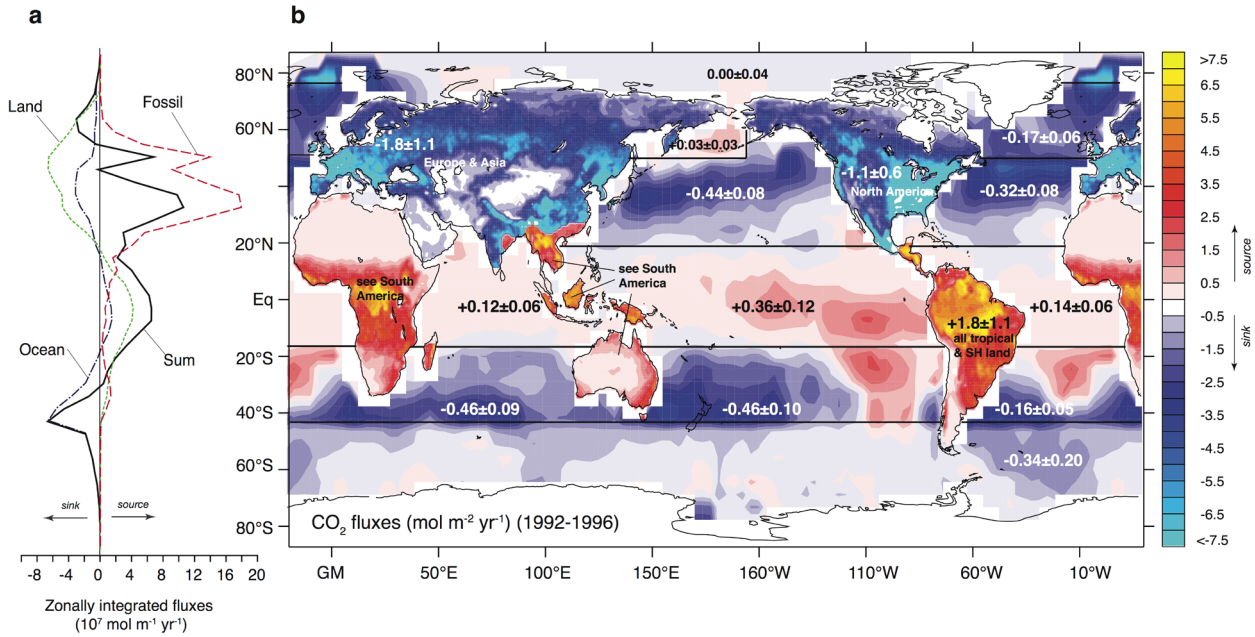


Figure 2.11: Global distribution of estimated sources and sinks for atmospheric $CO_2$ for the years 1992–1996: (a) Zonally integrated fluxes for the land, ocean, fossil fuel emissions, and their sum. (b) Global map of the sources and sinks based on a joint atmospheric ocean inversion for the land [Credits: Jacobson et al., 2007b] and on an oceanic inversion for the ocean [Credits: Mikaloff Fletcher et al., 2006, 2007], including the outgassing of river carbon. For (b), the regionally integrated estimates of the inversions (shown as numbers) were spatially mapped using an air-sea $CO_2$ flux pattern determined from surface $\Delta pCO_2$ measurements and a gas exchange model for the ocean fluxes, and the Net Primary Production (NPP) pattern of the CASA model for the land fluxes. As a consequence, the detailed spatial structure of the fluxes needs to be interpreted with caution, as it is not a result of the inversion, but an *a priori* input. The more highly resolved inverse flux estimates were first aggregated to 12 regions for the ocean and 3 regions for the land, and then mapped out using the spatial patterns. [Credits: Gruber, ETH]

model uncertainties will need to be improved before robust regional scale flux estimation becomes feasible, inverse modelling of tall tower measurements is certainly a promising direction. It is expected, however, that this application will remain limited to a few regions where tall tower networks exist, which does not provide a solution for the remaining landmasses, particularly in the tropics, that are virtually unserved by the current surface network. For high resolution inversions, boundary constraints from global models are an important prerequisite, making the A-SCOPE observations also key to the successful application of regional carbon source and sink estimates.

Using $CO_2$ measurements in the context of parameter inversions to optimise a set of uncertain model parameters is a fairly new approach in carbon cycle research. Here, the observations are used to solve for parameters of coupled process-based models of the fluxes, instead of solving for surface fluxes directly. Besides improving our understanding of the fundamental processes governing the exchange of carbon between the various components (atmosphere, land and ocean), the main advantage of this approach is its predictive power. If the coupled model system is fully prognostic, knowledge about the current carbon cycle can be applied to predict its evolution into the future. An example of a parameter inversion is the Carbon Cycle Data Assimilation System (CCDAS, Rayner et al., 2005), which is based

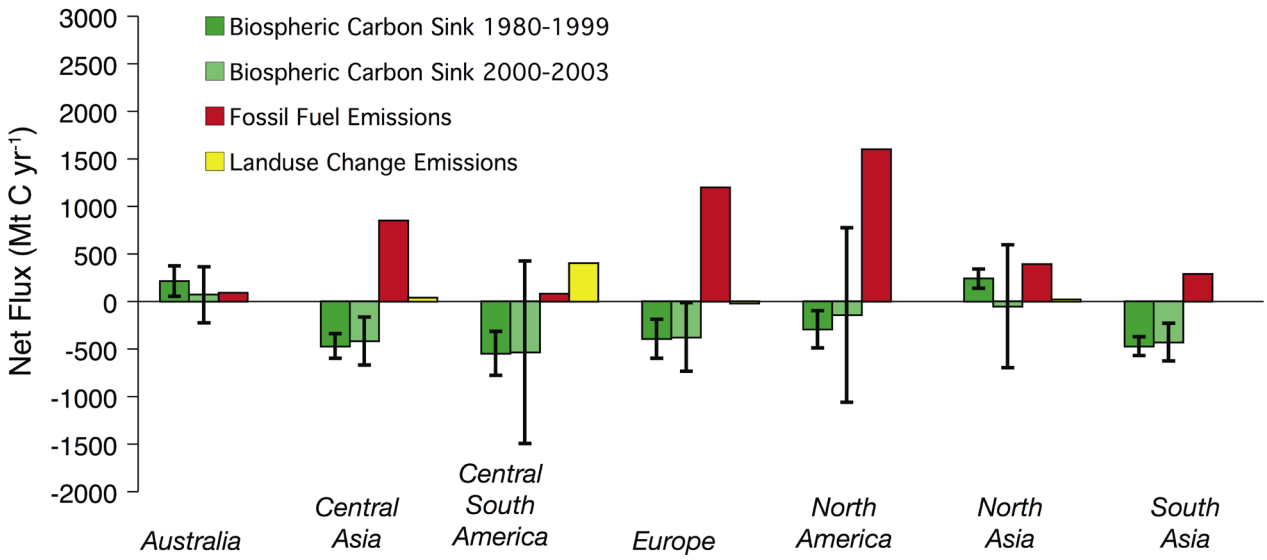


Figure 2.12: Terrestrial carbon uptake and associated uncertainties from 1979–1999 (assimilation period) and 2000–2003 (hindcasting period) for seven regions as estimated by CCDAS compared to fossil fuel and land use change emissions. [Credits: adapted from Scholze et al., 2007].

around a process-based, prognostic terrestrial biosphere model. Figure 2.12 shows the diagnosed and predicted (in this case 'hindcasted') long-term mean net carbon fluxes and their uncertainties over seven regions of the globe as an example of a CCDAS result (Scholze et al., 2007). There are, however, the same limitations for the existing parameter inversions as for the flux inversions: the constraint by the existing global flask sampling network is limited to about a dozen directions in parameter space (Rayner et al., 2005).

From an inverse modelling perspective, satellite missions, such as A-SCOPE, have the great advantage over surface measurements that global coverage can be obtained in several days. The large number of measurements and rather homogeneous measurement coverage has the potential to dramatically reduce the uncertainty of the $CO_2$ flux estimates at high spatial resolution in many parts of the world. Several Observation System Simulation Experiments (OSSEs) have been carried out to estimate the potential performance of space borne $CO_2$ observations (see Miller, 2007). These studies indicate that for instruments such as OCO and GOSAT, precisions of 1–10 ppm per single measurement should be sufficient to improve the uncertainty of current $CO_2$ source and sink estimates. Besides precision, however, observational biases are critical when introduced either by the instrument or – more importantly – by the retrieval. For passive satellite instruments operating in the short-wave infrared, such as SCIAMACHY, OCO and GOSAT, undetected cloud and aerosol layers are potential sources of important measurement bias. The impact of such biases on the performance of inversions strongly depends on their variation in time and space, but could already be detrimental to the estimated fluxes at the sub-ppm level. Instruments operating in the thermal infrared, such as AIRS and IASI, are less sensitive to aerosols, but have the important disadvantage that the measurements have a low sensitivity to $CO_2$ in the planetary boundary layer. The ability of flux inversions to constrain and resolve surface fluxes strongly improves with increasing measurement sensitivity to $CO_2$ at low altitudes, where

the concentration signals of the fluxes are largest. The A-SCOPE instrument concept compares favourably with any of the existing and planned $CO_2$ missions, since it combines a high sensitivity to the planetary boundary layer with a low impact of aerosols and clouds on the measurement accuracy.

### *2.3.3 Fundamental limitations at present*

In order to improve the ability to project the future evolution of atmospheric $CO_2$, and hence climate, an improved understanding of global $CO_2$ sources and sinks and the underlying processes is urgently needed. Inverse modelling is a powerful approach to reach that goal. However, its performance is currently limited by two factors: (i) measurement availability and (ii) the quality of the underlying models (for example, atmospheric transport, ocean and biosphere $CO_2$ exchange processes). As explained in the previous subsection, the coverage of the existing surface-monitoring networks is too low for the purpose of high resolution (a million square kilometres or better) inverse modelling of $CO_2$ sources and sinks. Expansion of the surface networks is not a realistic option, with the possible exception of a few highly developed regions on Earth. The monitoring of $CO_2$ from space is a highly promising alternative, but not well enough developed at present.

To take full advantage of a space-based $CO_2$ monitoring system, additional model development is needed. Transport model intercomparisons show a fairly consistent simulation of the large-scale dynamics. This can be explained by the fact that many models make use of meteorological fields derived from weather prediction models that are constrained by a network of meteorological observations that is dense enough to resolve the large-scale circulation. Much more uncertain, however, is the unresolved part of the atmospheric transport, including cumulus convection, turbulent mixing, and boundary layer dynamics. Further, it is known that the average residence time of stratospheric air is substantially underestimated in weather prediction models. This has implications for $CO_2$ as, for example, it increases the effective atmospheric volume into which the net annual emission is mixed. Therefore, the models are underestimating the actual $CO_2$ concentration. So far, transport models have mostly been validated using surface measurements. A recent development, however, is to use the expanding archives of aircraft measurements to evaluate the model performance in the free troposphere. In addition, the emerging Fourier Transform Spectrometer (FTS) and Total Carbon Column Observing Network (TCCON) allow initial verification of model-simulated total column $CO_2$, although the availability of high quality measurements is still limited and will have to be improved in the future. A-SCOPE will stimulate these activities and accelerate both future model development and the extension of the FTS network.

The most promising $CO_2$ flux monitoring system consists of various sources of both *in situ* and remote sensing measurements, each with their own strengths and weaknesses, to which A-SCOPE would make a key contribution. The combination of measurements from the various observational systems with models will provide a maximum constraint on the derived $CO_2$ fluxes and will allow verification of internal consistency, both of measurements and models.

## 2.4 Current and planned observational systems

### *2.4.1 Current surface networks*

Regular ground-based measurements of carbon dioxide in Mauna Loa started in 1958 (Figure 2.5). These began to show increasing levels of carbon dioxide in the atmosphere quite quickly. Since then, the number of sites making measurements of carbon dioxide and other trace gases has greatly increased, now numbering over 100 (Figure 2.13). Most of these sites contribute their results to the World Data Centre for Greenhouse Gases *(http://gaw.kishou.go.jp/wdcgg.html)* of the WMO's Global Atmosphere Watch (GAW), which coordinates quality control and centralised calibration facilities.

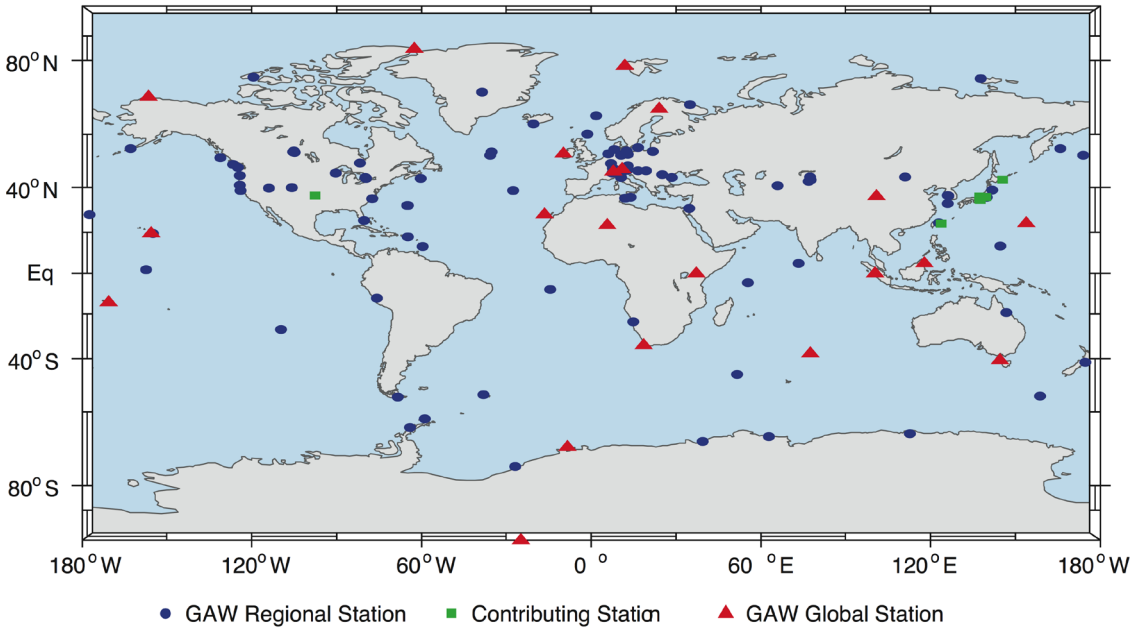


Figure 2.13: The locations of the surface stations measuring atmospheric $CO_2$ as of September 2008. The 24 GAW global stations are shown in red, while the regional and contributing stations are in blue and green respectively. [Credits: Image provided by the WMO/GAW Quality Assurance/Science Activity Centre (QA/SAC) at Empa, Switzerland, with permission]

The backbone of the GAW ground-based $CO_2$ measurement system is a network of 24 'global' stations. These key observatories are located at sites that are considered to provide good background values of atmospheric composition, often on small islands or continental mountains. Jungfraujoch in Switzerland and Danum Valley in Malaysia are the two most recent additions to this network. These stations are complemented by regional and contributing stations, which provide observations that are considered to be representative of a smaller geographical area. While most of these stations supply flask-based data on a weekly basis (Figure 2.14), the number of near-continuous measurement sites with *in situ* measurements of carbon dioxide is increasing. A map of all the sites that provide data to the GAW World Data Centre for Greenhouse Gases can be seen in Figure 2.13.

In addition to the ground-based measurement system, there are a number of tall tower sites around the globe, which provide *in situ* continuous measurements of

Figure 2.14: Summary of presently used sampling platforms and strategies for measuring atmospheric $CO_2$. Clockwise from bottom-left: Airborne sampling; Tall tower at Lamto, Ivory Coast; Observatory at the Pic du Midi, France; Flasks waiting for analysis; instrumentation for airborne continuous measurement; Flask semi-automatic analysis (center). [Credits: Francois-Marie Bréon, LSCE]

carbon dioxide and other trace gases at a variety of altitudes (Figure 2.14). These towers supply regionally representative measurements in the continental boundary layer. Seven of these towers are currently in operation in the US, run by NOAA's Earth System Research Laboratory *(ESRL – http://www.esrl.noaa.gov)*, and the network is currently expanding to 12. In Europe and Siberia there are another 6–8 sites operated by CarboEurope, and an expanded network is expected in the future as part of the construction of an Integrated Carbon Observing System, ICOS, in Europe *(http://icos-infrastructure.ipsl.jussieu.fr/)*.

Another ground-based measurement method is provided by the FTS, which allow for the measurement of the total column of carbon dioxide and other gases from the surface. There are few of these instruments worldwide at present: six are operational and five are in development *(http://www.tccon.caltech.edu)*. These high-precision instruments will provide a particularly useful tool for the calibration of satellite total-column measurements.

### *2.4.2 Airborne measurements*

Aircraft measurements, like tall towers, are important in that they provide information about the vertical distribution of trace gases in the atmosphere, though the use of aircraft allows these profiles to extend to much greater

altitudes. Many intensive but short time-scale field campaigns employ aircraft to make atmospheric measurements. However, for the purpose of carbon cycle modelling, measurements which span a longer time-scale are generally used. In order to reduce costs, many aircraft measurement sampling make use of the so-called platforms of opportunity provided by commercial aircraft. CARIBIC (*www.caribic-atmosphere.com*), which will be flying regularly until at least 2014, falls into this category. Similarly, Contrail *(http://www.jal-foundation.or.jp/html/shintaikikansokue/Contrail_index(E).htm,* a joint project between the JAL foundation and Japan Airlines, collected grab samples approximately twice monthly from April 1993 to December 2005 in the upper atmosphere between Australia and Japan. These samples were later analysed for trace gases, including carbon dioxide, methane, and carbon monoxide. In 2003 continuous $CO_2$-measuring equipment was installed on five aircraft, and observations are now being made worldwide.

Aside from those campaigns making use of commercial aircraft, some programmes make use of small aircraft on a regular basis (Figure 2.14). The most extensive of these is that of NOAA's ESRL, which carries out vertical profile measurements up to 8 km, of carbon dioxide, methane, ozone, and other trace gases several times per week at several North American sites. A similar, but smaller network is operated in Europe by the CarboEurope project.

### *2.4.3 Plans for surface network expansion*

Future expansion plans included in the WMO GAW Strategic Plan for the 2008–2015 period are more high-frequency measurements on the continents and more sampling stations, at high or low frequency, in the tropics, which are under-sampled at present. This plan also calls for more measurements of $CO_2$ vertical profiles through the use of both tall towers and aircraft, and the addition of atmospheric $CO_2$ measurements in the Ship of Opportunity Programme (SOOP) coordinated by JCOMM (the Joint WMO-IOC Technical Commission for Oceanography and Marine Meteorology).

The present surface network, or its planned expansion, is only very partially capable of resolving the time-evolving distribution of atmospheric $CO_2$. As a result, our ability to infer, by inverse methods, the spatial regional source/sink pattern is very limited using this sparse network. For example, the present network is insufficient to constrain whether large areas like North America or Eurasia are acting as sources or sinks for carbon from year-to-year with any uncertainty smaller than about 1 Pg C $yr^{-1}$, which corresponds to about a 100% uncertainty. The situation is even worse in the tropics, where the present network is largely blind for the large potential fluxes associated with deforestation and potentially enhanced growth in unperturbed tropical forests. Without a much more comprehensive coverage of atmospheric $CO_2$ measurements, further development and refinements of the methods used to infer sources and sinks are impossible, since the uncertainty cannot be easily assigned to transport model error, data error, or errors in the inversion procedures. Adding a few more ground-based stations here and there may help to better constrain fluxes within a few selected regions, but only a

revolutionary increase in the number of high-quality measurements will make it possible to infer the sources and sinks of $CO_2$ globally with much greater confidence than presently possible.

### *2.4.4 Satellite missions for $CO_2$ monitoring*

With the limitations of the surface or airborne $CO_2$ observation networks, it is natural to consider satellite capabilities. Even though satellite observation can probably not reach the level of accuracy provided by ***in situ*** sampling, this is likely to be compensated for by the huge number of observation, adequately distributed over the Earth. Indeed, OSSEs have shown that a satellite system could provide valuable information if the monitoring accuracy was better than about 1 ppm at the monthly 1000 km × 1000 km resolution.

There have been attempts to retrieve $CO_2$ concentration from current satellite measurements. Two remote sensing techniques may be applied with currently flying instruments: emission spectroscopy and absorption (solar) spectroscopy.

Emission spectroscopy uses high spectral-resolution measurements in the thermal infrared. These measurements are primarily used for temperature and water-vapour sounding for meteorological purposes. $CO_2$ concentration maps have been derived from TOVS and AIRS measurements. Similar fields are expected from IASI data. However, the concentration retrieved from these measurements is representative of the upper troposphere with very limited contribution from the mixing layer. It is then very difficult and highly uncertain to relate the measured concentration gradients to surface fluxes.

Absorption spectroscopy uses high spectral-resolution measurements of the sun light reflected by the Earth surface. The spectral absorption is related to the amount of absorbing material in the atmosphere which makes it possible to estimate its concentration. Measurements from SCIAMACHY have been used to estimate $CO_2$ column concentration with increasing success. Comparisons against FTIR show errors of the order of a few ppm. Although a random error of this order would be acceptable, there seems to be a large bias component in this error budget, so that the SCIAMACHY retrievals cannot be used reliably for $CO_2$ flux estimate. However SCIAMACHY had not been designed for the monitoring of $CO_2$.

Two missions are planned for launch in early 2009 that use the same broad concept as SCIAMACHY's, but with a focus on $CO_2$. These are the Orbital Carbon Observatory (OCO) scheduled for launch by NASA in January 2009 (*oco.jpl.nasa.gov*), and the Greenhouse gases Observation SATellite (GOSAT) (*www.gosat.nies.go.jp/index_e.html*) scheduled for launch by the Japanese space agency in early 2009. Both satellites fly on a polar orbit and carry a solar spectrometer to measure the depth of the $CO_2$ absorption lines which can be used to infer the $CO_2$ column density. In addition, GOSAT carries a thermal infrared spectrometer for day/night measurements of $CO_2$ concentrations, but with little sensitivity to the lower atmospheric layers. The mission documents suggest that the processing of OCO

and GOSAT observations will provide $CO_2$ column estimates with an accuracy of the order of 1 ppm. However, there are a number of hypothesis and limitations in these accuracy estimates, which raise some doubts that these goals are achievable. In addition, such accuracies have never been demonstrated from airborne campaigns. The main challenge faced by the passive instruments is their requirement to correct for atmospheric scattering, particularly by aerosols and clouds. This is needed as scattering changes the atmospheric path of the reflected sunlight, which must be known in order to correctly retrieve atmospheric $CO_2$. Observations in sun-glint mode make this challenge even larger, as the atmospheric path is even longer and may require substantially different correction for the downward and upward path of the photons. Scattering has a huge effect on the apparent $CO_2$ content, requiring corrections on up to several ppm in order to retrieve the *correct* $CO_2$ concentration. The measuring concept of OCO and GOSAT uses an $O_2$ absorption band as a proxy for the atmospheric path. However, because the $O_2$ and $CO_2$ absorption bands are far apart in wavelength, there are large uncertainties in the extrapolation of this proxy. As a result, the achievement of the stated accuracy will be a huge challenge for passive missions.

The A-SCOPE concept, thanks to its ranging capabilities, provides a direct measurement of the atmospheric path. It is therefore free from the main uncertainty of the OCO and GOSAT concept. In addition, it does not require the Sun as a light source, and can therefore provide both day and night measurements. It is argued, therefore, that A-SCOPE provides more extensive and much more reliable $CO_2$ concentration measurements than that of the passive missions.

## 2.5 A-SCOPE's observational system

### *2.5.1 Nature of the sampling*

Relative to the current surface-based network for atmospheric $CO_2$, A-SCOPE will increase the number of measurements by at least one order of magnitude. The majority of the current measurement stations sample the atmosphere every two weeks, resulting in about 5000 unique samples per year. Even if the increasing number of continuous sampling stations is taken into account, the current network produces less than 100 000 samples per year. In comparison, A-SCOPE will sample the atmosphere with about 100 000 unique observations in a single month (Figure 2.15). Even more importantly, these observations will be distributed globally, filling some of the large gaps in the current network, i.e. the regions in the tropics, subtropics, and some of the high-northern latitudes, where the current network is *blind* (Figure 2.13).

Furthermore, A-SCOPE will sample the atmosphere with a single instrument, while the surface network is based on a number of different instrumentations, requiring large efforts to ensure standardisation and an internally-consistent data set. The latter is extremely critical for $CO_2$ flux inversions, since the key information that enters these inversions are spatial and temporal gradients in atmospheric

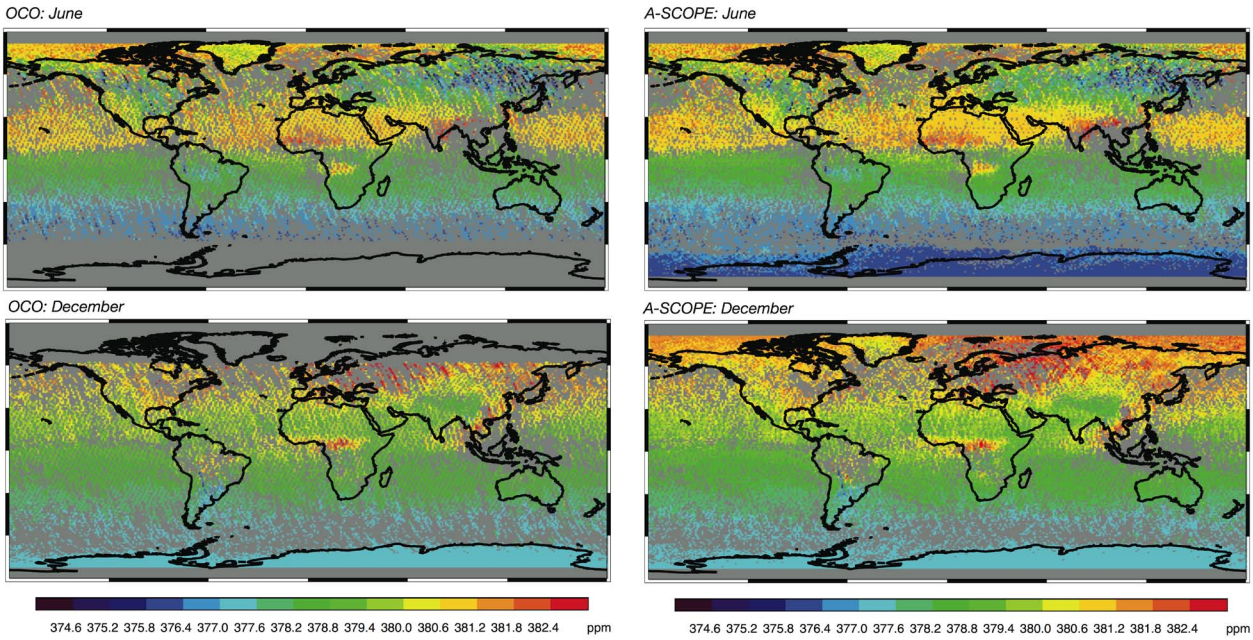


Figure 2.15: Expected sampling of the column averaged atmospheric $CO_2$ by OCO (first column) and A-SCOPE (second column) for the months of June and December. Relative to OCO, A-SCOPE will be able to provide high-accuracy atmospheric $CO_2$ data for all seasons and latitudes. Note in particular the absence of any observations by OCO in the high-latitudes of the winter hemisphere, leaving large gaps in the global distribution. A-SCOPE will also be able to resolve more detail in the spatial structure of atmospheric $CO_2$. The sampling shown for A-SCOPE can be considered as a lower-bound estimate, as the possibility for A-SCOPE to see through broken clouds has not yet been fully exploited. [Credits: Francois-Marie Bréon, LSCE, Sander Houweling, SRON]

$CO_2$ concentration, which are even more strongly affected by biases than the concentration itself.

Despite the large advancement that A-SCOPE provides relative to the existing network, the latter is regarded as very complimentary to A-SCOPE. This is because the backbone of the existing network, the NOAA-based stations, provide a consistent dataset with a level of accuracy and precision that is not achievable by A-SCOPE. A-SCOPE provides information about the column integral of $CO_2$ concentration, whereas the surface network provides information about the surface concentrations. Inversions with a combined A-SCOPE/surface network will outperform inversions with either of the two networks alone.

Relative to the planned satellite missions, i.e. OCO and GOSAT, A-SCOPE will provide an increase in the number of observations by a factor of two to three. There are several contributors to this increase:

- first, being an active system that does not have to rely on the presence of reflected sunlight, A-SCOPE can sample during the day and night, whereas the passive systems can only sample during the day,
- second, the passive systems can only reliably measure atmospheric $CO_2$ if the solar zenith angle is less than 70°, leading to large gaps in their sampling in latitudes polewards of 50 deg in winter time (Figure 2.15). Thus, large areas of

the globe will remain unsampled for several months each year. This is a serious limitation, particularly in the higher latitudes of the Northern Hemisphere, as these regions exhibit substantial fluxes during this period, as manifested by them having the largest seasonal variations in atmospheric $CO_2$ (Figure 2.9),

- third, with its small footprint of less than 100 m, A-SCOPE can take advantage of cloud holes that are too small for the substantially larger footprint of the passive instruments,
- fourth, the 6 am, 6 pm orbit will permit A-SCOPE to take advantage of the diurnal minimum in cloud cover, particularly in the tropics, where cloud cover increases by nearly a factor of two between 6AM and the early afternoon, when OCO is making its measurement,
- finally, the passive instruments are particularly sensitive to the presence of aerosols, leading to potentially large gaps in regions with relatively persistent high levels of aerosols, such as some tropical regions (e.g. India) or Southeast-Asia, i.e. in part exactly those regions, where the current *in situ* network is already very limited.

In contrast to the number of observations, there is little difference between the various observations systems with regard to the representativeness of their respective observations. For example, it makes little difference whether atmospheric $CO_2$ observations are obtained by scanning across a swath or along a single line or whether they are continuous or spot sampled. This is because the relatively strong transport and mixing in the atmosphere leads to relatively large correlation-length scales (> 100 km) for the column-weighted dry air mixing ratios of $CO_2$ so, that the majority of data within 50 km, along track or cross track, are highly correlated. In the atmospheric inversions used to estimate surface fluxes, such correlated measurements do not provide additional constraints. In contrast, any uncorrelated new measurement of atmospheric $CO_2$ will improve the estimation of the surface fluxes, irrespective of how and where it was sampled in space and time.

In summary, A-SCOPE is clearly superior to OCO and GOSAT in terms of its much better coverage and its more intense sampling, particularly in regions that are of crucial importance for characterising the global space-time distribution of atmospheric $CO_2$.

### *2.5.2 Nature of the data*

While A-SCOPE cannot compete with the *in situ* network with regard to the precision and accuracy, the stated target precision (0.5 ppm) and accuracy (0.05 ppm) are only a few times larger than the official WMO guidelines for *in situ* measurements. However, A-SCOPE has substantially higher precision and accuracy goals than GOSAT (stated precision of 4 ppm), and is very likely to exceed the precision and accuracy of OCO as well. OCO states a similar precision to A-SCOPE for measurements over land (0.5 ppm), but the precision over the ocean is much lower, i.e. 3 ppm (observations in the Sun-glint mode could improve upon this, though). In addition, these precisions are only achieved for high sun zenith-angles (more than 70°), while the random error for low solar zenith-angles is much higher.

While atmospheric $CO_2$ measurements made by A-SCOPE may only be marginally more *precise* than those made by OCO, they will likely be substantially more *accurate*. This is crucial for the objective of the mission, i.e. the determination of surface sources and sinks of $CO_2$, as the information that is being exploited to determine these sources and sinks by atmospheric inversion methods is the gradients in atmospheric $CO_2$. Thus any atmospheric $CO_2$ bias that varies in time and space and cannot accurately be accounted for will lead to biased flux estimates. Since the inversion is a global problem, all fluxes will become biased, making the detection of these biases extremely difficult.

OCO is expected to be substantially more prone to biases than A-SCOPE because its passive retrieval method makes it very sensitive to the presence of aerosols and thin clouds in the atmosphere. Under heavy aerosol loading, the inferred raw $CO_2$ concentration may need to be corrected by as much as 5 ppm, so that if there is only a 10% error in this correction, a bias of 0.5 ppm could exist in the retrieved atmospheric $CO_2$. Such a bias, if undetected, could cause flux biases of the order of 1 Pg C $yr^{-1}$, or an order of magnitude larger than the target for A-SCOPE. Another possible source of biases in OCO's observations is its need to switch between two modes of observations, i.e. nadir looking mode and sun-glint mode (over the ocean). Since the parameters of the retrievals are rather different for these two observational modes, there is a chance that a small, but persistent bias will emerge between the retrieved atmospheric $CO_2$ concentrations from these two modes. Again, a bias as small as 0.1 ppm, but persistent in time and/or space (for example, between land and ocean) could be sufficient for serious errors in the estimated fluxes. In comparison to OCO, A-SCOPE is exposed to much less risk of such biases, as it is insensitive to the presence of aerosols and because it uses a single observation mode.

In summary, A-SCOPE is the only mission currently planned that will make all-season, twice-daily, all-latitude, high-precision, high-accuracy measurements of atmospheric $CO_2$ concentrations from space. Thus, A-SCOPE is uniquely positioned to provide data that are urgently required to constrain atmospheric $CO_2$ inversion models to the level where real progress can be made regarding our ability to quantify and understand the global distribution of sources and sinks of $CO_2$ with confidence.

### *2.5.3 Expected improvement of source and sink estimation*

The goal of the A-SCOPE mission is to improve our ability to quantify sources and sinks of $CO_2$ at the Earth's surface by reducing the uncertainty from the present-level of a few tenths of a Pg C per year per continent (current surface network) to generally less than 0.02 Pg C per year per million square kilometres. In order to demonstrate this error reduction in detail, dedicated OSSEs have been performed using a state-of-the-art atmospheric $CO_2$ data assimilation system (for details, see Chapter 4).

Three atmospheric $CO_2$ observing systems considered:

- a surface-based network consisting of the current observing stations (Figure 2.13) and a modified one with the expected number of additional stations in about 2015,
- other existing or forthcoming space-borne instruments, primarily OCO (or GOSAT), and
- the A-SCOPE mission.

Figure 2.16 shows that the currently existing surface-based $CO_2$ measurement network is able to cause substantial (up to 60%) reductions in areas of good observational coverage, such as France and the U.S., but that the rest of the land areas remain largely unconstrained (error reduction of generally less than 10%). Clearly, without a very dense surface-based network it is not possible to properly constrain the fluxes everywhere.

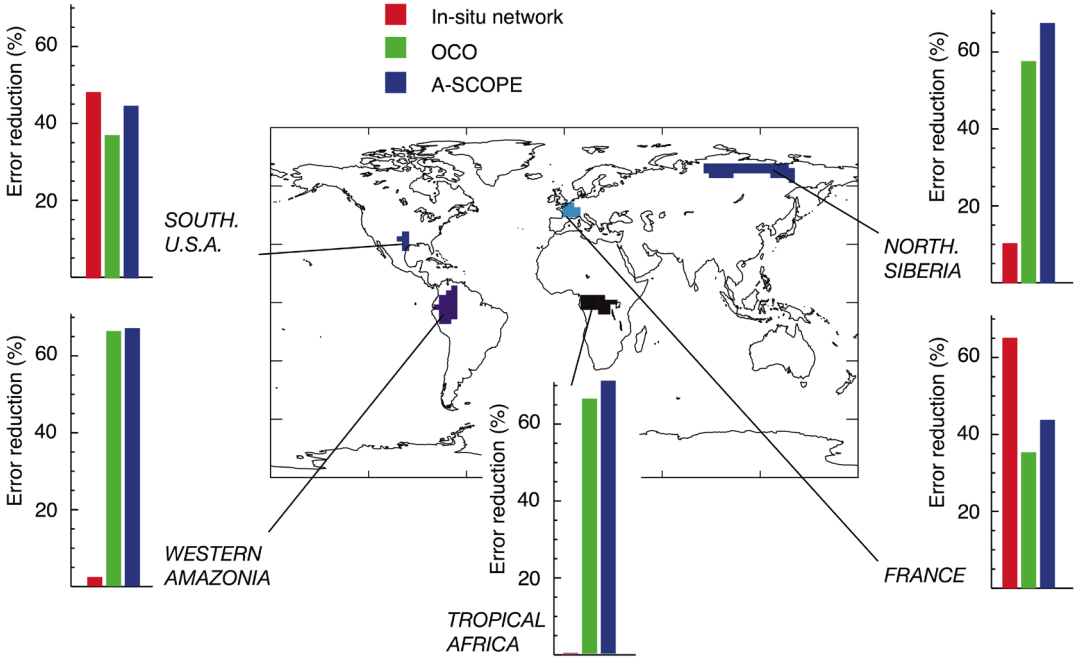


Figure 2.16: Additional benefit provided by A-SCOPE for constraining annual carbon fluxes for several, selected regions. The bars depict how much the data from the different observing systems are able to reduce the uncertainty of a prior flux estimate for a particular region. Shown are the relative reductions for the currently existing *in situ* network (red), for the planned OCO mission (green), and for the proposed A-SCOPE mission (blue). These results are obtained by an atmospheric data assimilation system as explained in more detail in chapter 4. It is important to note that all observations were assumed to be unbiased, whereas in reality, there is good reason to believe that OCO's measurements are at great risk to be biased. This is primarily because passive instruments need to correct for the influence of aerosols, which is very challenging. As a result, it can be expected that A-SCOPE will result in a larger reduction of the error relative to OCO than shown here. [Credits: Bréon, LSCE]

With the OCO observing system, the error reduction is 30 to 60% over most of the vegetated areas with much less variations between regions, thanks to the near-global coverage of OCO (Figure 2.15). However, there is a caveat: it is assumed

here that OCO's measurements are unbiased, while it had been shown before that OCO may be prone to biases because of its large sensitivity to undetected aerosols.

Thanks to its better coverage and its larger sensitivity to near-surface changes in atmospheric $CO_2$, A-SCOPE can provide an even larger error reduction than OCO. The additional benefit from active sensing is larger in the mid and high latitudes, and smaller in the tropics. There are two causes for this. First the higher near-surface sensitivity of A-SCOPE relative to OCO is not an advantage in the tropics, because the troposphere is relatively well mixed there. In contrast, the much more stratified troposphere in the mid- and high latitudes leads to stronger $CO_2$ variations near the ground, variations that A-SCOPE can detect better than OCO. The other reason is that A-SCOPE's active sensing provides observations at high latitudes in all seasons, while OCO is limited by the availability of sunlight. As a consequence, the high-latitude winter fluxes are poorly constrained by OCO, while A-SCOPE can provide important constraints during this period.

The additional benefit provided by A-SCOPE relative to OCO shown here is regarded to be a conservative minimum estimate. In reality, it is likely that the benefit will be larger. One reason is that the smaller footprint of A-SCOPE will permit more measurements under broken cloud conditions but that has not yet been included in the input studies. The second, and more important, reason, is that those OSSEs were undertaken under the assumption that all measurements were unbiased. With OCO being more prone to biases, and unknown biases representing a serious problem in atmospheric inversions, the error reduction provided by OCO is likely smaller than shown here, while A-SCOPE is expected to be largely unaffected by biases.

Although not yet investigated in the OSSE, it is expected that A-SCOPE will also provide additional benefits over the Southern Ocean. This region is globally one of the most important sink regions for anthropogenic $CO_2$ (Mikaloff Fletcher et al., 2006), and has been shown to respond rather sensitively to climate variations and change (e.g. Sarmiento et al., 1998; Lovenduski et al., 2008). In particular, there is mounting evidence that this region is already undergoing substantial changes in response to global climate change, having caused a reduction of its sink strength (LeQuéré et al., 2007). However, with the current surface-based observational network, this change is just at the edge of detection (see e.g. Law et al., 2008). *In situ* observations of the surface-ocean partial, pressure are preferable, but difficult and very expensive to obtain in the region, by necessity leading to large spatial and temporal gaps, particularly during wintertime. Not much improvement can be expected with OCO, due to its inability to observe atmospheric $CO_2$ over the Southern Ocean during austral winter. With its unique measurement capability during winter at high latitudes, A-SCOPE can be expected to provide the crucially needed atmospheric $CO_2$ observations that will permit us to assess the air-sea fluxes over the Southern Ocean and to determine how they are changing with time.

In summary, the OSSE simulations, as well as the theoretical arguments for the Southern Ocean, demonstrate that the A-SCOPE mission is poised to provide a big step forward in the ability to quantitatively determine the distribution and dynamics of the sources and sinks of carbon on a global scale.

### *2.5.4 Expected impact on process understanding*

Improved measurements of atmospheric $CO_2$ will also provide much needed constraints to improve the understanding of key global carbon-cycle processes, particularly on land. To demonstrate the large benefit of the A-SCOPE mission, an OSSE simulation with a process-based assimilation system was undertaken on the basis of the CCDAS (Rayner et al., 2005). The uncertainty reduction calculated by CCDAS for net $CO_2$ flux (net ecosystem production) and NPP, i.e. essentially the biomass increment, over Brazil, Europe and Russia are rather large: the posterior errors are between 98.5% and 99.3% smaller than their prior values which range between 0.45 Pg $Cy^{-1}$ for net ecosystem production over Europe and 4.9 Pg $Cy^{-1}$ for NPP over Brazil. Prior and posterior uncertainties are derived by propagating parametric uncertainties (prior and posterior, respectively, whereas posterior parameter uncertainties are derived by the assimilation method) onto diagnostic quantities. These large reductions are partly explained by the fact that CCDAS does not fully account for all uncertainties (for example, ocean $CO_2$ exchange fluxes are entering the calculation as prescribed background flux without any uncertainty assigned to them) and that its process formulations are assumed to be perfectly known except for the associated parameters, which are the quantities being optimised for.

Nevertheless, by employing a process-based model, CCDAS takes full advantage of the fact that the spatial and temporal variations of $CO_2$ fluxes are highly constrained by the underlying processes. Hence, information that is gained in one region has implications for fluxes in other regions with similar vegetation. The CCDAS approach has the potential to amplify the information content of the A-SCOPE measurements and thereby enhance its ability to quantify the exchange fluxes of $CO_2$. Of particular importance is the fact that the underlying optimised model can also be used for forward simulations in order to address the impact of future climate change on the global carbon cycle.

### *2.5.5 Expected impact on science and policy*

A-SCOPE can be expected to impact science and policy well beyond the determination of surface fluxes. Examples are the detection of biomass burning plumes and anthropogenic emissions from large cities and other hotspots. A-SCOPE will detect the ecosystem response to extreme climatological events, such as droughts and floods. The measurements will greatly stimulate scientific progress in the fields of atmospheric and carbon-cycle research, particularly in the areas of model development, interpretation, and verification of the data. Furthermore, high-precision $CO_2$ measurements provide a calibrated constraint on the $CO_2$ radiation fields used by satellite instruments to derive temperature profiles, which,

in turn, can improve the accuracy of numerical weather prediction, particularly when run in re-analysis mode.

Overall, A-SCOPE will greatly improve the understanding of the key processes that determine the exchange of $CO_2$ between the atmosphere, terrestrial biosphere and ocean. This will strengthen the ability to predict the feedback of the natural component of the carbon cycle to climate change and increasing $CO_2$ concentrations, which is needed to make reliable predictions of future $CO_2$ levels in support of the political decision-making. As such, A-SCOPE can make major contributions to the climate focus of the World Meteorological Organisation (WMO), namely the Global Climate Observing System (GCOS) and the International Global Observing System (IGOS). The mission will further contribute to the GEOSS initiatives directly by providing new global and reliable data on the spatial and temporal distribution of $CO_2$. The A-SCOPE observations contribute directly to GEO task EC-06-01, the support of an Integrated Carbon System.

On the policy level, the perhaps most important impact is the possibility to use A-SCOPE data for the verification of fossil fuel $CO_2$ emission reduction commitments, such as those currently negotiated under the UNFCCC for the post-Kyoto phase. For example, European mitigation measures aim to reduce national emissions by as much as 20% ($CO_2$ equivalent) by 2020. Recent G8 talks suggest even further reductions, up to 50%. Such drastic reductions are generally believed to be required to attain 'manageable' levels of climate change. Reduction strategies will increasingly involve the use of carbon markets, with considerable financial implications. Objective, unbiased, and independent verification of the compliance of countries with international treaties, as well as effectiveness of the implemented policy, will be of critical importance to all countries in the next few decades.

### *2.5.6 Ancillary benefits*

In addition to retrieving atmospheric $CO_2$, the A-SCOPE active-sensing system will also permit the retrieval of aerosol and cloud information, such as cloud height and cloud density. Although there are dedicated satellite missions to study these properties, the additional coverage that will be provided by the A-SCOPE mission permits a substantial extension of the study of the spatiotemporal dynamics of aerosols and clouds.

An active mission such as A-SCOPE can also provide estimates of the canopy height and vertical vegetation structure. Time series of canopy height can help to determine land use change activities such as deforestation and re-/afforestation, whereas information on the vertical vegetation structure can be linked to above-ground biomass. Both products would significantly enhance the value of the mission in terms of quantifying and understanding the global carbon cycle.

A third, ancillary benefit arising from the detailed knowledge of the atmospheric $CO_2$ concentration is improved retrievals of atmospheric temperature from satellites. It has

been shown that improved temperature soundings lead to substantial improvements in forecasted weather, as the current atmospheric temperature distribution is one of the most important determinants for the evolution of the weather over the following few days.

## 2.6 Uniqueness of A-SCOPE

Satellite-based measurements of the atmospheric $CO_2$ distribution are the only way to obtain the global coverage needed to solve for the sources and sinks on a global basis and with high regional resolution. While NASA's OCO and JAXA's GOSAT are expected to make a substantial step forward, it is recognised that an active $CO_2$ mission, such as A-SCOPE, is the only way to get truly global, all-season, twice-daily coverage under both clear and broken cloud conditions, and to obtain the scientifically desired accuracy and precision for atmospheric $CO_2$ retrievals.

A-SCOPE will exceed the currently existing surface-based network and the planned satellite missions with regard to the areas set out in the following paragraphs:

*Better sampling*

Relative to the current surface network, A-SCOPE will measure the atmosphere an order of magnitude more frequently and with a much higher spatial coverage (Figure 2.15 versus 2.13). Relative to OCO and GOSAT, A-SCOPE can make high-latitude measurements in winter time, can make measurements twice daily, and can make measurements under broken cloud conditions. It is expected that this will result in roughly three-times better coverage.

*Better data quality*

A-SCOPE will make atmospheric $CO_2$ measurements that are more precise and accurate than those of GOSAT and OCO. The main reason is that the passive measurement systems of OCO and GOSAT are prone to biases, particularly because of their high sensitivity to the presence of aerosols.

*Better surface fluxes*

Because of improved sampling and the better data quality provided by A-SCOPE it will be possible to reach the ambitious goal of being able to determine surface sources and sinks of $CO_2$ down to the required flux levels, to generally better than $\pm 0.02$ Pg C $yr^{-1}$ on an annual basis and over a region of 1000 km × 1000 km.

*Better process understanding*

The ability to constrain fluxes to that low level of uncertainty will permit the unprecedented study of the impact of variations in climate and weather on the land and ocean carbon cycle (for example, drought). In addition, the possibility to directly assimilate the high quality atmospheric $CO_2$ data into process-based carbon cycle models will permit much improved estimation of critical process parameters (for example, temperature dependency of soil respiration). Both approaches will substantially improve the assessment of the vulnerability of the global carbon-cycle to future climate change and other perturbations.

*Stronger policy impacts*

A benefit of the low level of uncertainty in the estimated fluxes is the possibility to constrain fossil-fuel emissions at a level that would permit the assessment of the compliance of countries with regard to their possible future reduction commitments.

*Ancillary benefits*

Relative to passive missions, the active measurement technique permits, without additional costs to the mission, the simultaneous determination of the atmospheric distribution of clouds and aerosols as well as the canopy height and the vertical distribution of the main terrestrial vegetation. Particularly the latter information is of great value for the development of a better process understanding of the terrestrial carbon cycle.

In summary, with A-SCOPE, carbon-cycle scientists can pave the way to determine the distribution and changes of the sources and sinks of $CO_2$ at the Earth's surface with an unprecedented accuracy. This will permit them to develop the understanding that is required in order to undertake reliable assessments of how the global carbon cycle and ultimately the Earth will change in the coming decades and centuries. With OCO and GOSAT about to be launched, A-SCOPE will be a second generation $CO_2$ mission, but one that is more likely to deliver the high quality observations needed to advance our understanding of the global carbon cycle to the next level.

# Chapter 3. Research Objectives

## 3.1 Introduction

The Earth Explorer A-SCOPE mission will fulfil the need for global and highly accurate carbon dioxide observations. These objectives are similar to those of the OCO and GOSAT missions but the coverage and accuracy provided by active remote sensing will allow a significant step forward in our understanding of the global carbon cycle. As such, the mission is addressing the challenges set out in the ESA Earth Observation Strategy (ESA, 2006), namely:

in terms of the *atmosphere* challenges

- to understand, model, and forecast atmospheric composition and air quality on adequate temporal and spatial scales, using ground-based and satellite data,
- to understand and quantify the natural variability and the human-induced changes in the Earth's climate system,

in terms of the *land* challenges

- to understand the role of terrestrial ecosystems and their interaction with other components of the Earth System for the exchange of water, carbon and energy, including the quantification of the ecological, atmospheric, chemical and anthropogenic processes that control these biochemical fluxes,
- to understand the effect of land-surface status on the terrestrial carbon cycle and its dynamics, by quantifying their control and feedback mechanisms for determining future trends,

and in terms of the *ocean* challenges

- to understand physical and bio-chemical air/sea interaction processes.

Indeed, although the A-SCOPE mission provides atmospheric observations, the quantitative analysis of its spatial and temporal gradients, using appropriate transport models, provides strong constraints for the monitoring of surface-atmosphere carbon fluxes, and therefore insight into biosphere dynamics.

## 3.2 The global carbon cycle and climate change

The overarching objectives of the A-SCOPE mission are an improved understanding and a better quantification of the global carbon cycle. The fundamental processes governing the exchange of carbon between the atmosphere, land, and ocean and their feedback mechanisms with the climate system are of paramount interest, so as to include them correctly and reliably in Earth System models. Such models are used to predict the rate of the greenhouse effect increase and climate change during the forthcoming centuries. Therefore, the A-SCOPE mission focuses on the current carbon cycle but is highly relevant for an improved prediction of the rate of

climate change. In addition, the understanding of vegetation dynamics, to which the A-SCOPE mission will contribute, will be needed to predict the fate of natural ecosystems in the context of such climate change.

A-SCOPE will meet these objectives by measuring the spatial and temporal gradients of atmospheric $CO_2$ with a precision and accuracy sufficient to constrain the $CO_2$ fluxes (sources and sinks) significantly better than with the current observation network or any forthcoming *in situ* or spaceborne observation systems.

More specifically, A-SCOPE will provide column-weighted dry-air mixing ratios of $CO_2$, referred to as $XCO_2$ in the following, over the satellite sub-track. Active sensing allows a global coverage not dependent on the availability of sunlight. Besides, the small footprint and the relative insensitivity to thin clouds will allow observations in tropical regions that are frequently cloud covered. The tropics are a key region for the global carbon cycle. These characteristics of the A-SCOPE mission will allow an unprecedented, true global, all-season, day-night, all-latitude coverage of the $CO_2$ concentration.

### 3.3 Surface fluxes and modelling

The A-SCOPE measurements, together with appropriate modelling and interpretative activities, will allow the constraining and further development of models of the terrestrial biosphere and of the oceans and thereby improve the projections of future trends in carbon sources and sinks. In addition, the mission will monitor the impact of large-scale climatic disturbances (such as El Niño) and other factors (such as forest fire, insect plagues or afforestation/deforestation) on regional carbon budgets. Such information is urgently needed, for example, for the development of optimal carbon mitigation strategies.

In most land areas, the current uncertainty on biospheric fluxes is much larger than that on fossil fuel emissions. Therefore, the objectives of the A-SCOPE mission primarily focus on the exchanges of $CO_2$ between the atmosphere and either land or oceans, rather than on fossil fuel emissions. Nevertheless, A-SCOPE will provide key data in the context of the international emission reduction agreements that may follow the Kyoto protocol. Indeed, specific human activities may be used to compensate the emissions due to fossil fuel burning, in particular through afforestation and novel agricultural practices. Accurate models of the long-term dynamics of soil-vegetation carbon storage are needed in this context. Such models will be a natural consequence of the scientific analysis of the data.

### 3.4 Emission inventories and protocols

In addition, A-SCOPE will provide key data to verify the consistency of anthropogenic emission inventories. Although the current uncertainties on fossil-fuel emissions in industrialised countries are too low to be significantly improved through spaceborne monitoring, the situation is different over the rest of the world. Indeed, there are considerable uncertainties on the $CO_2$ fluxes due to deforestation in the

tropical regions of America, Africa and Asia and due to local extraction and use of coal, for instance in China. Although the expected A-SCOPE mission cannot identify the anthropogenic contribution to the measured fluxes, it will certainly allow a consistency check on the emission inventories derived through bottom-up approaches and reported by the Kyoto protocol parties.

### 3.5 Conclusions

A-SCOPE will demonstrate the value of active remote sensing of carbon dioxide from space. As such, it will establish the basis for future missions of long duration, as required for the detection of trends. Indeed, large vegetation changes and associated carbon fluxes are expected during the 21st century as a response to climate change. Such changes can only be detected by long-term monitoring missions. A global and reliable monitoring of carbon fluxes will be essential in this context and A-SCOPE may be seen as a demonstration mission for this objective.

In conclusion, the Earth Explorer A-SCOPE mission is expected to provide key information for quantifying and understanding the global carbon cycle, and will open the way for a long-term monitoring of its evolution, which is the main driver of climate change

# Chapter 4. Observation Requirements

## 4.1 Introduction

This chapter defines and specifies the scientific mission requirements that are needed to fulfil the mission objectives as formulated in Chapter 3. In the following, it is assumed that the instrument will monitor $CO_2$ from space using an active optical technique. The primary data products of the A-SCOPE mission will be the column-weighted dry-air mixing ratio of $CO_2$ commonly referred to as $XCO_2$. Other geophysical quantities, referred to as spin-off products, comprise information on vegetation vertical distribution, on cloud and aerosol layers, and surface retro-reflectance.

The mission will have three levels of data products, defined as follows:

- Level 1a: data with all calibrations computed and appended, but not applied.
- Level 1b: data processed to Differential Absorption Optical Depth (DAOD) and Scattering Surface Elevation (SSE).
- Level 2: the geophysical data product $XCO_2$ and spin off products.
- Level 3: $CO_2$ fluxes at various spatial and temporal scales.

The Level 3 $CO_2$ flux is the parameter of prime scientific interest. The conversion of Level 2 to Level 3 involves inverse modelling using an atmospheric transport model. Several issues are being investigated, including the role of model uncertainties, model-data representation errors, and the question which set-up makes most efficient use of the data. It is expected that any $CO_2$ mission will, in the meantime, push model and assimilation technique development further. Therefore it has been chosen to formulate the observational requirements at Level 2, which more directly addresses instrument capability and performance than Level 3, and depends less on the modelling state of the art. Nevertheless, advantage is taken of the state of the art, because the Level 2 precision requirements are supported by inverse modelling experiments relating Level 2 and Level 3 statistical errors. These calculations consist of a series of OSSEs, simulating the impact of A-SCOPE measurements over a hypothetic range of instrument accuracy and measurement. OSSEs have been carried out as part of the scientific support studies for the mission (Ehret et al., 2005; Breon et al., 2008; Scholze et al., 2008).

This chapter is organised as follows: Section 4.2 discusses Level 3 target and threshold requirements, followed by a description of the procedure that was used to translate these requirements into Level 2 precision requirements (Section 4.3). Section 4.4 defines the observational requirements (Level 2) and their relation to the scientific scope and objectives of the mission as outlined in Chapters 2 and 3. Section 4.5 presents the observational requirements on the level of 'target' and 'threshold' for the primary data product. The working assumptions on the quality of required auxiliary input data are discussed in Section 4.6. Section 4.7 discusses optional additional requirement in support of the spin-off products. Finally,

Section 4.8 presents some results of performed OSSEs, illustrative of what would be the gain of A-SCOPE, given the specified observational requirements.

## 4.2 Target and threshold

The target and threshold observational requirements quantify the desired capabilities of the A-SCOPE mission to determine the sources and sinks of $CO_2$. The A-SCOPE performance level at 'target' and 'threshold' is based on the following considerations. The A-SCOPE mission objectives call for a significant improvement in the estimation of $CO_2$ fluxes in comparison with the expected performance on the basis of upcoming satellite missions and planned expansions of the surface measurement networks. The future development of inverse modelling will be towards higher spatial resolution. In Europe and the US, regional scale flux estimation is becoming feasible, which should be extended to the global domain using remote sensing techniques.

To improve our understanding of the global carbon budget will require accurate estimation of net annual fluxes. Estimation on the level of the driving processes using CCDAS is considered a promising future direction. Although the preferred time resolution for a specific process doesn't need to be annual, the annual timescale is nevertheless considered important. This is because the annual net fluxes are difficult to quantify by process modelling, whereas annual atmospheric concentration changes can be accurately observed and therefore provide powerful constraints. It is recognised that A-SCOPE will provide essential information on the carbon-cycle feedback to climatic anomalies, such as droughts, acting on sub-annual time scales. Nevertheless the annual time scale, which also reflects the impact of major weather anomalies, is preferred for the purpose of requirement definition.

Guided by these considerations, the A-SCOPE target requirement has been defined as the performance that is needed to quantify the sources and sinks of $CO_2$ on an annual timescale and a spatial scale of 1000 km × 1000 km within an uncertainty of 0.02 Pg C $yr^{-1}$, (i.e. 20 gC $m^{-2}$ $yr^{-1}$), or about 20% of the present-day uncertainty level. Threshold requirements correspond to the level at which A-SCOPE will deliver $CO_2$ measurements from space at a higher quality than any other existing or planned mission.

## 4.3 Translation of flux uncertainty to $XCO_2$ precision

OSSEs have been carried out to translate the required accuracy of the A-SCOPE estimated $CO_2$ surface fluxes, as defined in Section 4.2, into the Level 2 required precision of $XCO_2$ (Ehret et al., 2005). This procedure requires the specification of prior flux errors for each region, which are determined on the basis of the argument that the uncertainty scales with the magnitude of the fluxes, for which the heterotrophic respiration flux has been used as a proxy on land. The spatial and temporal correlations of these fluxes were defined by consensus among carbon-cycle experts and based upon the scientific literature. One year of synthetic

measurements was generated by 'flying' a conceptual A-SCOPE instrument over the domain of a global atmospheric transport model, sampling the model according to the instrument and orbit specifications accounting for cloud cover. Only cloud-free measurements were retained.

Several inverse modelling calculations have been carried out at a horizontal resolution of 8° × 10° (approximately 1000 km × 1000 km) for A-SCOPE measurement precisions ranging between 0.1 and 5 ppm. The instrument performance is quantified by averaging the annually integrated uncertainties of the inversion-derived posterior fluxes over land. A schematic overview of this procedure is shown in Figure 4.1. By varying the measurement precision a relationship is obtained between flux uncertainty and measurement precision. The intersection of this function with Level 3 flux uncertainty requirements yields corresponding Level 2 requirements on $XCO_2$ measurement precision. For more detailed information on these synthetic experiments see Ehret et al. (2005).

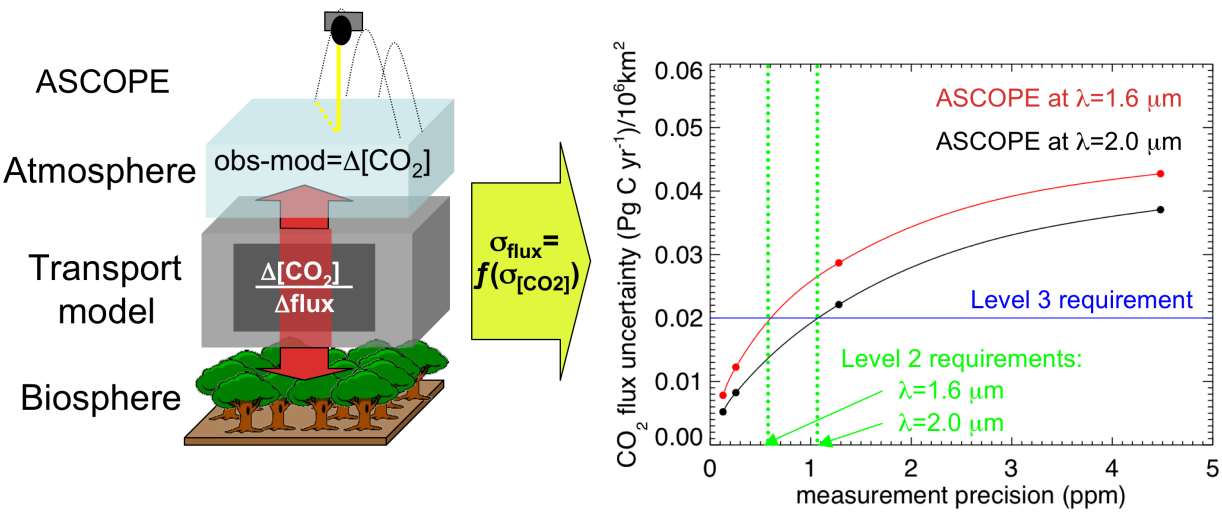


Figure 4.1: Schematic outline of the procedure to translate observation requirements on the accuracy of A-SCOPE derived $CO_2$ fluxes (Level 3) into precision requirements for $XCO_2$ (Level 2). The left side of the plot represents the inversion methodology, from which a relationship is obtained between the Level 2 and Level 3 uncertainties. This relationship is plotted on the right hand side for two wavelengths. The inferred requirements refer to the target precision for a uniform weighting function (typical for a measurement at λ=1.6μm) and for a weighting function that scales about linearly with pressure (typical for a measurement at λ=2.0μm). [Credits: Sander Houweling, SRON]

## 4.4 Requirement Definition

The quality of the $CO_2$ source and sink estimates, as derived from $XCO_2$ measurements through atmospheric transport inversion, is determined by measurement uncertainty, data density, and the sensitivity of the measurements to spatially and temporally separated sources and sinks. In addition, the ability to characterise and monitor in-flight data quality will require regular passes over several sites of the ground-based validation network (see Section 2.4.1). Besides a large number of high quality measurements, the capability to quantify sources and

sinks also depends on the quality of the models, i.e. atmospheric transport models and process-based models of sources and sinks that are used to translate observed $CO_2$ concentrations into flux estimates. This section, however, does not explicitly formulate model requirements, other than the basic requirement that the model quality should not limit the overall performance. It is assumed that future model development will keep up with improved measurement capabilities. For A-SCOPE the following observational requirements are considered.

### *4.4.1 Accuracy and precision*

The precision of the measurements directly impacts on the precision of the derived source and sink estimates. Synthetic model simulations have been carried out to determine this relationship, given measurement density and sensitivity, which led to the precision requirements listed in Section 4.5. Furthermore, synthetic model simulations show that measurement biases could significantly impact the retrieved sources and sinks. However, the magnitude of this impact is very much dependent on the spatial and temporal patterns of the bias. A global and constant bias has no impact, as only the gradients are linked to sources and sinks. However, for example, a bias that varies along the orbit would introduce artificial latitudinal $CO_2$ gradients, which could have a detrimental impact on the inversion-derived fluxes. On the other hand, biases that are highly localised in space and time can be interpreted as random errors, rather than biases. An important strength of satellite instruments, in comparison with surface measurements, is their capability to generate a large number of measurements, turning the inverse problem of source and sink estimation from an underdetermined problem into an overdetermined problem. The collective constraint of the measurements on the fluxes can only be effective if the individual measurements contribute largely independent pieces of information. In practice, this means that the level of systematic error (bias) should be substantially below that of precision.

### *4.4.2 Vertical sensitivity*

The signals of $CO_2$ sources and sinks are strongest near the Earth's surface, and, therefore, the effectiveness of $CO_2$ concentration measurements increases with increased sensitivity near the surface and, in particular, within the planetary boundary layer.

### *4.4.3 Coverage*

The estimation of sources and sinks benefits from a rather homogeneous measurement coverage in time and space in order to reduce sampling biases. Of specific interest are measurements over ecosystems that are poorly detected by the existing surface measurement network, such as tropical and boreal forests. In practice, the measurement coverage is limited by the overpass positions and frequency, and the presence of clouds.

### *4.4.4 Resolution*

The footprint size of the A-SCOPE measurements is not critical, to the extent that the typical horizontal resolution of active measurements is higher than any of the models that are used to interpret the data. However, horizontal measurement resolution is important in relation to measurement density and (homogeneous) coverage, since a small footprint substantially increases the number of cloud-free measurements.

### *4.4.5 Ranging capabilities*

The ranging capability of A-SCOPE directly influences its skill in determining the column length. Indeed, the measurement of $XCO_2$ using an active technique requires the knowledge of the pressure of the reflecting surface, which is derived from its elevation together with meteorological data. In addition, the ranging capability of an active technique opens the possibility of measuring vegetation structure information as a byproduct by interpreting the returned signal waveform.

### *4.4.6 Timeliness*

In the context of A-SCOPE, timeliness is defined as the timespan between measurement collection and the availability of corresponding Level 2 data. It should be realised, however, that the processing from Level 2 to Level 3 depends on the availability of meteorological fields and ***a priori*** emissions, which limits the timeliness of the scientific interpretation of the A-SCOPE measurements.

## 4.5 Observational requirements for $XCO_2$

Table 4.1 summarises the mission requirements for the primary data product, $XCO_2$. The random and systematic error requirements refer to a single observation, which is defined as an aggregation of individual (single shot) lidar soundings, usually referred to as an observation, along a distance of 50 km. Generally, the random and systematic error requirements depend on the sensitivity of the measurements to the $CO_2$ mixing ratio in the planetary boundary layer, as expressed by the vertical weighting function. The random and systematic error requirements as specified in Table 4.1 apply to a pressure-independent vertical weighting function, i.e. each $CO_2$ molecule in the vertical column receives equal weight. For an alternative (pressure dependent) weighting function, the corresponding precision requirement can be derived from Table 4.1, assuming an inverse relationship between precision and near-surface sensitivity. Surface sensitivity increased by a factor of two implies a relaxation of the precision by a factor of two and vice versa. Similarly, the mission simulations have assumed a near-polar orbit, with sampling continuously along the satellite sub-track. For a measurement configuration reaching global coverage with a significantly different number of observations, the precision requirement scales approximately with the square root of the number of observations.

| Parameter | Target | Threshold |
|---|---|---|
| Geophysical data product | $XCO_2$ | |
| Random error[1] | 0.5 ppm | 1.5 ppm |
| Systematic error | 0.05 ppm | 0.15 ppm |
| Coverage | Global | Global |
| Horizontal resolution:<br>Observation<br>Individual measurement | <br>50 km<br>< 100 m | <br>50 km<br>< 100 m |
| Vertical resolution | Total column | Total column |
| Local overpass time | 6 am/6 pm | 6 am/6 pm |
| Absolute accuracy of scattering surface elevation | 3 m | 10 m |
| Timeliness | 1 month | 1 month |

Table 4.1: Observational Requirements for the Primary Data Product.

[1] Assuming altitude independence of the measurement sensitivity to a $CO_2$ molecule.

The systematic error requirements in Table 4.1 refer to the sum of all systematic errors that cannot be corrected, for example by theoretical considerations or ground-based validation, and give rise to erroneous spatial and temporal variations in $XCO_2$ that are highly unpredictable. This includes non-random residual errors that remain after correction for any known source of systematic error. In the event that the spatio-temporal variation of a specific source of systematic error can be characterised, the potential impact of such an error on inversion-derived sources and sinks can be assessed, which may lead to a relaxation of the uncertainty requirement for that specific term in the error budget.

The horizontal resolution of 50 km corresponds to the spatial resolution of $CO_2$ source and sink estimation through inverse modelling that will be feasible when the mission is in operation. For small study domains even higher resolutions of the transport model may be used. However, the A-SCOPE mission target ranges from regional, i.e. several million square kilometres, to global. A footprint smaller than 100 m is needed to limit surface height variations within the field of view, to reduce the probability of cloud contamination, and to enable observation in broken cloud conditions. The coverage should be global, including the oceans and high latitudes, throughout the year. The local overpass time has been set to 6 am/6 pm, which corresponds to the maximum and the minimum of the $CO_2$ diurnal cycle in most land regions during the photosynthesis season. Besides offering the possibility of observing the full amplitude of the diurnal cycle from space, this is expected to facilitate the comparison of measurements and model simulations. The specified ranging capabilities expressed as 'Scattering Surface Elevation (SSE)' are needed to determine the local air mass with sufficient precision to meet the precision requirement for $XCO_2$. The threshold requirement of 10 m introduces an error of up to 1‰ (1 hPa) in the estimate of local surface pressure. The target requirement of 3 m would permit the full neglection of this contribution to the overall error budget, see also Section 4.6.

At least several years of data will be needed to obtain information on trends and inter-annual variations of $CO_2$ sources and sinks. The minimum required mission duration is set to three years, excluding commissioning. The timeliness requirement of one month will guarantee that the delivery of Level 2 data does not delay the processing to Level 3, since the availability of the meteorological fields and prior emission estimates that are needed in this processing step typically lag behind by several months. The application of A-SCOPE $CO_2$ measurements to numerical weather prediction does not target the actual forecast, but rather the post processing and re-evaluation of meteorological analyses ('re-analysis'), which do not require measurement availability in near real time.

## 4.6 Auxiliary data

Auxiliary data refers to external data that are essential to derive geophysical data products (Level 2) from raw (Level 0) measurement data. Such data would typically be provided by meteorological forecasting centres like the European Centre for Medium-range Weather Forecasting (ECMWF). Table 4.2 summarises the assumptions that were made regarding quality of the available data. The numbers refer to the vertical profile at the locations (and scale) of the A-SCOPE measurements and reflect the level of accuracy that is needed to avoid being the target performance of the instrument being limited by the quality of the auxiliary data.

| Parameter | Uncertainty[1] |
|---|---|
| Temperature | 1 K |
| Surface pressure | 1 hPa |
| Specific humidity | 10%[2] |

Table 4.2: Assumed Quality of Auxiliary Data.

[1] At the time and location of the observation.

[2] Since the atmospheric water vapour content is highly variable, the required accuracy is expressed as a percentage of the specific humidity (see text).

Auxiliary data are needed at several stages in the data processing as summarised below:

- *Absorption cross section:* The calculation of absorption cross sections requires information on the vertical profiles of temperature, water vapour and surface pressure. The spectroscopic implications of auxiliary data availability are discussed in Chapter 5.
- *Air mass factor:* The calculation of $XCO_2$ requires knowledge of the surface pressure at a reference altitude and of the water vapour column. The local surface pressure, at the exact location of the measurements, is derived from numerical weather prediction (NWP) archived surface pressure after correction for the difference between local surface elevation (as measured by A-SCOPE) and the elevation from NWP orography. This elevation difference is translated into a pressure difference using the hydrostatic equation and the NWP-derived vertical temperature profile. Finally, information on the water vapour column is needed to account for the contribution of water vapour to surface pressure.

The requirement on specific humidity corresponds to 1–2 g/kg for worse case conditions, encountered near the surface in the tropics. Even under these conditions, the contribution of the water vapour column to surface pressure remains within a margin of 1 ‰ (1 hPa).

The requirements listed in Table 4.2 have been compared with the current performance of NWP models, in particular the meteorological data that is made available by Météo France and ECMWF as part of A-SCOPE scientific support studies (see Figure 4.2 for surface pressure and e.g. Uppala et al. (2005) for temperature and humidity). It is concluded that the quality of the available auxiliary data should not limit the overall performance of A-SCOPE (Loth *et al*, 2005; Breon *et al*, 2008). Note that this conclusion holds for present-day data availability. A further improvement of the auxiliary data quality is expected when A-SCOPE is in orbit and operating.

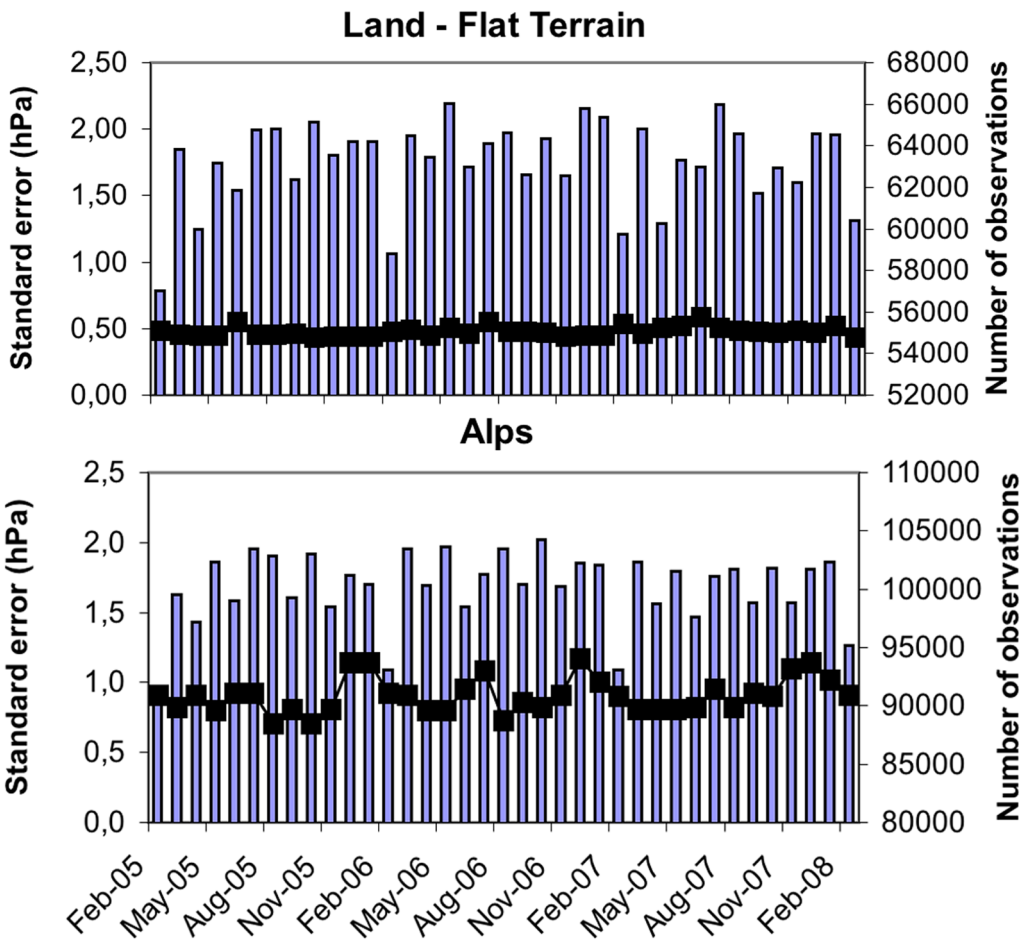


Figure 4.2: Monthly statistics of the difference between ARPÈGE/Météo France surface pressure forecasts and surface measurements for flat (top) and mountainous (bottom) terrain. The squares show the standard deviation of the difference between model and measurements (left-hand scale), while the bars are the number of measurements (right-hand scale). [Credits: Loth et al, 2005]

The atmospheric transport inversion, which translates the observed $CO_2$ concentration gradients into surface fluxes, is based on meteorological fields from numerical weather analysis, in particular wind vectors, temperature, and water

vapour profiles. These are routinely used in similar applications and should not cause specific difficulties for the A-SCOPE mission.

## 4.7 Spin-off products

Since the A-SCOPE mission will have a ranging capability, this can be used to measure vertical distributions of any scattering surface along the sub-satellite track. Clouds are a good example, for which Cloud-Aerosol Lidar and Infrared Pathfinder Satellite Observation (CALIPSO) has already demonstrated the usefulness of lidar measurements. For the detection of cloud and aerosol layers, a vertical resolution of 100 m is sufficient. More challenging, is to measure vegetation vertical distribution. Since vegetation is distributed over the first few meters, a ranging resolution of 1 m would be needed to resolve the main vegetation elements.

Compared with the primary data product, the spin-off products introduce few additional requirements on ranging capability, summarised in Table 4.3. However, it has to be emphasised that these requirements are not formal instrument requirements of the A-SCOPE mission. The requirements should be regarded as optional, in the sense that they would add valuable functionality, but they should not compromise the performance of the instrument in meeting the requirements for the primary product, or drive the cost of the mission.

| Parameter | Target | Threshold |
|---|---|---|
| Geophysical data product | Vegetation vertical distribution | |
| Surface return sampling (0–100 m)[1] | 1 m | 3 m |
| Geophysical data product | Cloud and aerosol layers | |
| Atmospheric return sampling (0 m–20 km)[1] | 20 m | 100 m |

Table 4.3: Observational Requirements for Spin-off Data Products.

[1] The number in parenthesis specifies the distance from a reference orography to which the ranging capability requirement applies.

As mentioned above, to detect the vegetation vertical distribution the ranging capability should be sufficient to resolve the main structural elements of vegetation. However, such a high vertical resolution is only needed within a rather shallow surface layer (0–100 m altitude). In contrast, to measure cloud and aerosol layers the vertical resolution needs to be of the order of 20–100 m. However, in this case measurements should be recorded from the surface up to the lowermost stratosphere, i.e. 0–20 km.

## 4.8 Performance simulations

The expected benefits of A-SCOPE for $CO_2$ surface-flux determination can be expressed in various ways. Several methods exist to infer information on $CO_2$ sources and sinks from the satellite measurements. The methodology that was used to relate the Level 3 to Level 2 requirements (see Figure 4.1) represents a specific choice. The choice has been to take the annual flux over $10^6$ $km^2$ of the terrestrial

biosphere, the main focus of A-SCOPE, as a benchmark. For this purpose a matrix inversion technique was used, that has the advantage that it explicitly calculates the full posterior covariance matrix, which is used to integrate the uncertainties annually. The disadvantage, however, is that it can only handle rather coarse spatial resolution.

Other inverse modelling methods, such as the variational approach, allow A-SCOPE performance estimation at higher resolution. Figure 4.3 demonstrates the level of uncertainty reduction that is gained for weekly fluxes at 4° × 3° resolution. The results demonstrate that also at this scale, a considerable uncertainty reduction will be achieved, in particular over regions such as Siberia and tropical forests, that are considered crucial in our ability to study the global carbon cycle. The results in Figure 4.3 suggest that the uncertainty improvement over the oceans remains limited. However, this is explained in part by a preliminary treatment of the *a priori* ocean flux uncertainties, which does not take into account the substantial difference in uncertainty between high and low latitudes. A more realistic treatment of these uncertainties is expected to increase A-SCOPE performance in the Arctic and Southern Oceans.

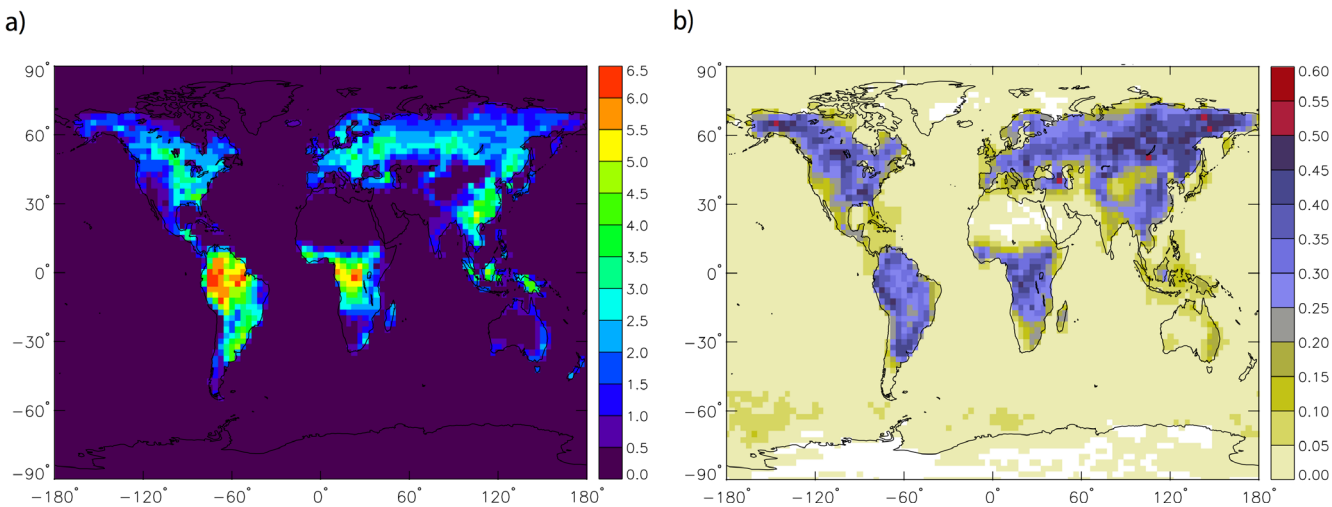


Figure 4.3: *A priori* assumed flux uncertainties in gC $m^{-2}$ $day^{-1}$ (left panel) and the estimated reduction in the $CO_2$ surface flux uncertainty gained by inverse modelling of A-SCOPE measurements (right panel). The uncertainty reductions represent the level of improvement as a fraction of the initial uncertainty (a value of 1 corresponds to the theoretical case in which a flux is determined without any remaining uncertainty). The uncertainty reductions refer to the 8-day mean flux and are derived from a flux inversion using a variational approach. [Credits: Bréon et al., 2008]

Even more desirable than surface flux estimation is the use of A-SCOPE to directly improve our understanding of the carbon cycle. Estimation on the process level is the primary focus of the CCDAS technique. Figure 4.4 presents the CCDAS performance as a function of A-SCOPE measurement precision. Besides obtaining information on the net $CO_2$ flux, we also gain information on the various processes regulating the terrestrial component of the carbon cycle. For example, Figure 4.4 shows the estimated uncertainty in the NPP, i.e. the photosynthetic biomass increment, an important component of the net flux. Note that the continental scale uncertainties are rather small in comparison with the results shown in Figure 4.1.

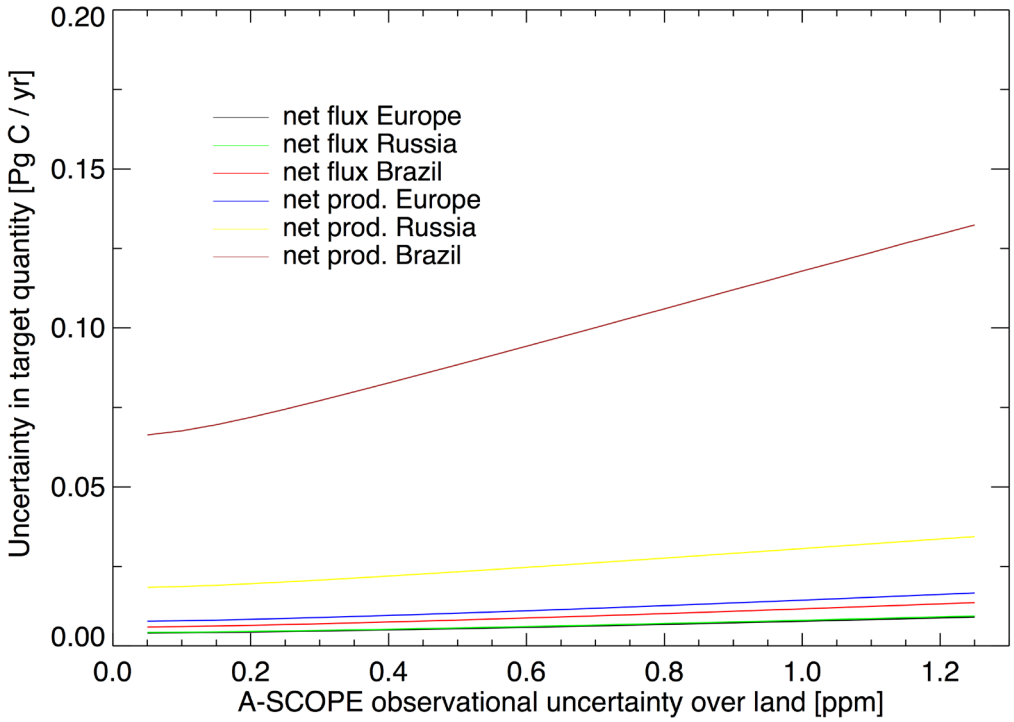


Figure 4.4: Model estimated uncertainty in the net $CO_2$ surface flux ('net flux') and NPP ('net prod.') as functions of the A-SCOPE measurements precision. The uncertainties refer to the annual uncertainty over selected large regions (Europe, Russia and Brazil) and are derived from CCDAS. [Credits: Scholze et al., 2008]

This is explained in part by the fact that CCDAS is under development and is at a stage which doesn't allow all prior uncertainties to be fully accounted for. However, CCDAS can already take full advantage of the fact that the spatial and temporal variations of $CO_2$ fluxes are highly constrained by the underlying processes. Because of this, for example, information that is gained in one location has implications for fluxes elsewhere. Hence, the CCDAS approach has the potential to amplify the information content of the A-SCOPE measurements and thereby enhance its ability to quantify the surface fluxes of $CO_2$.

## 4.9 Conclusions

In this chapter, the observational requirements at Level 2 have been specified based on Level 3 product requirements, i.e. $CO_2$ fluxes. Needs for auxiliary data enabling geophysical retrieval have been identified. This has been complemented by first performance simulations illustrating the potential of the mission for providing observations of unique quality.

# Chapter 5. The Mission Elements

## 5.1. Introduction

As already introduced in Chapter 3, the main geophysical product provided by the A-SCOPE mission will be $XCO_2$. As a novel feature, A-SCOPE will have its own light source emitting pulsed narrow-line laser radiation, not relying on sunlight. The $XCO_2$ values will be provided by a lidar technique with no bias due to particle-scattering in the light path, which can have strong regional variability. Using a range-gated receiver for detection of the signals scattered from the Earth surface, A-SCOPE can distinguish surface from cloud or aerosol backscatter, permitting high-precision retrievals of $XCO_2$ in the presence of particle layers with small/moderate optical depth, such as thin cirrus or aerosols (for example, from megacity plumes, desert, biomass burning). In the presence of clouds, the A-SCOPE measurement approach is capable of providing measurements in partially cloudy conditions. The lidar beam can reach the surface when gaps between clouds occur due to the near-nadir view and the small lidar footprint. A-SCOPE can also provide $XCO_2$ measurements above dense stratiform clouds, to be used as a reflective target instead of a surface target.

The A-SCOPE mission will provide a unique dataset with sampling twice daily and with all-season and all-latitude coverage. While building on OCO and GOSAT, A-SCOPE provides these unique attributes with respect to passive $CO_2$ monitoring missions that will significantly improve $CO_2$ flux estimates and enable new high-latitude carbon-cycle investigations. To meet the observational requirements outlined in Chapter 4, the A-SCOPE mission will have two main segments:

- a space segment, including as a main component a $CO_2$ Integrated Path Differential Absorption (IPDA) measurement system, to be used to perform measurements of $XCO_2$, as well as additional products as stated below,
- a ground segment for data processing and delivery to climate modelling centres as well as various research groups.

Outputs from NWP models will provide auxiliary data to be used in the processing of A-SCOPE data. This chapter outlines the proposed A-SCOPE Earth Explorer mission elements. The envisaged implementation concept for the segments of the mission is described in more detail in Chapter 6.

## 5.2 Space segment

The core element of the A-SCOPE mission is a quasi nadir-viewing $CO_2$ IPDA lidar system, which represents both a selective and sensitive method for measuring the number of $CO_2$ molecules in the path. This is shown schematically in Figure 5.1. The Earth's surface provides the return (backscattered) signals at two, namely 'on-line' and 'off-line', transmitted wavelengths denoted as $\lambda_{on}$ and $\lambda_{off}$, respectively. In principle, the IPDA technique is based on comparing the attenuation throughout the atmosphere of the two laser pulses at on-line and off-line wavelengths.

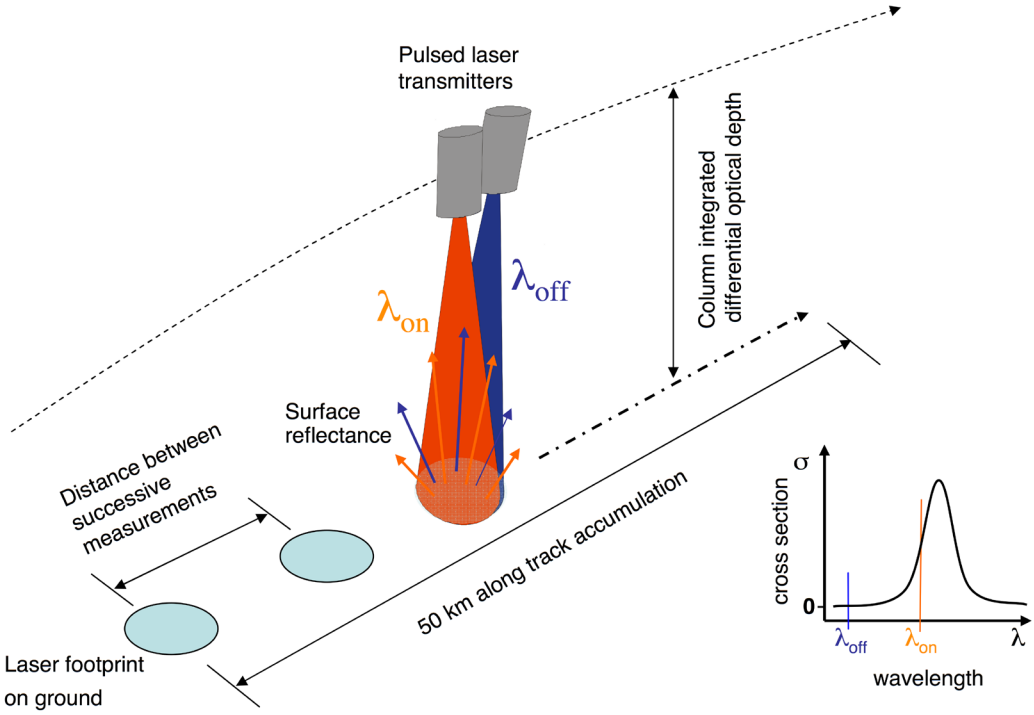


Figure 5.1: Principle of Integrated Path Differential Absorption (IPDA) measurement using surface targets. The integrated column extends from the surface to the top of the atmosphere. The light beam transmitted by on-orbit pulsed laser is scattered by the surface. The scattered light is collected by an on-orbit receiver telescope on the same platform. The figure represents 2 beams corresponding to the two laser pulses which encounter the same target on ground. The 50-km along track accumulation makes one 'observation'. Such along track accumulation is necessary to reach sufficient signal to noise ratio before processing. The insert shows schematically the shape of the molecular absorption cross section $\sigma$ as function of the wavelength $\lambda$ for a $CO_2$ absorption line in the near-infrared (NIR) spectral region (1.6 or 2 μm). Maximum absorption occurs at line centre. On-line setting in the wing of the $CO_2$ absorption line is marked by the vertical line in orange, off-line setting with negligible absorption is indicated by the blue line. The differential absorption cross section $\Delta\sigma$ is given by the difference in cross section for $\lambda_{on}$ and $\lambda_{off}$. [Credits: Ehret, DLR-IAP]

Accordingly, the IPDA technique does not require absolute radiometric calibration, in contrast to atmospheric backscatter lidars such as LITE (Winker et al., 1996) or CALIPSO (Winker et al., 2007). Considering two probing wavelengths only, the on-line wavelength is tuned to a specific offset from the centre of a selected carbon-dioxide absorption-line. The off-line wavelength is selected to be free from any other gas absorption. The on and off wavelengths are spectrally close enough to consider the atmospheric and surface properties to be identical with the exception of $CO_2$ absorption. Because the $CO_2$ line is pressure broadened throughout the entire troposphere, a significant detuning of the on-line wavelength with respect to the $CO_2$ absorption line centre permits the placing of a higher weight on the contributions from the lower troposphere.

### *5.2.1 Observational principle*

The IPDA lidar instrument introduced above will transmit alternatively two laser pulses which have slightly different wavelengths. Therefore, $XCO_2$ can directly be

calculated from the ratio of the two lidar signals $P_{off}$ and $P_{on}$ (see Figure 5.1) using the following equation:

Eq. 5.1
$$XCO_2 \equiv \frac{\int_0^{Psurf} w(p)\, WF(p)\, dp}{\int_0^{Psurf} WF(p)\, dp} = \frac{ln \frac{P_{off}}{P_{on}}}{2 \int_0^{Psurf} WF(p)\, dp}$$

$p$ denotes the atmospheric pressure, $p_{surf}$ is the surface pressure, $w(p)$ is the dry air $CO_2$ volume mixing ratio profile, and

Eq. 5.2
$$WF(p) = \frac{\sigma_{on}(p) - \sigma_{off}(p)}{\left(1 + \frac{M_{H2O}}{M_{air}} \rho_{H2O}(p)\right) \cdot g \cdot M_{air}}$$

$WF(p)$ is the weighting function under humid air conditions where

- $M_{H_2O}$, $M_{air}$ denote the molecular masses of water vapour and dry air molecules, respectively,
- $\rho_{H_2O}$ is the dry air volume mixing ratio of water vapour (number of water vapour molecules divided by the number of air molecules without water molecules),
- $g$ is the acceleration of gravity, and
- $\sigma_{on}$ - $\sigma_{off}$ is the differential absorption cross section for the selected wavelength pair that is a function of pressure (see Figure 5.1).

Absorption lines for $XCO_2$ retrievals are carefully selected in the NIR domain around 1.6 µm and 2 µm based on weak temperature dependency and negligible or small interference from any other gaseous species (Loth et al., 2005; Ehret et al., 2008). In order to favour the lower troposphere and planetary boundary-layer, soundings in the line wing corresponding to a weighting function peaking near the surface are preferred (see Figures 5.2 and 5.3).

In principle, the weighting function $WF(p)$ defined above (Equation 5.2) and shown in Figure 5.2 is at a particular pressure proportional to the contribution of a $CO_2$ molecule to the total measured Differential Absorption Optical Depth (DAOD). Using Equation 5.1, DAOD can be defined by

Eq. 5.3
$$DAOD \equiv \frac{ln \frac{P_{off}}{P_{on}}}{2}$$

which shows the direct link of DAOD to the measurement process inherent in the IPDA lidar observational principle. DAOD is proportional to the differential absorption cross-section ($\Delta\sigma = \sigma_{on} - \sigma_{off}$) displayed in Figures 5.1 and 5.3. For a uniform vertical-mixing ratio, the relative contribution of each layer of $CO_2$ molecules of geometrical thickness dz to the total DAOD can be obtained from multiplying the weighting functions depicted in Figure 5.2 by the atmospheric density profile.

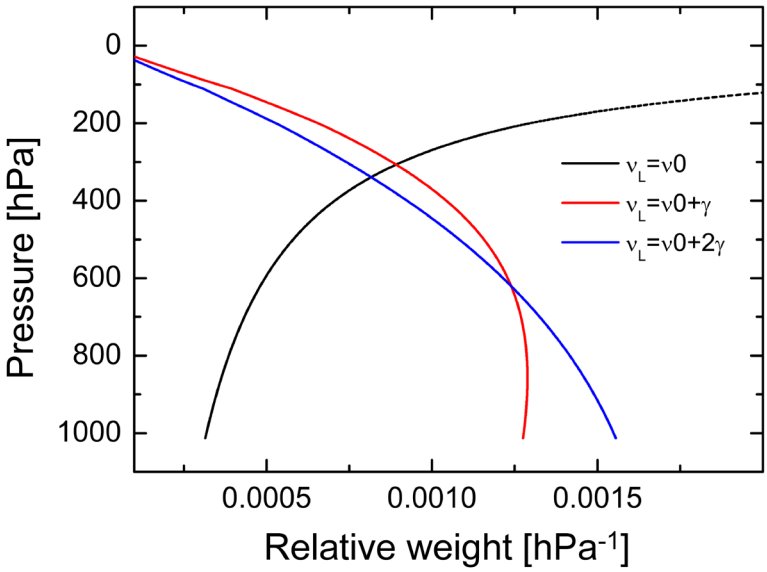


Figure 5.2: Relative weight of the $^{12}C^{16}O_2$ greenhouse gas column content as a function of pressure levels for three different on-line laser frequency positions ($\nu_L$) with respect to absorption line centre $\nu_0$ as indicated in Fig. 5.3. [Credits: Ehret et al., 2008, © Springer Publishing]

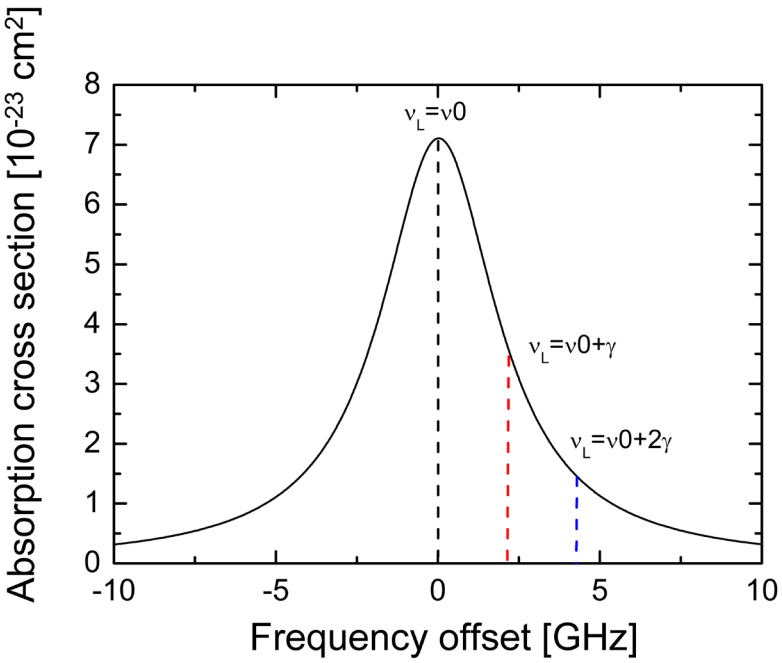


Figure 5.3: $^{12}C^{16}O_2$ molecule absorption cross section of line B1 (see Chapter 6) from $22^01$-$00^00$ band of $CO_2$ around 6348 $cm^{-1}$(1.57μm) as function of frequency detuning from line centre $\nu_0$ = 0 for T = 288 K and p = 1013 hPa. The dashed lines indicate the laser frequency detuning off line-centre in units of the collisional half-width $\gamma$. When the pressure decreases with altitude, $\gamma$ decreases and the line narrows. [Credits: Ehret et al., 2008, © Springer Publishing]

The observational requirements on $XCO_2$ entail very precise and bias-free measurements of DAOD. Possible errors emerging either from instrumental noise and platform pointing (see Chapter 6) or from uncertainties in the knowledge of the geophysical parameters (see Chapter 4) have to be taken into account when

defining the measurement requirements on DAOD. In the analysis, it is assumed that there is a rather equal share between the two error budgets (instrumental and geophysical). In addition, the relative contribution of the boundary layer, depending on the shape of *WF (p)* (see Figure 5.2), is considered in the definition of the overall error budget, which is formulated in Chapter 4 for a uniform *WF (p)*. As a result, the required measurement precision on DAOD is 0.074% for soundings at 1.57 µm and 0.15% for measurements at 2.05 µm, in order to meet the target requirement for the random error on $XCO_2$ (Bréon et al., 2007). To fulfil the systematic error requirement, these values have to be divided by a factor of 10. For the threshold requirements, the given error margins can be relaxed. Table 5.1 shows that the expected impact on the derivation of $XCO_2$ from uncertainty in the geophysical parameters, namely surface pressure, temperature and humidity, can be kept small. Thanks to the more favourable weighting function for soundings in the 2.05 µm spectral region, the error margins can be relaxed by a factor of two, as noted above. This helps to compensate for the increased sensitivity to surface-pressure uncertainty at those wavelengths.

| Parameter | Random error (RMS) [ppm] | | Uncertainty, assumption |
|---|---|---|---|
| | **Line B1 (1.57 µm)** | **Line B2 (2.05 µm)** | |
| Surface pressure | 0.26 | 0.62 | 1 hPa |
| Temperature | 0.07 | 0.17 | ARPÉGE error covariance matrix |
| Humidity | 0.10 | 0.12 | ARPÉGE error covariance matrix |
| **Total** | **0.29** | **0.65** | **Geometrically added** |

Table 5.1: Expected impact on the random error performance of A-SCOPE observations for the selected lines B1 and B2 (see Chapter 6) due to uncertainties in the geophysical parameters (Bréon et al, 2008). Error correlations of the Action de Recherche Petite Echelle Grande Echelle (ARPÉGE) climate model of Météo-France have been used.

### *5.2.2 Ancillary data requirement*

The determination of $XCO_2$ and *WF(p)* using Equations 5.1 and 5.2 will make use of an accurate knowledge of several key variables such as:

- Spectroscopic $^{12}C^{16}O_2$ absorption-line parameter-data are required for the determination of the absorption cross-section (see Equation 5.2), as well as information on possible interferences with other gaseous species including $CO_2$ isotopes. Information on this data will be obtained from existing databases, and on-going state-of-the-art spectroscopic measurements conducted in support of the OCO mission. If necessary, future studies will be conducted in support of A-SCOPE for the $CO_2$ absorption-line to be used for the lidar measurement;
- Meteorological variables i.e. surface pressure, temperature, and water-vapour profiles for the calculation of the absorption cross-section, see Equation 5.2. As discussed in Chapter 4, these data, required for the $XCO_2$ retrieval, will be provided by NWP models.

Two dedicated studies (Loth et al., 2005; Bréon et al., 2007) as well as a recent publication (Ehret et al., 2008) state the accuracy to which the relevant

absorption-line parameters will be needed to fulfil the measurement requirement for A-SCOPE. They specify a relative accuracy of 0.1% for air pressure broadening, 1% for air pressure-induced shift, and 0.5% for the temperature-scaling coefficient, which is not available from the latest version of the reference database HITRAN. To close this gap in view of OCO and A-SCOPE measurement accuracy requirements, the remote sensing community has already started to build a new database for the most relevant $CO_2$ lines in the NIR. These studies include determination of accurate data on line-centre position, line strength, line width, temperature-scaling exponent, and air-pressure induced line-shifts (Toth et al., 2008; Régalia-Jarlot et al., 2006; Joly et al., 2007). They also show that sophisticated parameterisation for the line shape, which is beyond the conventional Voigt profile-approximation, enables a better description of the spectral dependence of the absorption cross-section as function of the atmospheric parameters, as indicated in Equation 5.2.

## 5.3 Ground segment

The ground segment concept will include receiving stations located at mid-latitudes. Data will be processed by scientific centres and/or research institutes. Processed data shall be archived for a period of at least 10 years. Data processing includes the retrieval of:

(i) the $XCO_2$ data product, as well as flux inversion as the mission's main objective;

(ii) vegetation canopy height, vertical structure and metrics;

(iii) cloud/aerosol distribution and boundaries;

(iv) surface retro-reflectance.

Data processing includes the correction for systematic errors in the $XCO_2$ product, using ancillary instrument and spacecraft data. The latter 3 items, i.e. (ii) to (iv), are considered as mission spin-off products, so their processing is not discussed here.

## 5.4. Processing requirements for $XCO_2$

Starting from Level 1b, as detailed in Chapter 6, the following processing has to be performed to deliver Level 2 data products:

- calculation of the weighting function $WF(p)$ using the ancillary data described above (see Equation 5.2);
- calculation of $XCO_2$ using DAOD and $WF(p)$ (see Equation 5.1);
- quality control, for example, checking for consistency of the sequential values, including assessments of atmospheric-scattering effects, surface elevation and reflectance variability;

- calculation of the quality weight for the $XCO_2$ product using statistical properties for the variances of DAOD and *WF(p)*;
- calculation of the quality-weighted $XCO_2$ product at the observation level;
- correction for systematic errors in the $XCO_2$ product.

The Level 2 data sets will be used for flux-inversion investigations. The conversion of Level 2 to Level 3 involves inverse modelling using atmospheric-transport models. The latter step will be performed by the scientific end-user community as noted in Chapter 4.

## 5.5 Validation

An important activity of this mission will be the validation of $XCO_2$, which is the primary data product of the A-SCOPE mission. The observations shall be compared to temporally and spatially coincident measurements performed by independent instrumentation from various platforms, i.e. ground-based, aircraft, ship, balloon, at a variety of locations. A validation program shall be established by a group of scientists who have experience in ground-based and airborne $CO_2$ measurements, and representativeness issues. Campaign-mode observations of several continental-scale projects such as CarboEurope and the North American Carbon Project have shown how to determine representativeness errors at the regional scale. Such experimental campaigns, coupled to modelling efforts, are very valuable as validation tools for A-SCOPE observations. The validation exercise undertaken during the first year after launch will consider the full suite of high-accuracy and reliable techniques used for $CO_2$ measurements, including flask samples, *in situ* sensors, and remote sensors. Examples of the latter being pulsed Differential Absorption Lidar (DIAL) (Koch et al., 2004; Gibert et al., 2006), Laser Absorption Spectrometer (LAS) (Menzies and Spiers, 2008), and Fast Fourier Transform Infrared Radiometer (FTIR) (Yang et al., 2002; Washenfelder, 2006).

A-SCOPE provides total column content $XCO_2$ which is very difficult to measure with *in situ* sensors. An important validation component for A-SCOPE could be the already existing FTIR network used for OCO. Ground-based FTIR-sensors are able to verify the total column measurement from space with very high precision using the Sun as the radiation source (Washenfelder et al., 2006). The caveat is that these sensors will provide only daytime validation, thus it might be difficult to get true-coincident observations due to the envisaged 6AM-6PM orbit. DIAL instruments, in connection with appropriate modelling activities for the total $CO_2$ column, are considered to complement the FTIR network. They can operate during both day and night and could provide spatially and temporally coincident measurements to the satellite overpasses. The lidar community at various locations in Europe, the USA, and in Japan has already started to build-up new, ground-based and airborne $CO_2$ DIAL instruments operating in the 1.6 µm and 2 µm spectral regions (see Section 5.9).

As an example, the measurement of the troposphere $CO_2$ column-content by a ground based, pulsed 2-µm DIAL instrument has already been performed

using high-altitude dense clouds as targets (Gibert et al., 2008c). Recent field measurements using ground-based pulsed 2-µm or pulsed 1.57-µm DIAL instruments and various *in situ* sensors have shown good agreement (Gibert *et al*., 2008a, Amediek et al., 2008) and successfully address the representativeness issue between sensors (DIAL, *in situ*) at the same site or about 5 km apart (Gibert *et al*., 2008b). Ground-based DIAL operating in the NIR relies on aerosol content in the lower troposphere, especially in the Atmospheric Boundary Layer (ABL). Most of the $CO_2$ concentration variability is in the lower atmosphere.

## 5.6 Additional geophysical products

Various additional products can be derived from the observations of the A-SCOPE mission. A good example is the recent NASA's ICESat mission (Abshire et al., 2005; Schultz et al., 2005). This sensor was primarily designed for an accurate topography-ranging application, but also provided atmospheric data.

### *5.6.1 Canopy height and vertical structure*

As one spin-off product, A-SCOPE will provide estimates of the vegetation vertical structure and its temporal dynamics, with a view to obtaining reliable extra constraints on the location and extent of land-use change, especially deforestation and re-/afforestation activities. Estimates of the vegetation vertical structure also have the potential to improve knowledge of terrestrial above-ground biomass growth and its dynamics, because there is a direct and increasingly understood statistical relationship to above-ground carbon storage. Measuring above-ground tree biomass is, among others, a key observation for understanding terrestrial carbon cycling. Precise knowledge of the location and extent of forest disturbance and regrowth is an essential step towards a better quantification of the terrestrial carbon cycle and its impact on atmospheric $CO_2$ concentration. Deforestation represents a major source of $CO_2$ to the atmosphere whereas forest regrowth is a considerable sink of $CO_2$.

Satellite laser altimetry has a unique capability for estimating forest canopy-height and vertical structure (Lefsky et al., 2005; Boudreau et al., 2008). The off-line channel of A-SCOPE will be used to profile the structure of the canopy with a vertical resolution of about 1 m and a footprint of less than 100 m. The determination of forest height has been shown to be feasible from airborne lidar and can serve as an input parameter to estimate forest biomass, which is the most important forest structural parameter. As an example, a study has been conducted in Germany at the test site 'Nationalpark Bayerischer Wald' in a mountainous region ranging from 750–1130 m above sea level that consists of three major forest zones dominated by Norway spruce (Aulinger et al., 2005). The study concluded that the data from the lidar and the SARs are complementary and synergistic in estimating forest biomass.

ICESat waveforms were combined with ancillary topography from the Shuttle Radar Topography Mission (Lefsky et al., 2005) to estimate maximum forest height in

three ecosystems: tropical broadleaf forests in Brazil, temperate broadleaf forests in Tennessee, and temperate needle leaf forests in Oregon. This preliminary study shows that ICESat-derived maximum canopy heights for the Brazilian plots are quite well correlated with field estimates of above-ground biomass (correlation coefficient of about 0.73). In a subsequent study (Boudreau et al., 2008), airborne canopy lidar and ICESat waveforms were combined with a Landsat Enhanced Thematic Mapper Plus (ETM+) land-cover map, and a Shuttle Radar Topography Mission digital elevation model. These studies and all previous and on-going works conducted by the canopy lidar community paved the way for space applications.

### *5.6.2 Cloud boundaries and elevated aerosol layer*

A-SCOPE will have the capability to detect cloud boundaries, including cloud base for small to moderate cloud optical thickness (≤ 1). LITE, ICEsat and CALIPSO data are currently used for cloud-climatology studies. Their data are being used to derive cloud physical and statistical properties (Spinhirne et al., 2005; Wylie et al., 2007; Berthier et al., 2008). A-SCOPE will be one of a number of anticipated next-generation lidar missions that will add to cloud-climatology studies.

The A-SCOPE capabilities are sufficient to measure the vertical profiles of mineral-dust layers from Asian or African source regions, as well as biomass or forest fire aerosol layers as they are transported over large distances from the source regions. Airborne lidar observations of Asian dust layers extending several hundred km over the Pacific were reported by Spinhirne et al. (1997) and Menzies et al. (2002). From these observations it can be concluded that A-SCOPE's sensitivity will be sufficient to detect such layers during typical springtime dust-outbreak events (Liu et al., 2008a; Liu et al., 2008b; Uno et al., 2008). Examples of desert dust-outbreaks have been studied using the CALIPSO data since mid-2006 (Generoso et al., 2008).

The A-SCOPE sensitivity to aerosol backscatter enables detection of elevated aerosol layers associated with major forest fires and other biomass burning activities on spatial scales that provide plume-boundary information. An example is provided by the ICESat team observing a plume associated with a series of forest and brush fires in Southern California that burned an area of over 2750 $km^2$ in 2003 (Hoff et al., 2005).

### *5.6.3 Surface retro-reflectance*

With radiometric calibration of the A-SCOPE off-line channel, surface retro-reflectance values will be provided with a footprint of lower than 100 m. In-flight radiometric calibration over sites with well-characterised reflectance properties is convenient for comparison with lidar theoretical models, in order to assess lidar performance. The lidar retro-reflectance includes the hot-spot enhancement factor that applies to the broader angular reflectance normally observed using passive radiometers or imaging spectrometers. As noted in Bréon et al. (2002), observations of the hot-spot enhancement is of interest in remote

sensing of vegetation canopies. The A-SCOPE 1.6 or 2 µm wavelength observations supplement the shorter wavelength observations of POLDER (670 and 865 nm channels) and similar future solar-reflectance spectro-radiometers.

## 5.7 Summary of A-SCOPE geophysical products

The basic geophysical product is $XCO_2$ above the Earth's surface and, when possible, above dense cloud tops. Spin-off products will include vegetation canopy-height and structure, cloud boundaries, and elevated aerosol layers. Radiometric calibration of the A-SCOPE lidar will result in additional surface retro-reflectance measurements in clear-sky cases. Surface elevation with reference to geoid models will be provided as a Level 1b product. Table 5.2 provides a summary of the geophysical products that are expected from the A-SCOPE mission.

| Product | Mission objective | Comment | Remarks |
|---|---|---|---|
| Column-weighted dry-air mixing ratio of $CO_2$ ($XCO_2$) | Primary | It drives the A-SCOPE mission specifications and lidar instrument specifications | Ancillary data are required from NWP models:<br>• Surface pressure<br>• Temperature profile<br>• Water vapour profile<br>Accurate geoid models |
| Vegetation canopy height and metrics | spin-off | Compatible with high vertical resolution required for $CO_2$ total column | Accurate terrain numerical models (in addition to geoid models) |
| Elevated particle layers (detection, layer height, optical depth)<br>• Clouds<br>• Desert dust<br>• Biomass burning aerosols | spin-off | Availability depending on signal strength | Lidar radiometric calibration<br>Climatology of backscatter-to-extinction ration to derive optical depths |
| Surface retro-reflectance | spin-off | Available in clear-sky cases | Lidar radiometric calibration |

Table 5.2: Summary of A-SCOPE geophysical products.

## 5.8 Relation with other missions

The A-SCOPE mission can make major contributions to the GCOS and the IGOS. On the other hand, the Global Observing System (GOS) will provide auxiliary data to be used in the processing and monitoring of A-SCOPE data. The mission will benefit from/to all GOS system elements and environmental monitoring systems such as the Global Environmental Measurement System (GEMS).

A-SCOPE will be the first mission dedicated to the measurement of carbon dioxide with an active differential-absorption sensor. It will provide both continuity and enhancement of capability over missions currently being prepared for launch, i.e. NASA's OCO and JAXA's GOSAT. While these missions will represent a major step forward in our ability to determine the global-scale atmospheric $CO_2$ distributions, it is recognised that the limited coverage and the uncertainty and sampling biases

inherent in passive sensing will pose significant limitations on those missions. Only an active $CO_2$ mission has the capability to provide high-accuracy measurements combined with global, day/night coverage under both clear and broken cloud conditions. Thus, the A-SCOPE mission, as a second generation carbon mission, will provide new insight into carbon cycle aspects not accessible to existing and soon-to-be-launched missions i.e. SCIAMACHY, AIRS, IASI, OCO and GOSAT.

Simultaneous measurements of $CO_2$, aerosols, and clouds from this mission will provide continuity in key observations of EarthCARE data-products that can be assimilated into future operational environmental-monitoring systems such as GEMS.

A-SCOPE has triggered discussions in the international scientific community, leading to the refinement of mission objectives, and in the lidar community to the definition of instrument concepts, retrieval techniques and lidar specifications. Today, two missions, ASCENDS for column-integrated $CO_2$ mixing ratio and DESDynI for vegetation structure using a laser altimeter in combination with an L-band InSAR, are under discussion in the US for launch in the timeframe 2010–2016 as a result of the Decadal Survey (National Research Council, 2007).

## 5.9 Proof of concept

The methodology of DIAL for remote sensing of atmospheric trace-gases such as ozone or water vapour is mature as it has been developed and evaluated by many groups around the world (Schotland, 1974; Remsberg and Gordley, 1978; Mégie and Menzies, 1980). Regarding $CO_2$ measurement by DIAL techniques, several groups have developed different instruments that consider either the 1.6 or the 2.0 µm spectral domain, various pulsed or continuous-wave laser emissions, and direct or heterodyne detection. Table 5.3 provides an overview of recent progress in $CO_2$ DIAL.

Among the main results obtained today, the slope technique using range-resolved $CO_2$ measurements with an overall measurement precision error < 1% in the ABL have been demonstrated by Koch et al. (2004), and recent measurements in absolute value with high accuracy have been reported by Gilbert et al. (2006). Comparisons against various *in situ* sensors show agreement within a few percent (Gibert et al., 2008b; Koch et al., 2008; Amediek et al., 2008). Figure 5.4 displays i) the experimental site at École Polytechnique, 20 km south of Paris (France), where a 2 µm DIAL is deployed for $CO_2$ horizontal measurements in the ABL (Gilbert et al., 2006) and troposphere $CO_2$ column using high-altitude dense cloud (~ 6 km) as a hard target (Gibert et al., 2008c), ii) a facility 1.2 km away equipped with $CO_2$ and CO *in situ* sensors (laser diode spectrometer, LICOR[1] flasks), and iii) a research laboratory 5 km away conducting routine $CO_2$ and CO *in situ* measurements by gas chromatography. In addition to $CO_2$, the lidar has the capability of measuring atmospheric velocity

1 LI-COR Biosciences is the name of a manufacturer of instrument systems for biotechnology and environmental research.

and ABL structure. It is very convenient to link the $CO_2$ measurements made by lidar and *in situ* sensors in order to assess spatial representativeness. According to wind direction, the three locations can be imbedded in the same air mass or in different plumes from the city of Paris with significant horizontal gradients of $CO_2$ and CO concentrations. Figure 5.5 displays a time series of $CO_2$ measurements by the 2 µm DIAL and *in situ* sensors. The agreement is very good between 12:00 and 16:00 UTC when the ABL is fully developed (well mixed). Before 12:00 UTC the discrepancy is due to the difference in ABL vertical structure, while after 16:00 UTC the wind direction changes and the three locations are in different plumes from the city of Paris.

| Institution | Lidar technique | Peer reviewed publication and conference abstracts |
|---|---|---|
| IPSL, France | • 2.06 µm pulsed crystal-open path cavity<br>• Heterodyne detection<br>• Ground based<br>On-going new ground-based lidar development for the monitoring of a $CO_2$ geological sequestration site and new airborne lidar for carbon cycle application | Gibert et al., 2006<br>Gibert et al., 2008a<br>Gibert et al., 2008b<br>Gibert et al., 2008c |
| DLR, Germany | • 1.57 µm pulsed optical parametric oscillator, OPO<br>• Direct detection<br>• Either ground based or airborne | Amediek et al., 2008 |
| NASA–GSFC, US | • 1.57 µm pulsed fiber laser<br>• Direct detection<br>• Ground based | Abshire et al., 2008 |
| NASA–LaRC, US | • 2.05 µm pulsed crystal-open path cavity<br>• Heterodyne detection<br>• Ground based | Koch et al., 2004<br>Koch et al., 2008 |
| JPL–NASA, US | • 2.05 µm LAS (i.e. continuous wave, cw,<br>• constant power)<br>• Heterodyne detection<br>• Airborne | Menzies et al., 2008 |
| ITT and NASA LaRC, US | • 1.6 µm cw sinewave modulated power fibre laser<br>• Direct detection/lock-in<br>• Airborne | Browell et al., 2008 |
| NICT, Japan | • 2.05 µm pulsed crystal-open path cavity<br>• Heterodyne detection<br>• Ground based | Ishii et al., 2008 |
| Tokyo Metropolitan University, Japan | • 1.6 µm pulsed OPO<br>• Direct d-etection/photon counting<br>• Ground based | Sakaizawa et al., 2008 |

Table 5.3: Lidar techniques – relevant publications

In addition, the development of two airborne demonstrators for the A-SCOPE mission payload is in progress in Germany (DLR) and France (IPSL). Figure 5.6 depicts the airborne $CO_2$-DIAL system foreseen for operation on the DLR Cessna aircraft in a nadir-looking configuration, similar to the viewing direction of the A-SCOPE mission payload. The $CO_2$-DIAL system will use an OPO laser transmitter for generation of the on- and off-line wavelengths in the NIR at 1.57 µm and will be accompanied by two cameras operating in the VIS and NIR spectral region for the purpose of

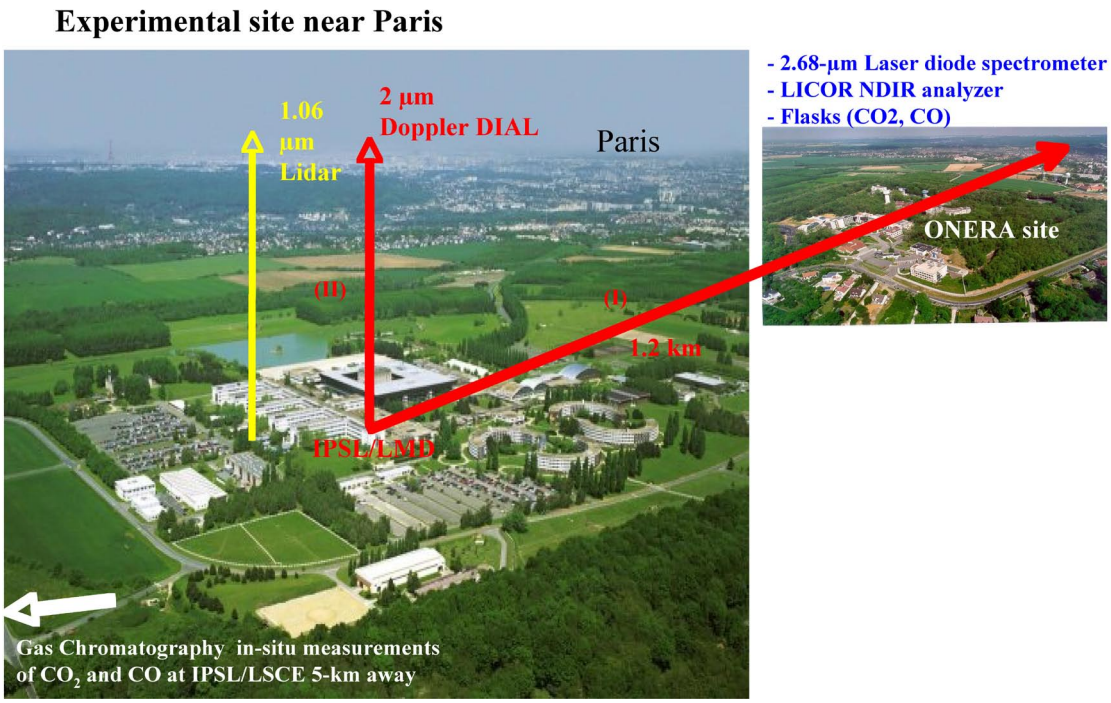


Figure 5.4: Experimental site at École Polytechnique near Paris, France, where a 2 µm DIAL is deployed for $CO_2$ horizontal measurements in the atmospheric boundary layer and vertical measurements using dense clouds as a hard target. *In situ* $CO_2$ and CO measurements are conducted at two locations 1.2 km and 5 km away for validation and geophysical applications. [Credits: Pierre Flamant, LMD]

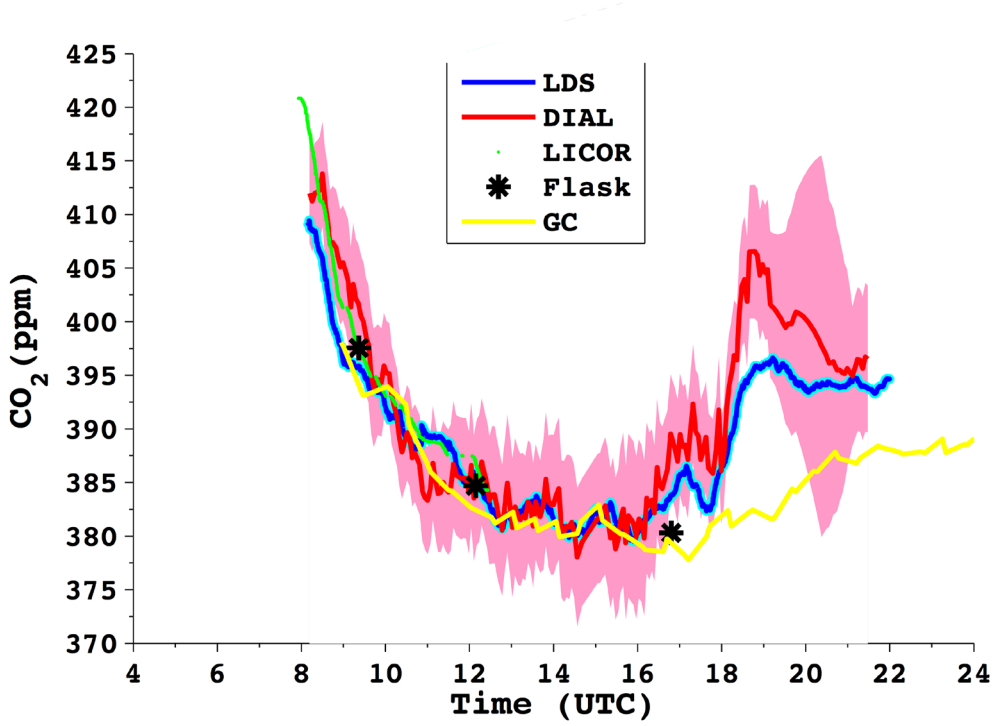


Figure 5.5: Time series of $CO_2$ mixing ratio measurements (September, 21, 2006) by 2 µm DIAL in red, *in situ* laser diode spectrometer (LDS) in blue, LICOR Non-Dispersive InfraRed (NDIR) analyzer in green, flasks (stars) and gas chromatography (GC) in yellow. 2µm DIAL measurements are averaged over a 1 km range gate and 30 min (red solid line) or 5 min (pink). [Credits: Pierre Flamant, LMD]

data interpretation. An initial version of this system, see photo on the right-hand side of Figure 5.6, operated at 1.57 µm. It was flown extensively around Europe for the purpose of studying the characteristics of surface reflectance. For example, its impact on the quality of the A-SCOPE primary data product was studied over complex terrain, snow and water surfaces as well as semiarid, densely forested or heavy agriculture areas (Fix et al., 2007). An example of surface reflectance measurements on a flight track from Cordoba to Valencia in southern Spain is shown in Figure 5.7. The measurement combines reflectance characteristics from olive groves, rocky and semiarid areas, the Mediterranean Sea, inland water, and agricultural land. As an initial result it was found that the relative reflectivity values between land and sea surfaces differ by a factor of 2 to 3. Over land they are highly variable, depending on the type of surface.

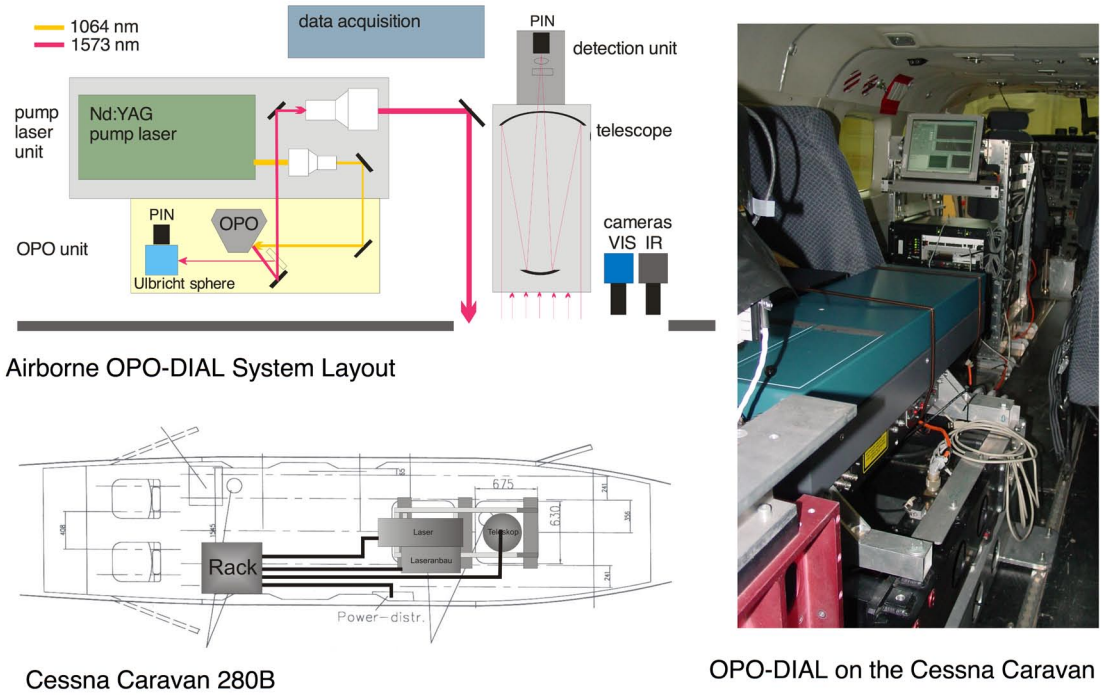


Figure 5.6: Optical layout (top left), aircraft installation (bottom left), and the system on-board the Cessna aircraft (right) for surface reflectance measurements. [Credits: Gerhard Ehret, DLR–IAP]

## 5.10 Summary

The IPDA lidar technique provides the column-weighted dry-air mixing ratio of carbon dioxide, namely $XCO_2$, with very low bias and very low cross sensitivity to other atmospheric parameters. $XCO_2$ can be measured in clear and partly-cloudy conditions due to the small footprint. When stratiform clouds are present, A-SCOPE will measure $XCO_2$ in the portion of the troposphere above the cloud tops.

In addition, the A-SCOPE mission will enable the measurement of various spin-off data products such as vegetation canopy-heights, cloud boundaries and cloud

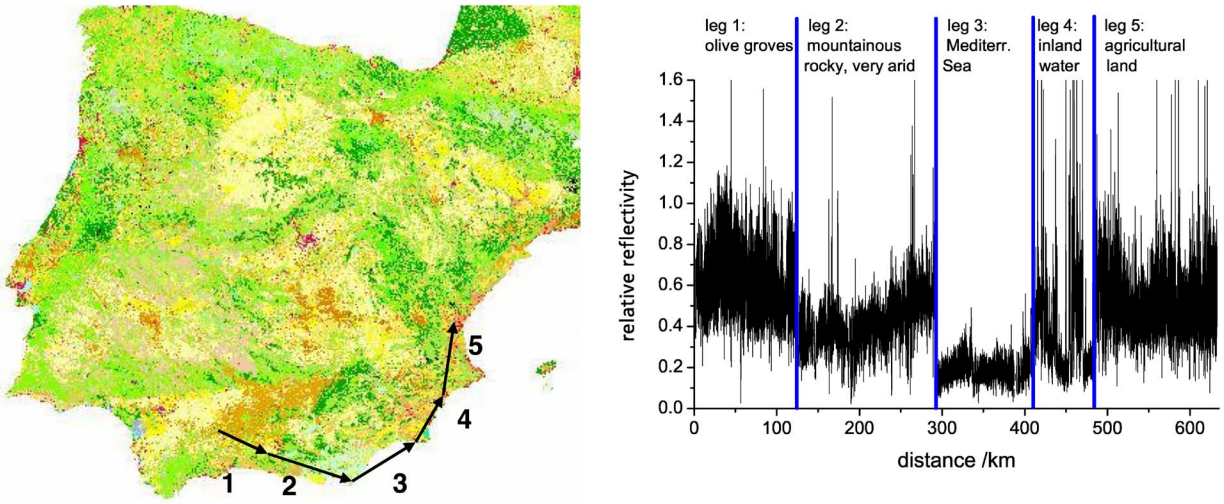


Figure 5.7: Relative surface reflectivity over the flight track from Cordoba to Valencia on the Iberian Peninsula depicted (left) measured by the airborne Lidar on June 13, 2008 (Fix et al., 2007) at 1.57 µm (right). The black arrows (left) indicate the different flight legs marked by the vertical blue lines on the right. [Credits: Gerhard Ehret, DLR–IAP]

optical thickness, optical thickness and distribution of elevated aerosol layers, and surface retro-reflectances.

The instrument operates in day and night-time conditions and over water and land surfaces, thus offering near-global coverage. This is a major advance over the data from the sparse network of surface stations or passive satellite observations which need sunlight. The combination of sensitivity to the lower troposphere, day-night observational capability, and full-latitude and full-seasonal coverage will provide an unprecedented capability to investigate the carbon cycle pertinent to a wide variety of ecosystems.

The A-SCOPE payload will provide continuity in observation of $XCO_2$ provided by the two dedicated satellite missions GOSAT and OCO. However, the quality of the A-SCOPE measurements with respect to coverage and sampling biases will be substantially better than the data from those dedicated, passive missions. A-SCOPE can therefore make a major contribution to a better understanding of the global carbon cycle.

# Chapter 6. System Concept

## 6.1 Introduction

This chapter provides the technical description of the A-SCOPE mission, as derived from the preparatory activities at Phase 0 level, for implementation as an Earth Explorer in the frame of ESA's Living Planet Programme. It shows how candidate implementation concepts can respond to the scientific mission requirements defined in the previous chapters. To this end, the expected system performance at Level 1b is also described.

The system description is mainly based on the results of the work performed during parallel Phase 0 system studies by two industrial consortia (EADS Astrium GmbH, 2008; Thales Alenia Space Italy, 2008). When necessary, two concepts are described in order to present significantly different approaches capable of meeting the mission requirements.

After an overview of the mission architecture and the proposed orbit (Sections 6.2 and 6.3) the space segment is described in detail (Section 6.4), followed by the ground segment and operations concept (Sections 6.5 and 6.6). The overall mission performance is described in Section 6.7.

## 6.2 Mission architecture overview

The A-SCOPE mission aims at improving our understanding of the global carbon cycle and at determining the carbon fluxes at regional scale through the near-global accurate measurement of column-weighted dry air mixing ratios of $CO_2$ ($XCO_2$), as outlined in previous chapters. The high precision, the low bias-error, and the geographic and seasonal coverage are the key performance parameters of A-SCOPE compared with other $CO_2$ missions.

The mission will provide estimates of the vegetation vertical structure as by-products and will have the capability to detect cloud boundaries and elevated aerosol layers, as well as to determine surface retro-reflectance.

The accurate measurement of $XCO_2$ gradients and temporal variations from space is challenging because the low concentration (about 380 ppmv) of $CO_2$ is relatively homogeneous in the atmosphere, with maximum variations of a few percent. The atmospheric backscatter signal is too weak to enable vertically-resolved measurements with the current lidar technology. The most promising way to achieve an accurate measurement from space is to integrate the whole atmospheric column relying on the echo from the surface (ground, canopy or stratiform clouds). This measurement technique, called IPDA, has already been described in Chapter 5. This will be realised in space for the first time on A-SCOPE. The main architectural elements of the A-SCOPE mission are depicted in Figure 6.1.

Figure 6.1: A-SCOPE mission architecture elements.

The space segment consists of a single satellite in a near-polar Sun-synchronous orbit at a reference altitude in the range 325–400 km and operating a near-nadir pointing IPDA lidar. For the latter, two different concepts have been assessed, one operating at wavelengths around 1.57 µm and the other at 2.05 µm.

The baseline Vega launcher will inject the spacecraft into its target orbit. The A-SCOPE satellite is also compatible with a launch by Rockot, Dnepr or PSLV, considered as back-up launchers.

The generic structure of the A-SCOPE Ground Segment follows the generic Earth Explorer Ground Segment infrastructure and is composed of:

- The Flight Operation Segment (FOS), which includes the Telemetry, Tracking and Command (TT&C) Ground Station and the Flight Operations Control Centre (FOCC);
- The Payload Data Ground Segment (PDGS), which includes the Science Data Acquisition Station, the Processing and Archiving Element and the Mission Planning and Monitoring Element.

## 6.3 Orbit

The orbit selected for the A-SCOPE satellite is a near-polar dawn-dusk Sun-synchronous orbit with a reference altitude in the range 325–400 km.

The selection of the orbit altitude calls for a compromise between the conflicting needs of the IPDA lidar payload and those of the supporting platform. For the lidar, a lower altitude translates, for a given performance target, into a lower requirement for the emitted power and/or the surface of the collecting optics. For the supporting platform, a lower altitude implies a higher atmospheric drag, affecting the Attitude and Orbit Control System (AOCS) and the propulsion subsystem, and an increase of atomic-oxygen concentration requiring adequate protection of the exposed surfaces.

The dawn-dusk orbit ensures benign environmental conditions for the satellite and for the IPDA lidar in terms of relatively stable Sun illumination and thermal environment. These features are particularly important for A-SCOPE in view of the demanding stability requirements applicable to the power monitoring subsystem, to the laser spectral properties and to the knowledge of the instrument Line-of-Sight (LOS).

The mission requirements do not impose stringent constraints on orbit maintenance. The only orbital parameters to be controlled are the orbit altitude and the Local Time of the Descending Node, in order to maintain the same Sun illumination conditions over the whole mission duration. For the lower orbit altitude, the interval between orbit-control manoeuvres is about 8 days.

Eclipses occur around the winter solstice over the Northern Hemisphere. The maximum eclipse duration is about 25 minutes for the 325 km orbit.

Though not an explicit mission requirement, exactly repeating orbits in this altitude range have been selected to ease the operational timeline and the calibration/validation operations.

## 6.4 Space segment

The A-SCOPE space segment consists of a single satellite carrying the $CO_2$ IPDA lidar instrument. Two different instrument concepts that meet the requirements have been identified. The instrument concepts impose different requirements on the satellite platform and on the overall satellite configuration. Nevertheless the configurations share a similar modular approach with a clear separation between the payload module and the platform module, as well as significant similarities in terms of conceptual architecture and subsystems. Alternative concepts and solutions will therefore be presented when relevant. Following the payload concepts description in Section 6.4.1, the satellite platform is described in Section 6.4.2 and complemented with the description of the overall satellite configuration and budgets in Section 6.4.3.

### 6.4.1 Payload

#### Observation principles

The A-SCOPE mission aims to observe total-column carbon dioxide with a quasi-nadir-looking pulsed lidar. The lidar needs to point slightly off-nadir, i.e. by 2° across-track, to avoid specular reflections on ice clouds (Hu et al. 2007).

The A-SCOPE lidar instrument transmits two laser pulses at slightly different wavelengths. One laser wavelength (on-line) is selected within a $CO_2$ absorption line, while the other laser wavelength (off-line) is selected close to the first one but with sufficient separation to encounter a significantly smaller absorption. The set of useful laser wavelengths has been identified based on spectroscopy data from Hitran04 (Rothman et al., 2005) and on more recent measurements of pressure shifts (Toth et al., 2008) through a careful optimisation of the combined atmospheric and instrument performance. The results of the current wavelength selections discussed in Chapter 5 are displayed in Figure 6.2 for spectral channels around 1.57 µm and 2.05 µm.

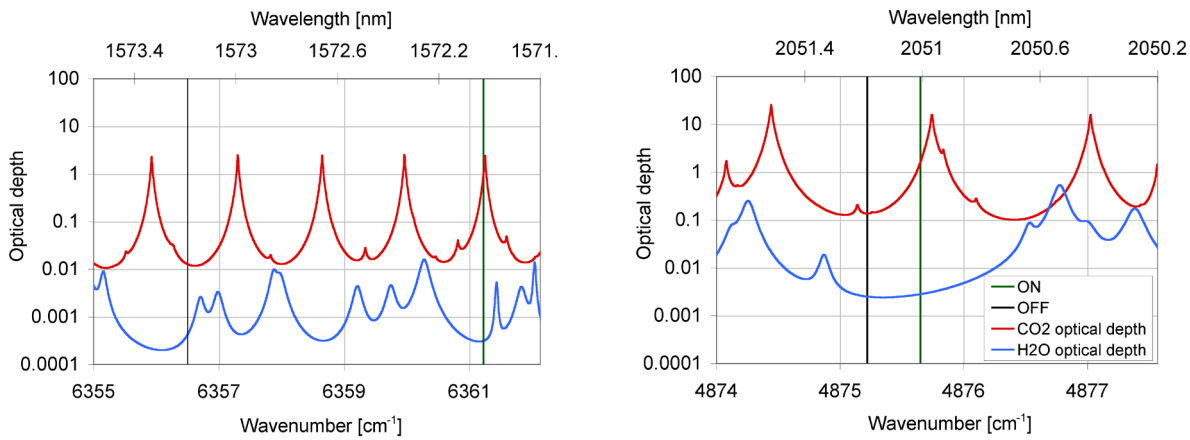


Figure 6.2: One-way $CO_2$ and $H_2O$ optical depths around 1.57 µm (left) and 2.05 µm (right). Selected on/off- lines are 6361.2246/6356.50 $cm^{-1}$ and 4875.6487/4875.22 $cm^{-1}$..

The ratio of the return signals normalised by the associated transmitted laser energies gives a measurement of the total column $CO_2$ DAOD. The differential-measurement principle avoids the need for an absolute radiometric calibration of the received signal. However, unavoidable instrument parameter instabilities generate the need for an accurate measurement of the relative energy of each laser pulse.

To make high accuracy measurements of species with small variability, as is the case for atmospheric $CO_2$, a high Signal-to-Noise Ratio (SNR) is required, which can be provided by an IPDA lidar. Indeed, the ground echo is much stronger than the atmospheric return, so that the required instrument size is significantly reduced and comparable to existing spaceborne lidars.

In order to separate the ground echo from the atmospheric return, a vertical sampling capability of 1 m is required close to ground. This also allows the retrieval of additional information about vegetation canopy height. Otherwise, for quality control of each atmospheric return, a coarser vertical sampling is required higher-up in the troposphere. This data provides additional information about aerosol and cloud layers.

### *Main instrumental aspects*

In order to meet the A-SCOPE requirements the specific functionalities and properties of the instrument have been defined, independently of the possible technical implementations, and are summarised here.

*Radiometric properties:* An IPDA instrument requires an on-board measurement of the relative pulse-energies. To this end, a small portion of the outgoing beam must be picked-up and sent to the detector, which will accurately monitor the fluctuations in the pulse-energy ratio between the on-line/off-line transmissions. The routing optics must be laid out such that the variation of relevant beam parameters (pointing variation relative to the receiver Field Of View (FOV), polarisation, speckle) does not significantly affect the ratio. The power monitoring path includes attenuation by several orders of magnitude in order to provide a signal on the detector of the same magnitude as the ground-return signal.

*Spectral properties:* As shown by the variation of the optical depths in Figure 6.2, the on-line frequency position relative to the absorption line must be accurately known. This requires implementing a frequency stabilisation setup in the sub-MHz range. However, if the stabilisation of the frequency proves too demanding, an accurate measurement of the actual frequency can be performed and used as a correction parameter during data processing. Not only the on-line frequency position, but also the signal's spectral purity must be well controlled. Spurious broad-band and narrow spectral impurities are sources of systematic error. As the spectral purity cannot be easily measured on-board, it has to be minimised by the laser design.

*Pointing:* Pointing jitter causes a similar Doppler effect to that caused by spectral jitter. Accurate monitoring of the Doppler effect imposes requirements on spacecraft pointing and on laser-pointing jitter. This monitoring makes it possible to label each single shot with pointing information that can be used on-ground to correct the Doppler shift. In addition, accurate co-alignment of the transmitter footprint and the receiver FOV needs a fine pointing control mechanism which allows compensation for slow pointing variations.

*On-off overlap:* In an IPDA lidar, the DAOD is retrieved from the ratio of the return on- and off-line signals (see Figure 5.1). In order to minimise the measurement error caused by the imperfect overlap of the two illuminated spots on ground, the time separation of the two pulses has to be as low as possible, yet still such as to avoid

any ambiguity between the echoes from ground and from high cirrus clouds, and compatible with the capabilities of a single laser source to generate two pulses in a row.

### *Instrument architecture*

The IPDA instrument operates on the basis of incoherent detection. Following the recommendations of previous ESA studies (Loth et al., 2005; Ehret and Kiemle, 2005), direct detection has been selected in order to design an instrument of reasonable size at both wavelengths.

Figure 6.3 shows the different subsystems of an IPDA instrument in a functional block diagram. Both instrument concepts share the same subsystems, even though their implementation differs. A bistatic configuration is preferred in order to simplify the separation of the transmitter and receiver paths. This configuration is further justified by the fact that different beam sizes and wavefront properties are found in the transmit and receive paths. The power monitoring path, which after proper attenuation redirects part of the transmitted beam onto the main detector, is also shown.

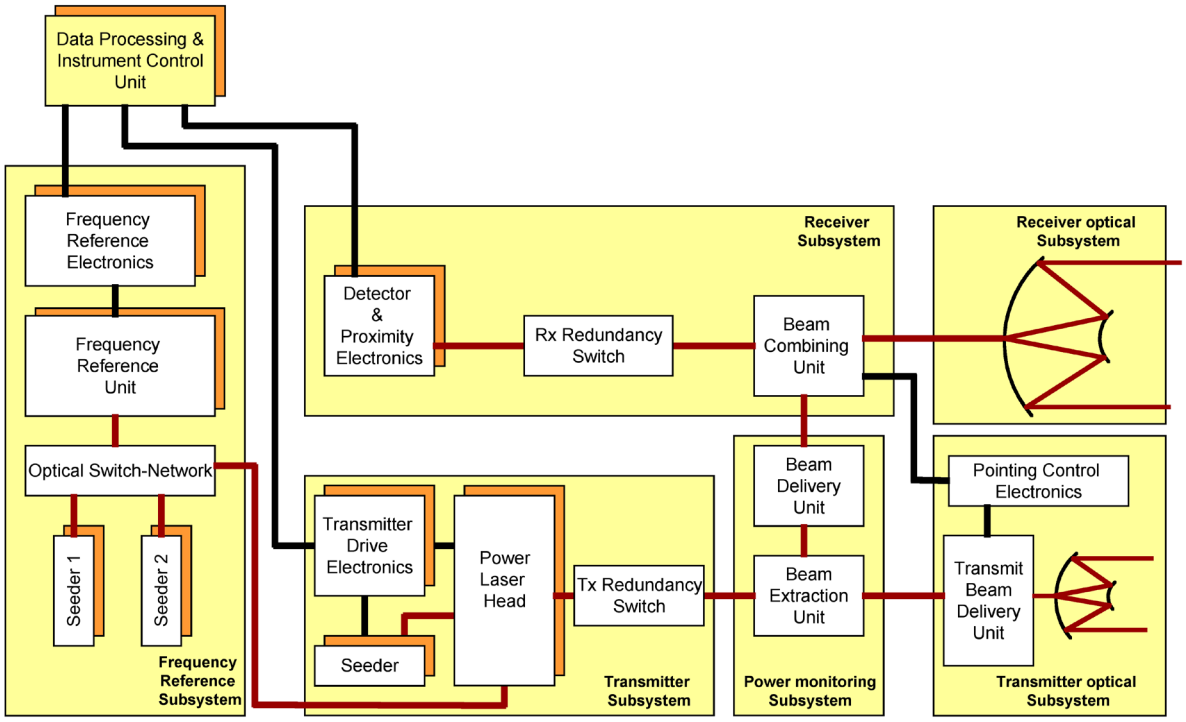


Figure 6.3: functional block diagram of one selected IPDA instrument concept, with the redundant units shown as shadows.

The directions of the transmitted beam, the return echo and the calibration beam are measured with 2D-array sensors, not shown in the block diagram, enabling dynamic compensation of slow drifts. An optimal co-alignment of all three beams is required to minimise biases in the instrument operation.

The instrument provides a vertical sampling of 1 m from ground to 100 m height and of 20 m up to 20 km. The pulse repetition frequency has been set to 50 Hz, which, for 50 km integration length, translates into averaging about 350 pairs of pulses. The on- and off-lines are separated in time by 200–250 µs.

The instrument and data management functions are included in a dedicated data processing and instrument control unit, interfacing with the spacecraft controller.

The overall mechanical design aims at ensuring the co-alignment of the receiver and transmitter optical axes and at decoupling the optical structure from the main structure. In one design option (Figure 6.4, left), it is proposed to use two optical plates spaced by isostatic mounts in order to separate the subsystems with high thermal dissipation (laser optics and laser drive electronics) from those that need a stable thermal environment (receiver, pointing control, frequency stabilisation). In another option (Figure 6.4, right), a single optical plate supports on one side the primary mirror and on the other side all the optical subsystems. The primary mirror is mounted by means of an isostatic support on the payload baseplate, which in turn provides the mechanical link to, and thermal isolation from, the platform through isostatic bipods.

Figure 6.4: Overall opto-mechanical configuration options.

In one concept, a highly-stable redundancy switch, based on a flip-flop mechanism, is used in order to switch between nominal and redundant systems at transmitter level or at receiver level. The second concept uses the displacement of the optical fibre in the focal plane of the telescope for redundancy at receiver level and passive optics at transmitter level.

## *Key payload subsystems and functionalities*

*Transmitter*

For each spectral channel, a candidate laser source has been selected. Both options need the generation of a pair of pulses (at on- and off-line wavelengths) at an overall pulse repetition frequency of 50 Hz, with a pulse energy of about 50 mJ. For the generation of double pulses at 1.57 µm, the Nd:YAG Master Oscillator/Power Amplifier laser at 1.064 µm, combined with an OPO/OPA (Optical Parametric Oscillator/Amplifier) as frequency converter, is preferred. At 2.05 µm a direct emission laser based on a thulium (Tm) pumped holmium (Ho) power oscillator is preferred. At 2.05 µm, an OPO/OPA based laser could be implemented as well.

Injection seeding is needed in both cases to generate the on- and off-line wavelengths. Seeders at 1.57 µm are based on external-cavity diode lasers, while at 2.05 µm a diode-pumped stable resonator with a Co-doped Tm:Ho crystal is selected. Fast optical switches provide a way to rapidly inject the on-line and off-line seeder signals into the cavities. In the OPO/OPA configuration, an additional seeder is required to generate the proper 1.064 µm pump signal for ensuring the spectral requirement with a high efficiency.

*Receiver*

The telescope is a 1 m-class Cassegrain-like design with a real focal plane used to place a field stop limiting the footprint to about 100 m diameter on ground. It is followed by an optical unit that combines the optical beams needed for pointing and for the radiometric calibrations. The collected backscattered energy is finally focused on a detector with mono-pixel functionality. A relatively large sensor has been selected (about 150 to 200 µm), in order to maintain the etendue of the beam and to ease the design of the focusing optics. Two optical configurations have been studied for the receiver. In one option (Figure 6.5 bottom), free propagation has been selected, while the second option (Figure 6.5 top) uses optical fibres between the receiver telescope secondary focal plane and the detector optical assembly, as well as for the calibration path from the laser output to the detector optical assembly. The background light, lower at 2.05 µm than at 1.57 µm, is efficiently blocked by a single interference filter with a bandwidth of 1 nm at 2.05 µm and of 2 nm at 1.57 µm.

*Detector*

The detector is a low-noise Avalanche PhotoDiode (APD) (see Figure 6.6). A relatively narrow bandwidth (< 20 MHz) is sufficient to fulfil the sampling requirements. Some challenging detector noise characteristics are derived from the random error requirement. The receiver response must be well characterised and stable to constrain the systematic error. For the relevant dynamic range, a requirement on the stability of the response of the detector of about 0.01% has been identified. The proximity electronics needs to be placed in the same package as the detector. An active temperature-control system, based on a thermoelectric cooler, is needed to reduce the dark current and the variations of any non-linear behaviour. In view of the demanding linearity requirement, one concept assumes a regular in-orbit

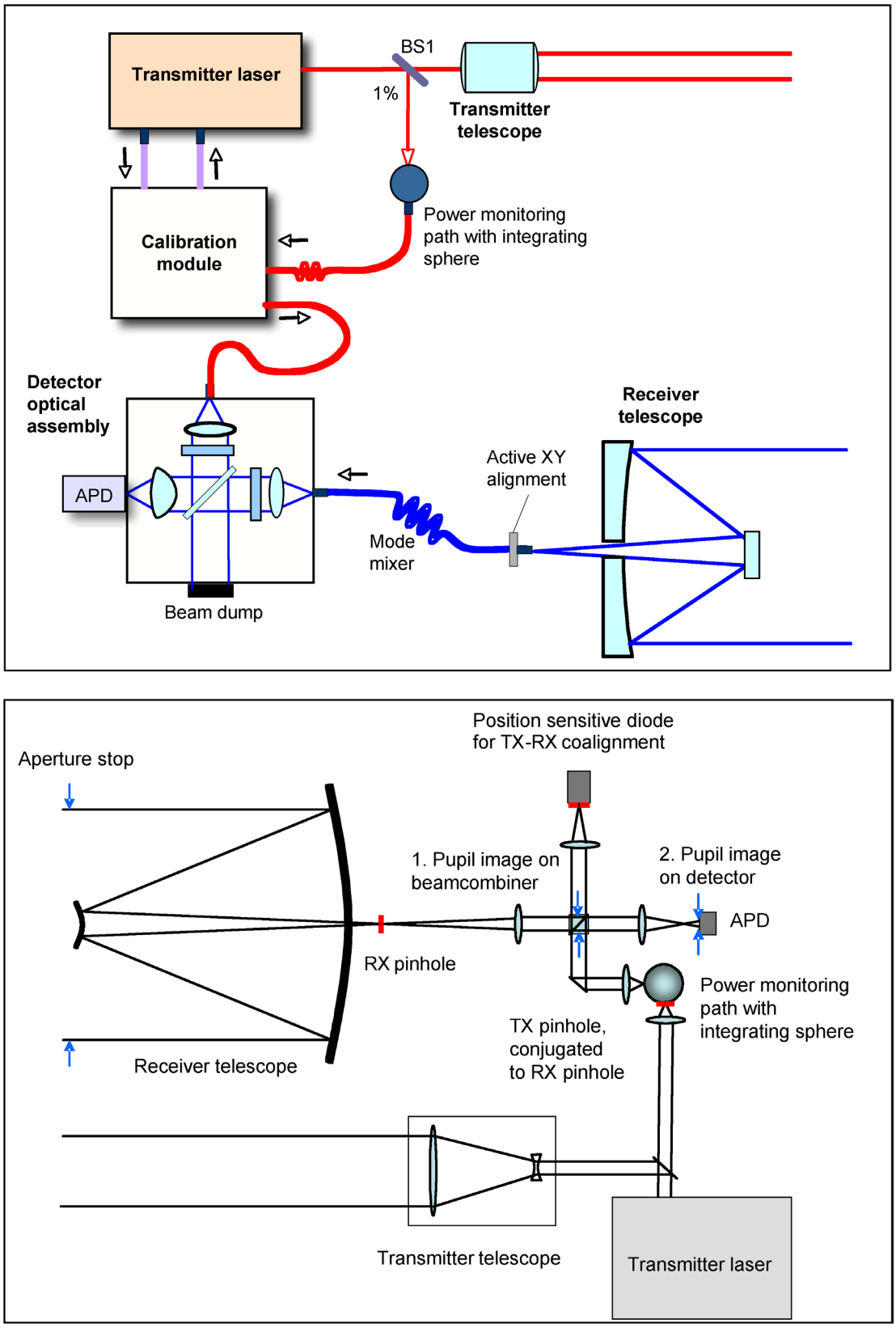


Figure 6.5: Operation principles and optical configurations of the two transmit-receive concepts.

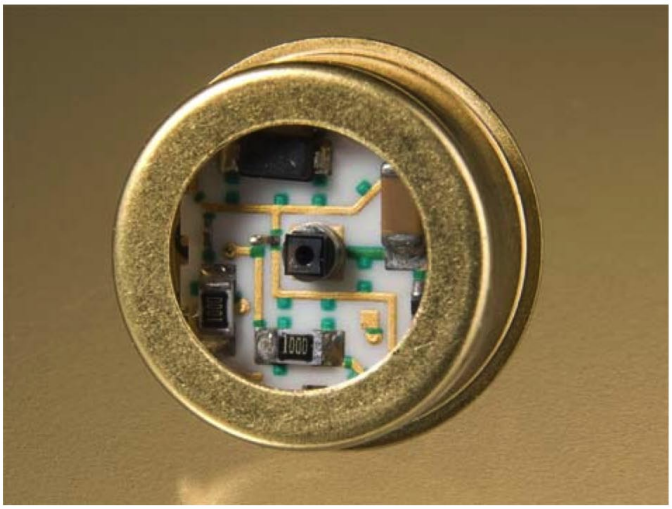

Figure 6.6: Low noise avalanche photodiode / amplifier hybrid receiver at 1.55 µm. – [Copyright: Laser Components GmbH.]

measurement of linearity. To this end, a calibration signal is generated by a highly stable blackbody source. The coupling between the calibration source and the detector is performed by a fibre optics beam splitter.

### *Frequency reference*

Maintaining the position of the on-line pulse, which is about 50 MHz wide, on the side of the $CO_2$ absorption line, which is about 1 GHz wide, to about 100 kHz requires the use of state-of-the-art stabilisation schemes. For both wavelengths, the optical frequency-comb technique has been identified as a possible way to reach the requirements. However, for each wavelength a different strategy is envisaged. One way to stabilise the seeders at the on- and off-lines is to beat them with an optical frequency-comb signal locked to a GPS-synchronised Ultra Stable Oscillator. Another option is to stabilise the seeder to a $CO_2$ absorption line to a somewhat relaxed requirement, while acquiring the knowledge of the spectral position of each laser pulse using a high-resolution wavelength meter accurately calibrated with an optical frequency-comb.

### *Power monitoring*

The power monitoring subsystem combines elements from both transmit and receive paths. In order to meet the accuracy of the relative pulse-energy measurement, an integrating sphere has been retained as it provides the most suitable way to achieve the attenuation of the calibration laser beam and to mitigate the effect of any spatial beam variability on the detector surface. The integrating sphere can operate with both free-propagating beams or coupled with multimode fibres. However the predictable accuracy of the integrating sphere is driven by the material properties of its components, which are not yet well-enough characterised.

### *Pointing control*

Pointing control is a functionality spread across power monitoring, receiver and transmitter optical subsystems. Pointing control is achieved either by monitoring and controlling the transmit beam or by monitoring and adjusting the field stop in the receive path. In the free-beam propagation concept, a piezo-controlled tip/tilt mirror has been selected, while in the fibre-based concept a piezo-controlled fibre holder ensures the co-alignment between receive and transmit paths.

### *Data processing*

A single active receiver is used for all measurement and calibration signals, which can be separated by time de-multiplexing. In order to cope with the signal dynamics, two analogue-to-digital converters (ADCs) are combined with different gains. With 14-bit ADC components, the dynamic range is then extended to 20-bit at 50 MHz sampling rate, which is sufficient to cover both the noise floor and the peak return-signal.

In Figure 6.7 the general timing structure of the receiver signal is shown for a pulse pair. The pulse pairs are repeated at the instrument Pulse Repetition Frequency (PRF), i.e. 50 Hz. Five measurements are needed to deduce one DAOD and SSE value. The minimum time separation between the two pulses is driven by the capability of the pump laser, which is typically longer than the time required to avoid ambiguity of atmospheric echoes, i.e. 200–250µs.

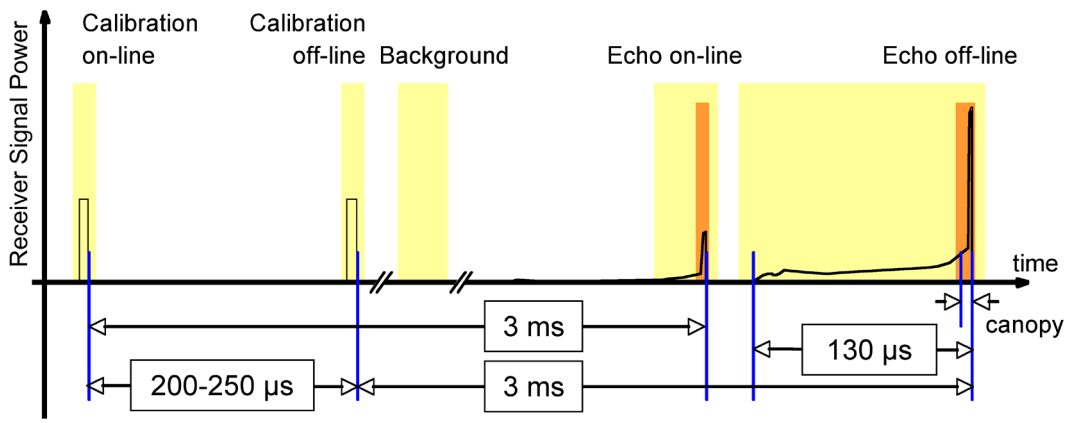


Figure 6.7: Receiver signal timing; background observation should be as close as possible to the echo measurements.

The low duty-cycle of the measurement process (about 20%) can be used to include a settling time for the next pulse and a calibration of the system, if needed.

### *Operation modes*

In addition to the standard mode of operation, the instrument operation includes modes dedicated to warm up and calibration.

### 6.4.2 Platform

The proposed satellite platform concepts have significant heritage from satellite systems under development in the frame of already approved Earth Explorers (ADM-Aeolus, EarthCARE) and of GMES Sentinel missions. In the following sub-sections the main platform subsystems are outlined.

#### Structure

The platform structural concept is based on a central cylinder providing the main load path to the launcher and supporting the propellant tanks. Four shear panels connect the cylinder to the lateral panels, where the platform equipment and the thermal radiators are accommodated. Parts of the instrument electronics are accommodated in the platform (see Figure 6.8).

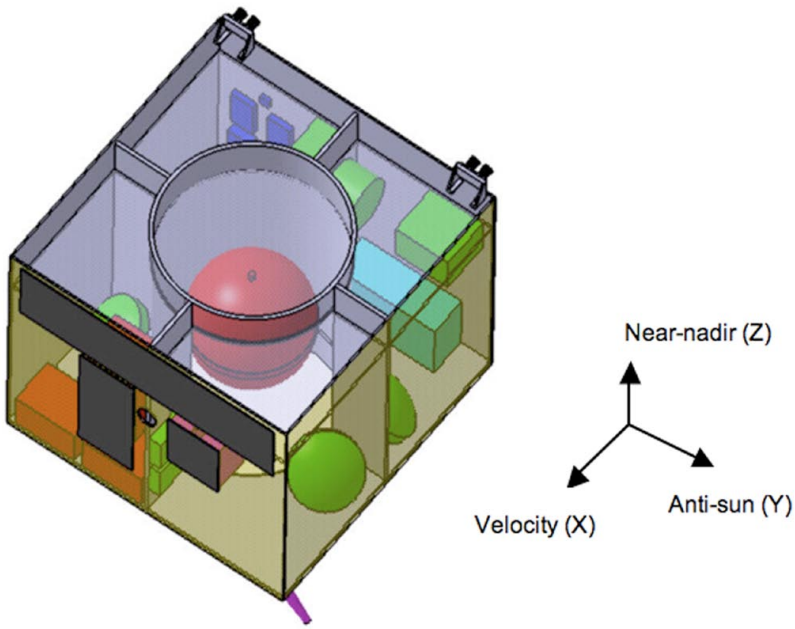


Figure 6.8: A-SCOPE platform structure.

The baseplate of the optical bench is connected to the platform via isostatic mounts in order to thermo-elastically decouple the receive and transmit telescopes from the platform structure. In order to improve the instrument LOS pointing knowledge, the attitude sensors are mounted directly on the optical bench.

#### Thermal control

The thermal control design is driven by the need to radiate the high power dissipated by the instrument (approximately 500 W) and by the platform units. The selected dawn-dusk orbit provides for one side of the spacecraft to be always shadowed from the sunlight, offering sufficient radiating surface. Depending on the configuration and on the location of parts of the instrument equipment

(laser control electronics) within the payload module, dedicated thermal control and radiators for parts of the instrument might be required. For the platform equipment, radiators can be accommodated also on the velocity and anti-velocity panels of the spacecraft. Figure 6.9 shows a possible accommodation of the radiators.

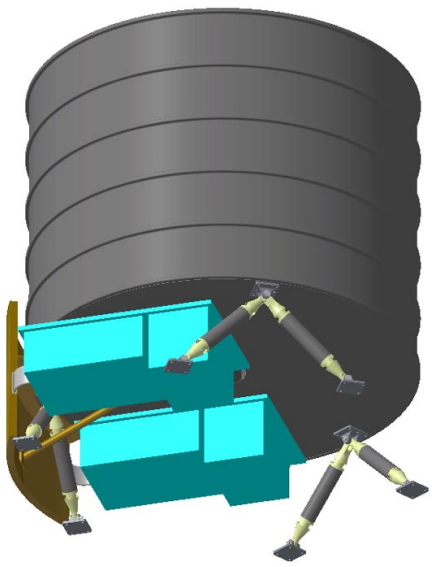

Figure 6.9: Instrument radiator in the payload module.

The thermal control subsystem relies on passive means (multi-layer insulation, radiators) and on heaters to maintain the appropriate thermal environment in the cold case. Heat pipes are used within the platform module to provide the thermal paths between the units mounted on the shear panels and the radiating panels located on the side walls.

### *Power and energy storage*

The electrical power generation is provided by two deployable solar array wings for a total surface of about 9 $m^2$, located on the velocity and anti-velocity sides of the spacecraft and connected to the platform by yokes. Thanks to the favourable Sun geometry in the selected dawn-dusk orbit, the panels are kept in a fixed position after deployment. Triple-junction GaAs cells are used. Energy storage is provided by Li-ion batteries with a capacity of about 100 Ah. The power conditioning and distribution can be based on either direct energy transfer or maximum power-point tracking architectures.

### *Data handling and transmission*

The data handling and transmission architecture for the A-SCOPE satellite does not pose any significant challenges. The proposed architecture (see Figure 6.10) is based on a redundant on-board computer in charge of reception and storage of telecommands, distribution of commands to the relevant units, acquisition and monitoring of relevant satellite parameters, provision of processing capabilities for

the implementation of the relevant command and control functions (propulsion, AOCS), formatting and transmission via the TT&C subsystem of the housekeeping telemetry.

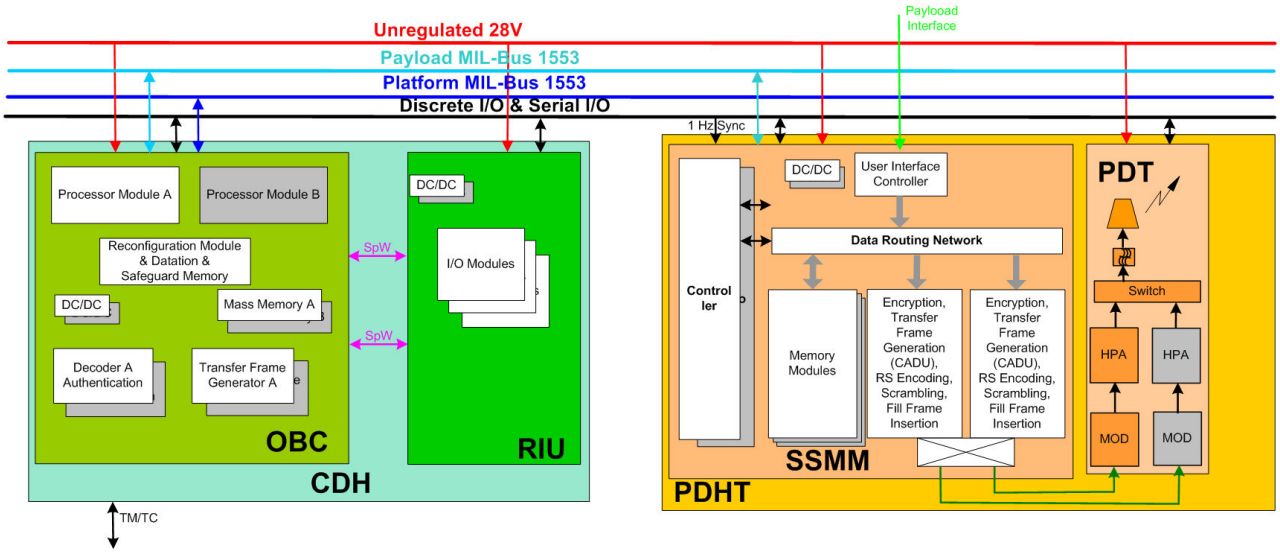


Figure 6.10: Command, data handling and transmission architecture.

The Payload Data Handling and Transmission (PDHT) consists of a solid-state mass memory to store the raw data produced by the instrument and of the processing functions needed to format and code the data stream, which is finally sent to the payload data-transmission subsystem.

The data downlink is performed at X-band. The expected data rate is in the range 260–300 Mb/s, assuming a single ground station is used and depending on the level of data reduction and averaging performed on-board. The design aims at achieving a minimum number (one or two) of contacts per day in order to simplify the operation timeline and reduce cost. This is compatible with the use of off-the-shelf PDHT equipment.

### *Telemetry, tracking and command*

Telemetry, Tracking and Command functions are implemented via a traditional architecture using S-band communications, consisting of a fully redundant transponder and two isoflux antennas accommodated on the nadir and anti-nadir sides of the platform. The TT&C subsystem will support telecommand uplink at 2 kb/s and telemetry downlink at 8 kb/s.

### *AOCS*

The pointing performance requirements are not demanding in terms of the absolute pointing error and the measurement accuracy when compared to on-going

developments like ADM/Aeolus or to the capabilities offered by the platforms used in the GMES programme, which are adequate candidate solutions for the A-SCOPE mission.

The Relative Pointing Error (RPE) requirements apply over the (short) time scales relevant to the consecutive emission of the on-line and off-line pulses and therefore require the limiting of any micro-vibrations via suitable design solutions (for example structural damping, limitation of reaction wheel angular rates) since the frequency domain relevant to the RPE is outside the control bandwidth of the AOCS.

However, different considerations apply to the stability of the measurement error over the mission lifetime, as required to constrain the contribution to the stability of the measurement bias coming from the Doppler shift. The relevant requirements are more demanding for the IPDA lidar at 1.57 µm compared to the one at 2.05 µm, as explained in the performance section (13 µrad and 66 µrad, respectively). The required performance implies a limit to the contribution of the attitude-sensor bias as well as an adequate characterisation/calibration of the misalignment between the attitude sensors and the telescope caused by launch and thermo-elastic effects in orbit. A detailed assessment of the relevant performance and calibration procedures is outside the scope of the Phase 0 and will have to be performed in later phases.

In summary, with the above reservation about the pointing-knowledge stability, the A-SCOPE AOCS architecture can be based on a 'standard' solution using commercial off-the-shelf equipment, i.e. high-end star-trackers and gyroscopes as attitude sensors and reaction wheels as actuators. Earth- and Sun-sensors are used to support non-nominal AOCS modes. Wheel de-saturation is performed with the support of a magnetometer/magnetotorquer package. As an alternative, reaction-control thrusters can be used.

Position, velocity and time data is provided by the on-board Global Navigation Satellite Systems (GNSS) receiver. On-ground position determination to about 2 m accuracy is sufficient to ensure the required performance for the SSE determination.

### *Propulsion*

Despite the relatively low altitude, chemical propulsion has been selected as the most attractive solution in terms of overall complexity and cost, the alternative being electric propulsion.

A hydrazine mono-propellant system operated in blow-down mode is proposed, with two redundant branches of four thrusters for in-plane manoeuvres.

### 6.4.3 Satellite

#### Configuration

Figure 6.11 and Figure 6.12 show the A-SCOPE spacecraft configurations for the two concepts studied. Both concepts share the same modular approach, with a clear separation between the platform and the payload module, the latter being mounted on top of the platform via isostatic mounts to limit the thermo-elastic coupling between the instrument and the platform structure. The main differences are the positions of the yokes of the solar array and the inclusion in one concept of a dedicated instrument radiator in the payload module.

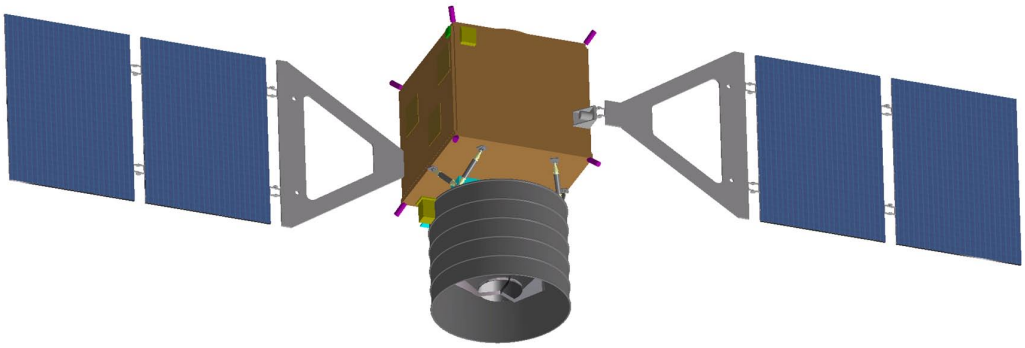

Figure 6.11: A-SCOPE spacecraft configuration – 2.05 μm IPDA lidar concept.

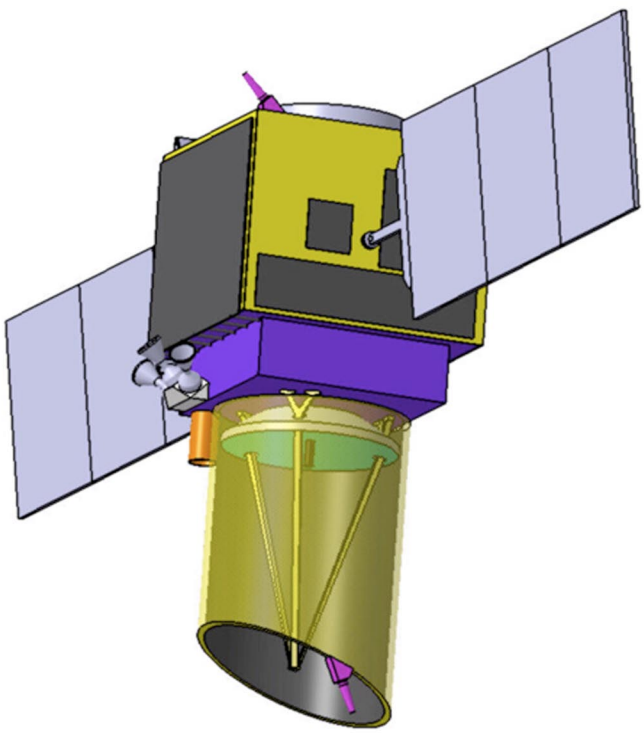

Figure 6.12: A-SCOPE spacecraft configuration – 1.57 μm IPDA lidar concept.

The 2.05 µm lidar concept includes a dedicated instrument radiator accommodated in the payload module on the anti-Sun-side of the spacecraft. In the 1.57 µm lidar concept, the solar array is canted to optimise the Sun illumination conditions.

*Budgets*

Table 6.1 summarises the main satellite budgets. The ranges correspond to the budgets for the two concepts.

| Mass Budget | (kg) |
|---|---|
| Payload module | 280–380 |
| Platform | 570–730 |
| Satellite (dry mass, including margins) | 850–1110 |
| Propellant (3 years) | 80–130 |
| Satellite (launch mass) | 1000–1200 |

| Power Budget | (W) |
|---|---|
| Payload | 490–520 |
| Platform | 500–800 |
| Battery charging | 500 |
| Total | 1500–1800 |

| Payload Data Rate | |
|---|---|
| Instrument data rate | 0.38–1.7 Mb/s |
| On-board raw data storage | 2–9 Gb/orbit |

| Delta V Budget (3 years) | (m/s) |
|---|---|
| Orbit insertion dispersion | 11–15 |
| Orbit maintenance | 36–160 |
| Total | 50–170 |

Table 6.1: A-SCOPE satellite budgets.

### *6.4.4 Launcher*

The A-SCOPE satellite configuration and launch mass is compatible with a Vega launcher, with comfortable mass margins. As a back-up, Rockot (marginal), Dnepr or PSLV could be considered. Figure 6.13 shows both concepts embarked on the Vega launcher.

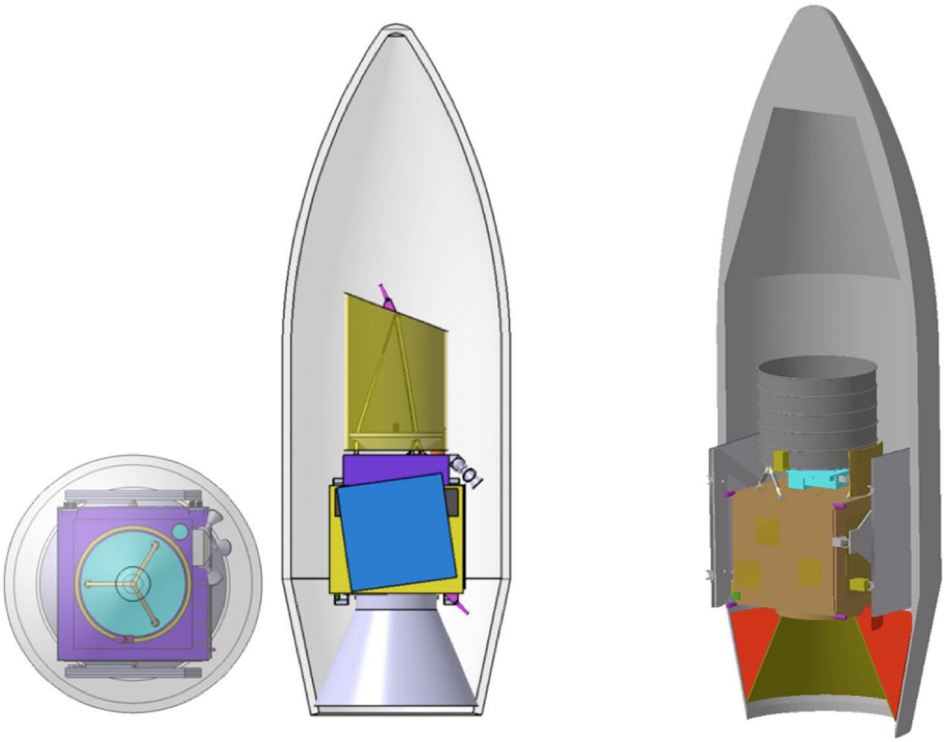

Figure 6.13: Accommodation of the two A-SCOPE satellite concepts under the Vega fairing.

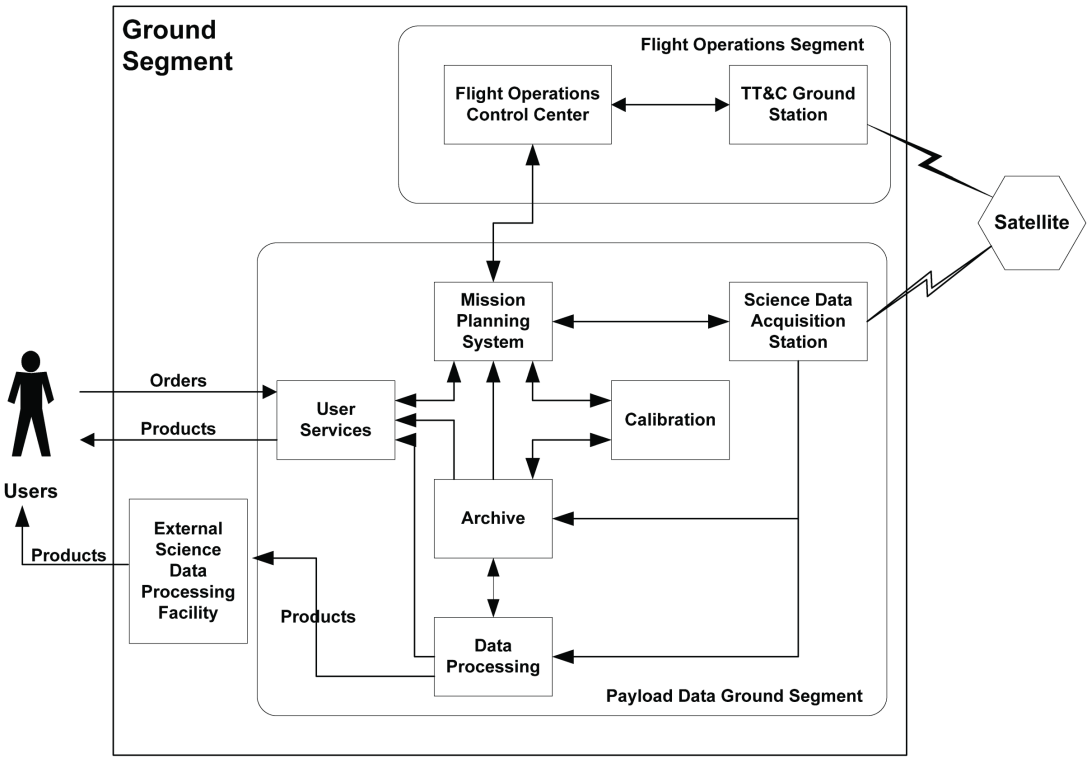


Figure 6.14: A-SCOPE Ground Segment Architecture.

## 6.5 Ground segment and data processing

### *6.5.1 General*

The A-SCOPE Ground Segment is based on the infrastructure developed to support the Earth Explorers as well as other ESA missions. It consists of two main components, the PDGS and the FOS.

### *6.5.2 Ground segment elements*

The overall A-SCOPE ground segment architecture is presented in Figure 6.14.

The FOS includes the TT&C Ground Station and the FOCC.

The TT&C Ground Station provides the following main functions:

- house-keeping telemetry acquisition,
- telecommand uplink,
- satellite tracking, and
- data transmission to the FOCC.

For both mission implementation concepts, the amount of data to be downlinked is very low, compared to the capacity of a standard space-ground link. Therefore contacts with a single ground station in the range from once per day to once every three days are sufficient.

The TT&C function uses a frequency in the S-band and the Science Data Acquisition function one in X-band. With the above contact frequency, a single ground station that could perform both functions in parallel is the preferred concept. A station at, for example, Kiruna or Maspalomas could be used.

During the Launch and Early Operations Phase (LEOP), the operations are supported by a dedicated LEOP ground station network.

The FOCC is based at ESOC and provides the following main functions:

- satellite monitoring and control,
- flight dynamics and manoeuvre planning,
- TT&C ground station network control,
- overall satellite operations planning,
- on-board software maintenance,
- mission simulation,
- FOS supervision,
- spacecraft system data distribution, and
- interface with the launch site for LEOP.

The Payload Data Ground Segment (PDGS) consists of the Science Data Acquisition Station, the Processing and Archiving Element and the Mission Planning and Monitoring element.

The Science Data Acquisition Station is in charge of acquiring the raw payload-data and of transmitting them to the Processing and Archiving Element.

The Processing and Archiving Element and the Mission Planning and Monitoring Element are implemented through maximal re-use of existing ESA Multi-mission Facility Infrastructure elements, and their final location will be selected in later phases.

They provide the following main functions:

- acquisition of payload data from the Science Data Acquisition Ground Station(s),
- acquisition of required ancillary data from appropriate providers,
- generation and quality control of calibration, Level 1 and higher level products,
- long-term archiving of mission products and related auxiliary files and reports,
- implementing the payload planning strategy (routine and calibration) and forwarding it to the FOS,
- instrument/mission performance monitoring,
- systematic and on-request distribution of mission products to the user community, and
- provision of user services.

The specific processing needs of the A-SCOPE mission are described in the following section.

### *6.5.3 Data processing*

The data-processing chain is required to provide the necessary algorithms and functions to process raw lidar data from the payload into various Level 0, Level 1, and Level 2 products. Table 6.2 below summarises the standard products provided by A-SCOPE up to Level 1b.

The Level 0 data products contain the ground returns and raw backscatter profiles (aerosols and clouds), together with ancillary data such as laser pulse energy, time, position, pointing, and any other calibration information relevant at the level of individual laser shots or at larger time scales.

Level 1a data products are generated by subtracting background and offset to separately obtain the on- and off-line signals and their respective radiometric calibrations. All other calibration information is made available at shot level. Time,

position, velocity and pointing information is also made available. All the Level 1a data associated with a single laser pulse are transmitted to ground.

| LIDAR Data Products | Level | Example Products |
|---|---|---|
| Time ordered raw data | 0 | Raw data after restoration of the chronological data sequence for the instrument operating in observation mode. |
| Annotated data | 1a | Level 0 data with all calibrations computed and appended, but not applied. Annotation from time, satellite position, velocity and pointing. |
| Geo-located and calibrated instrument products | 1b | Level 1a data with radiometric calibration applied, processed to get the Differential Atmospheric Optical Depth (DAOD) and Scattering Surface Elevation (SSE) at observation-level, annotated with<br>• observation-level calibration information<br>• preliminary pulse classification<br>• geo-location and time. |

Table 6.2: A-SCOPE data products.

The Level 1b data products are generated for each observation by appropriately processing the shot-level information. Level 1b includes the DAOD and the SSE. The radiometric calibration is included in the calculation of the DAOD. Additional calibration information relevant to the DAOD, the geo-location and time information as well as the preliminary quality flags are calculated and made available at observation level.

## 6.6 Operation and utilisation concept

The A-SCOPE spacecraft is designed for an operational lifetime of three years. Once the system has been commissioned and is operating nominally, the operations are driven by the need to maintain the stability of the lidar configuration.

Payload data acquisition is performed continuously, all along the orbit. Mission planning is expected to be very simple for this mission. All commanding activities are pre-programmed and loaded onto an on-board mission scheduler.

Given that the timeliness requirements are not challenging and that the amount of data is relatively small, the possibility of operating this mission with a simplified concept is being considered in order to reduce the long-term operation costs. For example, the science dumps and TT&C passes could be reduced to a minimum. A low-cost beacon system could alert the ground to on-board problems without having to wait for the next dump.

In the IPDA instrument, calibration is nominally applied as an integral part of the operational mode: pointing, energy and wavelength have to be either stable or measured for each pulse during the whole mission lifetime. Additionally, if the stability of the linearity of the detector cannot be guaranteed, it needs to be calibrated. The time needed for the pulse to return from the top-of-atmosphere to the spacecraft is advantageously used to calibrate the linearity of the detector.

## 6.7 Performance Aspects

For performance assessment, $CO_2$ mixing ratios ranging from 370 ppmv to 450 ppmv have been considered. Various atmospheric scenarios have been envisaged and results are presented here for a US Standard Atmosphere, taking into account both molecular (Rayleigh) and aerosol scatterings. The nominal instrument parameters from the system studies are summarised in Table 6.3.

| | Unit | B1 | B2 |
|---|---|---|---|
| Wavelength | µm | 1.57 | 2.05 |
| **Instrument** | | | |
| Laser pulse energy | mJ | 50 | 55 |
| Telescope diameter | m | 1 | 1.2 |
| FOV | mrad | 0.476 | 0.220 |
| Integration time = Δt | ns | 200 | 160 |
| Receiver path transmittance | - | 0.65 | 0.64 |
| Filter bandwidth | nm | 2 | 1 |
| PRF | Hz | 50 | 50 |
| **Detector** | | | |
| Quantum efficiency = $Q_e$ | - | 0.74 | 0.75 |
| Excess noise factor = F | - | 5.5 | 1.5 |
| Noise Equivalent Power = NEP | $fW/Hz^{0.5}$ | 46 | 100 |
| **System** | | | |
| Spacecraft altitude | km | 435 | 350 |
| Measurements within 50 km = N | - | ~ 350 | |

Table 6.3: Instrument parameters for performance assessment.

### *6.7.1 Random errors and instrument sizing*

The random errors (RE) are mostly constrained by the instrument size. Specifically, shot and detector noise, which are the main RE contributors, scale directly with laser transmitted power, receiver aperture diameter and detector performance. These REs show different dependencies with signal strength S.

Due to differences in detector performance, whereas B1 is dominated by shot noise (Eq. 6.1), the detector noise is more significant for B2 (Eq. 6.2). Other RE terms, such as background light from Sun irradiance reflection on Earth and on-line frequency jitter, have only marginal effects. A significant RE contribution is generated by the lack of overlap between on-line and off-line footprints on ground due to the change

Eq. 6.1
$$RE_{shot} \propto \frac{1}{DAOD}\frac{1}{\sqrt{N}}\frac{1}{\sqrt{S}}$$

Eq. 6.2
$$RE_{NEP} \propto \frac{1}{DAOD}\frac{1}{\sqrt{N}}\frac{NEP\sqrt{\Delta t}}{S}$$

in lidar reflectivity. To properly assess this, an aircraft campaign was performed with the aim of quantifying lidar reflectivity statistics for various geophysical contexts, as described in Chapter 5.

All RE terms, combined as statistically independent contributors, are to be compared to the requirements of Table 6.4.

| Wavelength | B1 | B2 |
|---|---|---|
| RE target | $7.4 \times 10^{-4}$ | $1.5 \times 10^{-3}$ |
| RE threshold | $2.2 \times 10^{-3}$ | $4.5 \times 10^{-3}$ |

Table 6.4: DAOD random error requirements as defined in Chapter 5.

For the nominal instrument parameters, the radiometric performance is computed against surface scattering elevation for the two extreme cases of lidar reflectivity. A minimum value of 0.035 $sr^{-1}$ is associated with an average reflectivity over ocean (Bréon and Henriot, 2006). A maximum value of 0.3 $sr^{-1}$ accounts for strong backscattering, as could be observed above deserts. Figure 6.15 shows that the performance of both concepts meets the threshold requirement with good margins under all conditions. The target requirements are met with ample margins by both concepts in the high-reflectivity case. In the low-reflectivity case, thanks to the relative homogeneity of $CO_2$ above ocean, the performance is assumed to improve by further averaging.

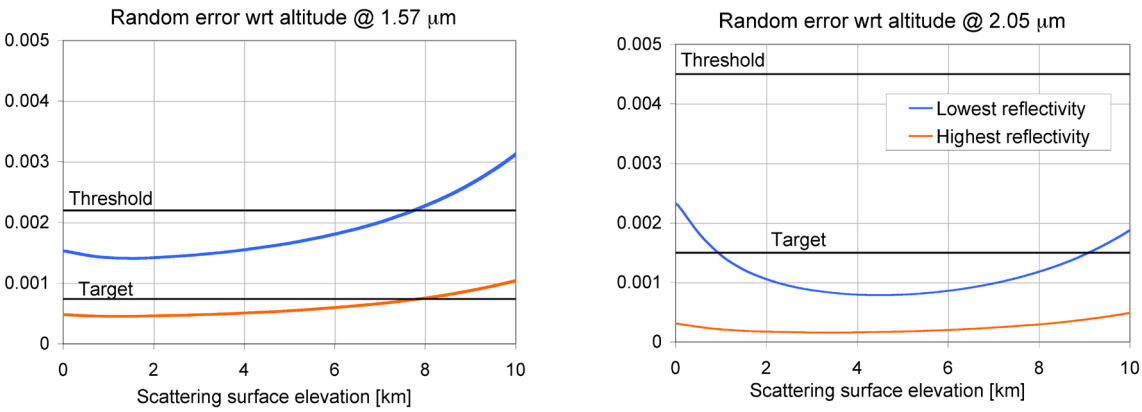


Figure 6.15: DAOD relative random error performance computed as a function of the ground elevation for the two sets of instrument parameters.

### *6.7.2 Systematic errors and measurement accuracy*

Instrumental Systematic Errors (SE) that are not linked to instrument size also play a major role in the accuracy of the measurements. The most important SE have been identified to be: the laser frequency stability (from the laser and from LOS de-pointing through Doppler effects); the laser spectral purity; the laser linewidth knowledge and stability; the power monitoring accuracy; and the detector non-linearity stability. As established in Chapter 4, the difference of SE between any two distinct scenes must not exceed 10 % of the RE.

The allocation of the different contributors to the SE is presented in Table 6.5. The associated instrumental requirements are to be understood as constraining the possible relative variations of DAOD values averaged over 1000 km × 1000 km scenes that might occur between any two scenes, due to changes in instrumental or geophysical conditions. In most cases these variations can be interpreted as caused by ageing (over the mission lifetime) or by the changing thermal environment. It should be noted that, in terms of the expected performance, only the satellite-pointing stability and the transmitter-bandwidth stability are experimentally demonstrated. The other contributors still lack experimental verification and reflect a budget allocation designed to meet the threshold requirements, rather than a consolidated performance assessment.

| Parameter | B1 | B2 |
|---|---|---|
| Power monitoring | $9 \times 10^{-5}$ | $2 \times 10^{-4}$ |
| Detector linearity error | $1.4 \times 10^{-4}$ | $1.2 \times 10^{-4}$ |
| Transmitter frequency stability (drift) | 70 kHz | 100 kHz |
| Pointing | 13 µrad | 66 µrad |
| Transmitter bandwidth stability | 2.5 MHz | 1 MHz |
| Transmitter spectral purity stability | $5.0 \times 10^{-4}$ | $6.8 \times 10^{-4}$ |

Table 6.5: Budget of the contributors to the systematic error. The combination of the statistically independent contributors is sized to meet the threshold requirements defined in Chapter 5.

### *6.7.3 Scattering surface elevation*

Another primary data product is the SSE, defined as the elevation of the scattering surface with respect to the WGS-84 reference ellipsoid. This is determined from the satellite altitude provided by the GNSS receiver, the lidar pointing knowledge and the lidar ranging capability. The SSE differs from the topography determined from altimetry since it is an optical effective elevation, weighted by the various elevations and lidar reflectivity of the backscattering elements within the laser footprint.

The measurement of SSE is affected by several error sources quantified in Table 6.6:

- inaccuracies in the electronic detection chain,
- spacecraft pointing errors,
- errors in spacecraft position determination.

| Parameter | B1 | B2 |
|---|---|---|
| Single shot ranging error from SNR | 0.5 m | 1.5 m |
| Pointing errors | 0.4 m | 0.3 m |
| Spacecraft location errors | 2 m | 2 m |
| Final error | 2.1 m | 2.5 m |

Table 6.6: Summary of the contributors to SSE error.

Assuming that the spacecraft pointing error is about 20 µrad, the overall SSE error is about 2 m, thus meeting the target level of 3 m with comfortable margins.

### *6.7.4 Comparison B1/B2*

With the given set of spectroscopic parameters, two instrument concepts that meet the radiometric requirements have been defined. As explained in Chapter 5, due to the different weighting functions the expected scientific return obtained in the lower troposphere is more favorable for B2 than for B1, which allows for requirement relaxation by a factor of two. Similar instrument sizes have been considered for both wavelengths, with the nominal power-aperture product per wavelength equal to 2 $Wm^2$ for B1 and to 3 $Wm^2$ for B2. Design margins are illustrated for both wavelengths in Figure 6.16, where the required pulse energy is plotted against the telescope diameter so that each instrument design meets threshold and target requirements.

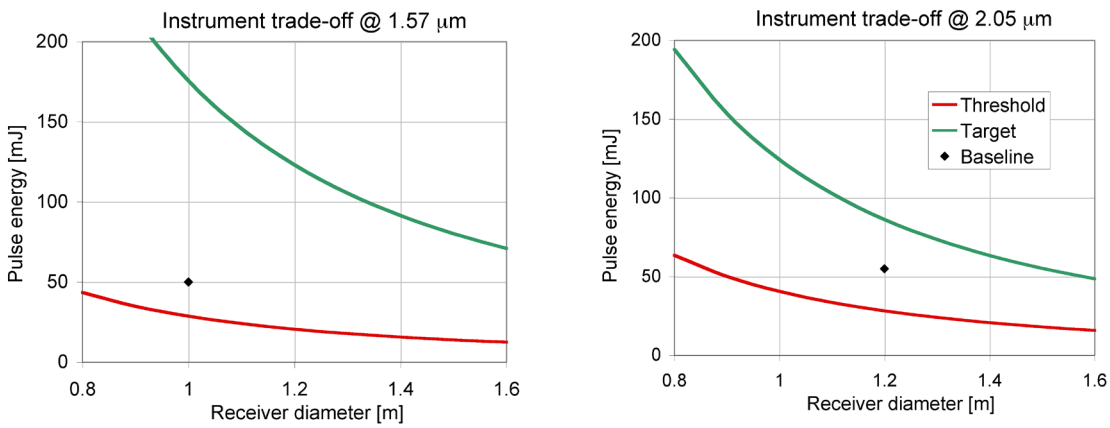


Figure 6.16: Pulse energy versus telescope diameter required to meet the threshold and target random error requirements.

Care must be taken when comparing B1 and B2 wavelengths, not only due to different measurement strategies (for example, assumptions on integration time) but also to differences in technological maturity and risks between the two wavelengths, as explained in Chapter 7. In short, it can be stated that, even though the requirements are more demanding for B1, the confidence in achieving them is higher as the technology developed at this wavelength is more mature. B2 benefits from less demanding requirements, but lacks technological maturity, especially with regard to the detector. In any case, the lidar operation point will have to be re-assessed and the on- and off-line wavelengths fine-tuned in future phases taking improved $CO_2$ spectroscopic data and new achievements in critical technologies into proper account.

# Chapter 7. Programmatics

## 7.1 Introduction

This chapter presents the technical maturity, the heritage and the risks associated with the implementation concepts developed in the frame of the Phase 0 studies. The overall development approach and schedule are briefly introduced and discussed with respect to the compatibility with a target launch date for the seventh Earth Explorer Core Mission during 2016.

## 7.2 Technical maturity, critical areas and risk

No critical elements have been identified for the A-SCOPE satellite platform development since there is a strong heritage from the on-going Earth Explorers and other Low Earth Orbit (LEO) missions.

Substantial development risks are however associated with specific elements of the $CO_2$ IPDA lidar. This chapter lists the most critical sub-systems, provides an assessment of their technical maturity together with any applicable heritage and underlines the status of related on-going activities or the need for pre-development activities.

Four areas are considered to be critical with respect to the maturity of the relevant technologies and the capability to achieve the desired performance, namely the transmitter, the detector, the frequency stabilisation, and the power monitoring subsystems.

### *7.2.1 Transmitter*

The proposed concept for the laser at 1.57 µm is a seeded OPO-OPA frequency converter pumped by a Nd:YAG laser. For the laser at 2.05 µm, the proposed concept is a Tm-pumped Ho power oscillator seeded by a co-doped Ho:Tm:YAG laser. Only a subset of the transmitter performance requirements has been demonstrated so far. The combination of the relatively high pulse energy and beam quality, the very-high frequency stability and spectral purity, as well as the space compatibility, have not yet been demonstrated. The transmitter development will draw substantially from the experience accumulated in Europe with the ALADIN and the ATLID lidars, which are both Q-switched high-power systems, though not at the same wavelengths considered for A-SCOPE.

Injection-seeded OPOs have been developed at 1.57 µm for a ground-based $CO_2$ DIAL lidar, achieving a pulse energy of 10 mJ with good beam quality and 99.9 % spectral purity (Amediek et al., 2008; Burris, 2008) . The Agency has initiated an activity to develop an OPO/OPA laser system meeting the A-SCOPE requirements with the exception of the spectral stability and purity. As to the pump source, in the frame of the pre-development activities related to EarthCARE, a laser source has been developed demonstrating energy up to 100 mJ with high electro-optical efficiency

(up to 10%). This pump source development includes all the space-relevant aspects such as redundancy, conductive cooling and reliability. Further pre-development activities on the laser transmitter are required during Phase A.

For the 2.05 µm transmitter, the power oscillator concept based on Ho:Tm laser has been developed at NASA, demonstrating 90 mJ at 5 Hz (Koch et al., 2008) in a $CO_2$ DIAL ground system, and at NICT (Japan), demonstrating 50 mJ at 20 Hz (Ishii et al., 2008). In Europe, expertise on the high repetition rate lasers can be found, but not with high-energy systems. Two developments have been initiated by the Agency to develop laser sources at 2.05 µm, based on an OPO/OPA concept and on a fibre-laser concept, respectively. Also in this case a pre-development of the laser source would be required and, in view of the lower maturity of this solution, the results should be available during the course of Phase A to allow informed design choices to be made.

Apart from the development of the laser system itself, a number of components need to be developed in space qualified versions. Critical issues may be expected from the radiation darkening of fibre lasers, the radiation effects on new crystals or the lifetime of laser diodes at 793 nm.

### *7.2.2 Detector*

Both instrument concepts need APD. These detectors are not commercially available at 2 µm. Recent developments at NASA have demonstrated both phototransistor and advanced HgCdTe APD at 2 µm in an atmospheric $CO_2$ lidar profiling system (Refaat et al., 2008; Abedin et al., 2008). Two developments have been initiated by the Agency to develop new 2 µm APD, one based on InGaAs material, the other based on HgCdTe material. The developments include the proximity electronics, since the combination of both detector and amplifier is required to demonstrate the overall performance. APD's at 1.57 µm with the required performance are commercially available. The mechanisms underlying the non-linearity of APD's have to be investigated. For silicon photodiodes, linearity to within $3 \times 10^{-5}$ have been reported (Haapalinna et al., 1999). Some effort will have also to be devoted to the detector characterisation to the needed accuracy and to the modelling required to improve confidence in the performance simulations.

### *7.2.3 Frequency stabilisation*

One concept relies on the stabilisation of the on-line frequency to values around 100 kHz. Using an optical frequency-comb synchronised with GPS signals is a new technique that can provide the required absolute frequency. Commercial systems are available but need to be space qualified (on-going ESA TRP activity). Suitable seeders are commercially available and need to be space qualified. A specific development is required for the frequency-reference electronics.

Another concept has been proposed to relax the stabilisation requirement and to measure each out-going pulse. In this case, several elements requiring development and space qualification are needed:

- $CO_2$ gas absorption cell, which could be based on Photonics Crystal Fibre,
- Long FP etalons (~ 150 mm) with modest working aperture and finesse,
- IR detector array (on-going ESA TRP activity),
- Electro-Optical Modulators, currently commercially available,
- High-resolution wavelength meter.

For both concepts, an early design and development of a complete frequency stabilisation and measurement breadboard is required.

### *7.2.4 Power monitoring measurements*

Very accurate measurements of relative pulse energies require a design that gives the best stability of the path from the pick-up of the outgoing pulse down to the detector, or a frequent calibration of the detector. Both concepts have been analysed and the need to develop and qualify specific elements has been identified, namely for:

- Blackbody at a temperature of about 1400K,
- Integrating sphere with accurate knowledge of the reflectivity properties,
- Specific coatings that guarantee the high (< 1%) accuracy of the power monitoring path,
- Fibre optics at 2 µm,
- Optical switches.

For both concepts an early design and development of a complete power-monitoring breadboard is required.

## 7.3 Development approach and schedule

The development approach proposed for the A-SCOPE system assumes a platform model philosophy based on a Structural and Thermal Model (STM) and a Proto-Flight Model (PFM).

At instrument level the risks associated to the low maturity of the key technologies will require an approach based on the breadboarding of critical elements and on an Optical-Structural and Thermal Model, an Engineering Qualification Model (EQM) and a PFM.

Some of the outlined pre-development activities have already started (laser source, detectors), while a few other activities could start at the same time as the Phase A as they are sufficiently well defined. They include the assessment and selection of key components (optical switches, optical frequency-combs, integrating sphere).

The remaining required pre-development activities, mainly related to the breadboarding of the power monitoring and of the frequency stabilisation and measurement, can only start after refining the design of these modules within Phase A.

The critical path in the overall development plan is determined by the instrument development activities. The required technology pre-developments and the demanding development and qualification programme indicate that the A-SCOPE mission would not be compatible with a launch within 2016.

## References

Abedin M. N., T. F. Refaat, S. Ismail, G. Kock, and U. N. Singh, 2008: Progress of 2-micron detectors for application to lidar remote sensing, *Proc. Earth Science Technology Conference ESTC2008*, B8P3.

Abshire J. B., H. Riris, G. Allan, S. R. Kawa, J.-P. Mao, E. Wilson, M. Stephen, M. A. Krainak, X. Sun, and C. Weaver, 2008: Laser Sounder Approach for Global Measurement of Tropospheric CO2 Mixing Ratio from Space, Reviewed and Revised Papers, 24th International Laser Radar Conference, 23–28 June, Boulder, Colorado, USA, p. 637–640.

Abshire J. B., X. Sun, H. Riris, J. M. Sirota, J. F. McGarry, S. Palm, D. Yi, and P. Liiva, 2005: Geoscience Laser Altimeter System (GLAS) on the ICESat Mission: On-orbit measurement performance, *Geophys. Res. Lett.*, 32, L21S02, doi:10.1029/2005GL024028.

Amediek, A., A. Fix, M. Wirth, and G. Ehret, 2008: Development of an OPO system at 1.57 µm for integrated path DIAL measurement of atmospheric carbon dioxide, *Appl. Phys. B*, 92, 295–302.

Aulinger, T., T. Mette, K.P. Papathanassion, L. Hajnsek,, M. Heurich, P .Krzystek, 2005: Validation of heights from interferometric SAR and lidar over the temperate forest site "Nationalpark Bayerischer Wald", *Proc. 2nd International Workshop POLINSAR 2005*, 17–21 January 200, ESRIN, Frascati, Italy, ESA SP-586. Available from *http://www.esa.int/esapub/conference/toc/tocSP586.pdf*

Baker, D. F. et al., 2006: TransCom 3 inversion intercomparison: Impact of transport model errors on the interannual variability of regional CO2 fluxes, 1988–2003, *Global Biogeochem. Cycles*, 20, GB1002, doi:10.1029/2004GB002439.

Berthier S., P. Chazette, J. Pelon, and B. Baum, 2008: Comparison of cloud statistics from spaceborne lidar systems, *Atmos. Chem. Phys. Discuss.*, 8, 5269–5304. Available from *http://www.atmos-chem-phys-discuss.net/8/5269/2008/*

Boudreau J. , R.F Nelson, H. A. Margolis, A. Beaudoin, L. Guidon, and D. S. Kimes, 2008: Regional Aboveground Forest Biomass Using Airborne and Spaceborne Lidar in Québec, *Rem. Sens. Env.*(in press).

Bréon, F. B., F. Maignan, M. Leroy, and I. Grant, 2002: Analysis of hot spot directional signatures measured from space, *J. Geophys. Res.*, 107, 4282–4296.

Bréon F. M. and N. Henriot, 2006: Spaceborne observations of ocean glint reflectance and modelling of wave slope distributions, *J. Geophys. Res.*, 111, C06005.

Bréon F. M., S. Houweling, I. Aben, G.Ehret, F. Chevallier, J. Marshall, P. Flamant, D. Bruneau, and P. Rayner, 2008: Observation Techniques and mission concepts for the Analysis of the Global Carbon Cycle, *ESA Contract* No. 20839, study in progress.

Browell E. V., M. E. Dobbs, J. Dobler, S. Kooi, Y. Choi, F. W. Harrison, B. Moore III, and T. S. Zaccheo, 2008: Airborne Demonstration of 1.57-Micron Laser Absorption Spectrometer for Atmospheric CO2 Measurements, Reviewed and Revised Papers, 24th International Laser Radar Conference, 23–28 June, Boulder, Colorado, USA, p. 697–700.

Burris J., 2008: Development of a CO2 DIAL lidar at 1570 nm, Reviewed and Revised Papers, 24th International Laser Radar Conference, 23–28 June, Boulder, Colorado, USA, p.681–682.

Cox, P. M., R. A. Betts, C. D. Jones, S. A. Spall, and I. J. Totterdell, 2000: Acceleration of global warming feedbacks due to carbon-cycle feedbacks in a coupled climate model, *Nature*, 408, 184–187.

EADS ASTRIUM GmbH, 2008: Phase 0 study of the six candidate Earth Explorer Core Missions, Final Report, *ESA Contract* No. 20706.

Ehret, G., and C. Kiemle, 2005: Requirements Definition for Future DIAL Instruments, *ESA Study Report*, ESA-CR(P)-4513.

Ehret, G., C. Kiemle, M. Wirth, A. Amediek, A. Fix, and S. Houweling, 2008: Space-borne remote sensing of CO2, CH4, and N2O by integrated path differential absorption lidar: a sensitivity analysis, *Appl. Phys. B* , 90, 593–608, DOI: 10.1007/s00340-007-2892-3.

European Space Agency (ESA), 2006: *The Changing Earth – New Scientific Challenges for ESA's Living Planet Programme*, ESA SP-1304, 83p.

Fix A. A. Amediek, and G. Ehret, 2007: Breadboarding of Critical Technologies for Future Lidar Instruments, *ESA Contract* No. 18256, study in progress.

Friedlingstein P., 2008: A steep road to climate stabilization. *Nature*, 451, 297–298.

Friedlingstein P. et al., 2006: Climate-Carbon Cycle feedback analysis: results from the C4MIP Model Intercomparison, *J. Clim.*, 19, 3337–3353.

Generoso, S., I. Bey, F.M. Bréon, and M. Labonne, 2008: Aerosol vertical distribution in dust outflow over the Atlantic, 2008: Comparisons between GEOS-Chem and CALIPSO, *J. Geophys. Res.*, accepted.

Gibert F., P.H. Flamant, D. Bruneau, and C. Loth, 2006: Two-micrometer heterodyne differential absorption lidar measurements of the atmospheric CO2 mixing ratio in the boundary layer, *Appl. Opt.*, 45, 4448–4458.

Gibert F., L. Joly, I. Xueref-Remy, M. Schmidt, A. Royer, P. H. Flamant, M. Ramonet, B. Parvitte, G. Durry, and V. Zéninari, 2008a: Inter-comparison of 2-µm Heterodyne Differential Absorption Lidar, Laser Diode Spectrometer, LICOR NDIR analyzer and flasks measurements of near-ground atmospheric CO2 mixing ratio, ***Spectrochimica Acta Part A: Mol. Biomol. Spectrosc***.. 71, doi:10.1016/j.saa.2008.07.010.

Gibert, F., I. Xuéref-Rémy, L. Joly, M. Schmidt, J. Cuesta, K. Davis, M.l Ramonet, P. H. Flamant, B. Parvitte, and V. Zéninari, 2008b: A case study of CO2, CO and particles content evolution in the suburban atmospheric boundary layer using a 2-µm Doppler DIAL, a 1-µm backscatter lidar and an array of in-situ sensors, ***Bound. Layer Meteor.***, 128, 381–401, doi:10.1007/s10546-008-9296-8.

Gibert F., P.H. Flamant, J. Cuesta, and D. Bruneau, 2008c: Vertical 2-µm heterodyne differential absorption lidar measurements of mean CO2 mixing ratio in the troposphere, ***J. Atmos. Ocean. Technology***, 25, 1477–1497, doi:10.1175_2008JTECHA1070.1.

Gurney K.R. et al., 2002: Towards robust regional estimates of CO2 sources and sinks using atmospheric transport models, ***Nature***, 415, 626-630.

Haapalinna A., T. Kübarsepp, P. Kärhä, and E. Ikonen, 1999: Measurement of the absolute linearity of photodetectors with a diode laser, ***Meas. Sci. Technol.***, 10, 1072–1078.

Hoff, R. M., S. P. Palm, J. A. Engel-Cox, and J. Spinhirne, 2005: GLAS long-range transport observation of the 2003 California forest fire plumes to the Northeastern US, ***Geophys. Res. Lett.***, 32, L22S08, doi:10.1029/2005GL023723.

Houghton, R. A., 2003: Revised estimates of the annual net flux of carbon to the atmosphere from changes in land use and land management 1850–2000, ***Tellus***, Ser. B, 55, 378–390.

Hu, Y., 2007: Depolarization ratio-effective lidar ratio relation: theoretical basis for space based lidar cloud phase discrimination, ***Geophys. Res. Lett.,*** 34, L11812.

Intergovernmental Panel on Climate Change (IPCC), 2007a: ***Climate Change 2007 - The Physical Science Basis - Summary for Policymakers***, IPCC Secretariat, c/o WMO, Geneva, 18p.

Intergovernmental Panel on Climate Change (IPCC), 2007b: ***Climate Change 2007 -, The Physical Science Basis*** - Contribution of Working Group I to the Fourth Assessment Report of the Intergovernmental Panel on Climate Change [Solomon, S., D. Qin, M. Manning, Z. Chen, M. Marquis, K.B. Averyt, M. Tignor, and H.L. Miller (eds.)]. Cambridge University Press, Cambridge, United Kingdom and New York, NY, USA.

Ishii S., K. Mizutani, H. Fukuoka, T. Ishikawa, H. Iwai, P. Baron, J. Mendrok, Y. Kasai, T. Aoki, A. Sato, K. Asai, and T. Itabe, 2008: Development of 2 Micron Coherent Differential Absorption Lidar, Reviewed and Revised Papers, 24th International Laser Radar Conference, 23–28 June, Boulder, Colorado, USA, p. 689–692.

Jacobson, A. J., S. E. Mikaloff Fletcher, N. Gruber, J. L. Sarmiento, and M. Gloor, 2007a: A joint atmosphere-ocean inversion for surface fluxes of carbon dioxide: 1. Methods and global fluxes, *Global Biogeochem. Cycles*, 21, GB1019, doi:GB1029/2005GB002556.

Jacobson, A. J., S. E. Mikaloff Fletcher, N. Gruber, J. L. Sarmiento, and M. Gloor, 2007b: A joint atmosphere-ocean inversion for surface fluxes of carbon dioxide: 2. Regional results, *Global Biogeochem. Cycles*, 21, GB1020, doi:GB1029/2006GB002703.

Joly, L., F. Gibert, B. Grouiez, A. Grossel, B. Parvitte, G. Durry, and V. Zéninari, 2007: A complete study of CO2 line parameters around 4845 $cm^{-1}$ for Lidar applications, *J. Quant. Spectr. Rad. Trans.*, 109, 426–434, doi:10.1016/j.jqsrt.2007.06.003.

Koch G. J., B. W. Barnes, M. Petros, J. Y. Beon, F. Amzajerdian, J. Yu, R. E. Davis, S. Ismail, S. Vay, M. J. Kavaya, and U. N. Singh, 2004: Coherent differential absorption lidar measurements of CO2, *Appl. Opt.*, 43, 5092–5099.

Koch, J.G., J.Y. Beyon, F. Gibert, B.W. Barnes, S. Ismael, M. Petros, P.J. Petzar, J. Yu, E.A. Modlin, K.J. Davis and U. Singh, 2008: Side-Line Tunable Transmitter for Differential Absorption Lidar Measurements of CO2: Design and Application to Atmospheric Measurements, *Appl. Opt.,* 47. 944–956.

Law, R.M., R. J. Matear, and R. J. Francey, 2008: Comment on "Saturation of the Southern Ocean CO2 Sink Due to Recent Climate Change", *Science*, 319 (5863), 570a, doi:10.1126/science.1149077.

Le Quéré, C. et al., 2007: Saturation of the Southern Ocean CO2 sink due to recent climate change, *Science*, 316, 1735–1738.

Lefsky, M. A. D. J. Harding, M. Keller W. B. Cohen, C. C. Carabajal, F. Del Bom Espirito-Santo, M. O. Hunter, and R. de Oliveira Jr., 2005: Estimates of forest canopy height and aboveground biomass using ICESat, *Geophys. Res. Lett.*, 32, L22S02, doi:10.1029/2005GL023971.

Liu, Z. et al., 2008a: CALIPSO lidar observations of the optical properties of Saharan dust: A case study of long-range transport, *J. Geophys. Res.*, 113, D07207, doi:10.1029/2007JD008878.

Liu, D., Z. Wang, Z. Liu, D. M .Winker, and C. Trepte, 2008b: A height resolved global view of dust aerosols from the first year CALIPSO lidar measurements, *J. Geophys. Res.*, 113, D16214, doi:10.1029/2007JD009776.

Loth, C. P. Flamant, F. M. Bréon, D. Bruneau, P. Desmet, T. Pain, A. Dabas, P. Prunet, and J. P. Cariou, 2005: Future Atmospheric Carbon Dioxide Testing from Space, Observation Techniques and Sensor Concepts for the Observations of CO2 From Space, *ESA Study Report*, ESA-CR(P)-4544.

Lovenduski, N.S., N. Gruber, and S. C. Doney, 2008: Toward a mechanistic understanding of the decadal trends in the Southern Ocean carbon sink, *Global Biogeochem. Cycles*, 22, GB3016, doi:10.1029/2007GB003139.

Mégie G. and R. T. Menzies, 1980: Complementarity of UV and IR differential absorption lidar for global measurements of atmospheric species, *Appl. Opt*., 19, 1173–1183.

Menzies R. T. and G. D. Spiers, 2008: Airborne Laser Absorption Spectrometer for IPDA Measurement of Atmospheric Effects on Attainable Precision and a Technique for Cloud and Aerosol filtering , Reviewed and Revised Papers, 24th International Laser Radar Conference, 23–28 June, Boulder, Colorado, USA, p. 643–646.

Menzies, R.T. D.M. Tratt, J.D. Spinhirne, and D.L.Hlavka, 2002: Aerosol layers over the Pacific Ocean: Vertical distributions and optical properties as observed by multi-wavelength airborne lidars, *J. Geophys. Res.*, 107, 10.1029/2001JD001196.

Mikaloff Fletcher, S.E. et al., 2006: Inverse estimates of anthropogenic CO2 uptake, transport, and storage by the ocean, *Global Biogeochem. Cycles*, 20, GB2002, doi:10.1029/2005GB002530.

Mikaloff Fletcher, S.E. et al., 2007: Inverse estimates of the oceanic sources and sinks of natural CO2 and the implied oceanic carbon transport, *Global Biogeochem. Cycles*, 21, GB1010, doi:10.1029/2006GB002751.

Miller, C. E. et al., 2007: Precision requirements for space-based XCO2 data, *J. Geophys. Res.*, 112, doi: 10.1029/2006JD007659.

National Research Council, 2007: *Earth Science and Applications from Space - National Imperatives for the Next Decade and Beyond;* Committee on Earth Science and Applications from Space, National Academies Press, 456p.

Peylin P., P. Bousquet, C. Le Quéré, S. Sitch, P. Friedlingstein, G. McKinley, N. Gruber, P. Rayner, and P. Ciais, 2005: Multiple constraints on regional CO2 flux variations over land and oceans. Global Biogeochem. *Cycles*, 19, GB1011, doi:10.1029/2003GB002214.

Rayner, P., M. Scholze, W. Knorr, T. Kaminski, R. Giering, and H. Widmann, 2005: Two decades of terrestrial Carbon fluxes from a Carbon Cycle Data Assimilation System (CCDAS). *Global Biogeochem. Cycles*, 19, doi:10.1029/2004GB002254.

Refaat T. F., S. Ismail, M. N. Abedin, S. M. Spuler, S. D. Mayor, and U. N. Singh, 2008: Lidar backscatter signal recovery from phototransistor systematic effect by deconvolution, *Appl. Opt.*, 47, 29, 5281–5295.

Régalia-Jarlot L., V. Zéninari, B. Parvitte, A. Grossel, X. Thomas, P. von der Heyden, and G. Durry, 2006: A complete study of the line intensities of four bands of CO2 around 1.6 and 2.0 µm: a comparison between Fourier transform and diode laser measurements, *J. Quant. Spectro. Rad. Trans.*, 101, 325–338.

Remsberg E. and Gordley, 1978: Analysis of differential absorption lidar from the space shuttle, *Appl Opt.*, 17, 624–630.

Rothman L. S. et al., 2005: The HITRAN 2004 molecular spectroscopic database, *J. Quant. Spectro. Rad. Trans.*, 96, 139–204.

Sabine, C. L. et al., 2004: The Oceanic Sink for Anthropogenic CO2, *Science*, 305, pp. 367–371.

Sakaizawa D., C. Nagasawa, M. Abo, Y. Shibata, and T. Nagai, 2008: Development of a 1.6 µm CO2 DIAL Transmitter using the OpM-OpO, Reviewed and Revised Papers, 24th International Laser Radar Conference, 23–28 June, Boulder, Colorado, USA, p. 683–686.

Sarmiento, J.L. and N. Gruber, 2002: Sinks for anthropogenic carbon, *Phys. Today*, 55(8), 30–36.

Sarmiento, J. L., T. M. C. Hughes, R. J. Stouffer, and S. Manabe, 1998: Simulated response of the ocean carbon cycle to anthropogenic climate warming, *Nature*, 393, 245–249.

Scholze, M. et al., 2008: Quantifying the benefit of A-SCOPE data for reducing uncertainties in current and future terrestrial carbon uptake, *ESA Contract* No. 21061, study in progress.

Scholze, M., T. Kaminski, P. Rayner, W. Knorr, and R. Giering, 2007: Propagating uncertainty through prognostic CCDAS simulations. *J. Geophys. Res.*, 112, doi:10.1029/2007JD008642.

Schotland R. M., 1974: Errors in the lidar measurement of atmospheric gases by differential absorption, *J. Appl. Meteor.* , 13, 71–77.

Schultz B. E., H. J. Zwally, C. A. Shuman, D. Hancock, and J. P. DiMarzio, 2005: Overview of the ICESat Mission, *Geophys. Res. Lett.*, 32, L21S01, doi:10.1029/2005GL024009.

Spinhirne, J. D., S. Chudamani, J. F.Cavanaugh, and J. L.Bufton, 1997: Aerosol and cloud backscatter at 1.06, 1.54, and 0.53 micron by airborne hard-target-calibrated Nd:YAG/methane Raman lidar, *Appl. Opt.*, 36, 3475–3490.

Spinhirne, J. D., S. P. Palm, and W. D. Hart. 2005: Antarctica Cloud Cover for October 2003 from GLAS Satellite LIDAR Profiling. *Geophys. Res. Lett.*, 32: L22S05, doi:10.1029/2005GL023782.

Thales Alenia Space Italy, 2008: Phase 0 study of the six candidate Earth Explorer Core Missions, Final Report, *ESA Contract* No. 20844.

Thornton, P. E., J.-F. Lamarque, N. A. Rosenbloom, and N. M. Mahowald, 2007: Influence of carbon-nitrogen cycle coupling on land model response to CO2 fertilization and climate variability, *Global Biogeochem. Cycles*, 21, GB4018, doi:10.1029/2006GB002868.

Toth, R.A., L.R. Brown, C.E. Miller, V. M. Devi, and D.C. Benner, 2008: Spectroscopic database of CO2 line parameters: 4300-7000 $cm^{-1}$, *J. Quant., Spectrosc. Rad. Trans.*, 109, 906–921.

Uno, I., K. Yumimoto, A. Shimizu, Y. Hara, N. Sugimoto, Z. Wang, Z. Liu, and D. M. Winker, 2008: 3D structure of Asian dust transport revealed by CALIPSO lidar and a 4DVAR dust model, *Geophys. Res. Lett.*, 35, L06803, doi:10.1029/2007GL032329.

Uppala, S. M. et al., 2005: The ERA-40 re-analysis, *Quart. J. R. Meteor. Soc.*, 131, pp 2961–3012.

Washenfelder, R. A., G. C. Toon, J.-F. Blavier, Z. Yang, N. T. Allen, P. O. Wennberg, S. A. Vay, D. M. Matross, and B. C. Daube, 2006: Carbon dioxide column abundances at the Wisconsin Tall Tower site, *J. Geophys. Res.*, 111, D22305, doi:10.1029/2006JD007154.

Winker, D. M., R. H. Couch, and M. P. McCormick, 1996: An overview of LITE: NASA's Lidar In-space Technology Experiment, Proc. IEEE, 84, 2, 164–180.

Winker, D. W. Hunt, and M. J. McGill, 2007: Initial performance assessment of CALIOP, *Geophys. Res. Lett.*, 34, L19803, doi:10.1029/2007GL030135.

Wylie, D. et al., 2007: Comparison of Cloud Cover Statistics from the GLAS Lidar with HIRS, *J. of Climate*, 20, 4968–4981.

Yang, Z., G.C. Toon, J.S. Margolis, and P.O. Wennberg, 2002: Atmospheric CO2 retrievals from ground-based near IR solar spectra, *Geophys. Res. Lett.*, 29, 1339, doi:10.1029/2001GL014537.

## Acronyms

| | |
|---|---|
| ABL | Atmospheric Boundary Layer |
| AIRS | Atmospheric Infrared Sounder |
| ADC | Analogue to Digital Converter |
| AOCS | Attitude and Orbit Control System |
| APD | Avalanche PhotoDiode |
| ARPÉGE | Action de Recherche Petite Echelle Grande Echelle |
| ASCENDS | Active Sensing of $CO_2$ Emissions over Nights, Days, and Seasons |
| CALIPSO | Cloud-Aerosol Lidar and Infrared Pathfinder Satellite Observation |
| CCDAS | Carbon Cycle Data Assimilation System |
| $CO_2$ | Carbon dioxide |
| CW | Continuous Wave |
| DAOD | Differential Absorption Optical Depth |
| DESDynI | Deformation, Ecosystem Structure, and Dynamics of Ice |
| DIAL | Differential Absorption Lidar |
| ECMWF | European Centre for Medium-range Weather Forecasting |
| ENSO | El Niño Southern Oscillation |
| EQM | Engineering Qualification Model |
| ESA | European Space Agency |
| ESOC | European Space Operation Centre |
| ESRIN | European Space Research Institute |
| ESRL | Earth System Research Laboratory |
| ETH | Eidgenössische Technische Hochschule |
| ETM+ | Enhanced Thematic Mapper Plus |
| FOCC | Flight Operations Control Centre |
| FOS | Flight Operation Segment |
| FOV | Field Of View |
| FTIR | Fast Fourier Transform Infrared Radiometer |
| FTS | Fourier Transform Spectrometer |
| GAW | Global Atmosphere Watch |
| GC | Gas Chromatography |
| GCOS | Global Climate Observing System |
| GEMS | Global Environmental Measurement System |
| GLAS | Geoscience Laser Altimeter System |
| GNSS | Global Navigation Satellite Systems |

| | |
|---|---|
| GOS | Global Observing System |
| GOSAT | Greenhouse gases Observing SATellite |
| HITRAN | High-resolution transmission molecular absorption database |
| IAP | Institute for Atmospheric Physics |
| IASI | Infrared Atmospheric Sounding Interferometer |
| ICESat | Ice, Cloud, and land Elevation Satellite |
| ICOS | Integrated Carbon Observing System |
| IGOS | International Global Observing System |
| IOC | Intergovernmental Oceanographic Commission (of UNESCO) |
| IPCC | Intergovernmental Panel on Climate Change |
| IPDA | Integrated Path Differential Absorption |
| JAXA | Japan Aerospace Exploration Agency |
| JCOMM | Joint WMO-IOC Technical Commission for Oceanography and Marine Meteorology |
| LAS | Laser Absorption Spectrometer |
| LDS | Laser Diode Spectrometer |
| LEO | Low Earth Orbit |
| LEOP | Launch and Early Operations Phase |
| LITE | Lidar In-space Technology Experiment |
| LMD | Laboratoire de Météorologie Dynamique |
| LOS | Line Of Sight |
| LOSU | Level of scientific understanding |
| LSCE | Laboratoire des Sciences du Climat et de L'Environnement |
| LTDN | Local Time of the Descending Node |
| NASA | National Aeronautics and Space Administration |
| NDIR | Non-dispersive infrared |
| NEP | Noise Equivalent Power |
| NIR | Near-infrared |
| NPP | Net Primary Production |
| NWP | Numerical Weather Prediction |
| OCO | Orbiting Carbon Observatory |
| OPA | Optical Parametric Amplifier |
| OPO | Optical Parametric Oscillator |
| OSSE | Observation System Simulation Experiment |
| OSTM | Optical, Structural and Thermal Model |

| | |
|---|---|
| PDGS | Payload Data Ground Segment |
| PDHT | Payload Data Handling and Transmission |
| PFM | Proto-Flight Model |
| PRF | Pulse Repetition Frequency |
| RE | Random Error |
| RF | Radiative Forcing |
| RPE | Relative Pointing Error |
| SCIAMACHY | SCanning Imaging Absorption SpectroMeter for Atmospheric CartograpHY |
| SE | Systematic Error |
| SNR | Signal to Noise Ratio |
| SOOP | Ship of Opportunity Programme |
| SRON | Stichting Ruimte Onderzoek Nederland |
| SSE | Surface Scattering Elevation |
| STM | Structural and Thermal Model |
| TCCON | Total Carbon Column Observing Network |
| TT&C | Telemetry, Tracking and Command |
| UNFCCC | United Nations Framework Convention on Climate Change |
| UoB | University of Bristol |
| USO | Ultra Stable Oscilator |
| VU | Vrije Universiteit Amsterdam |
| WMO | World Meteorological Organization |
| $XCO_2$ | Column-weighted dry-air mixing ratio of carbon dioxide |

**CONTACT**

**ESA HQ**
France
+33 1 5369 7654

**ESTEC**
The Netherlands
+31 71 565 3006

**ESOC**
Germany
+49 615 1900

**ESRIN**
Italy
+39 0694 1801

**ESAC**
Spain
+34 91 813 1100

**EAC**
Germany
+49 2203 60010

**An ESA Communications Production**
SP-1313/1 | ISBN 978-92-9221-406-7 | ISSN 0379-6566
Copyright © 2008 European Space Agency